AD NUMBER:	AD0361916
CLASSIFICATION CHANGES	
TO:	Unclassified
FROM:	Confidential
LIMITATION CHANGES	
TO:	Approved for public release; distribution is unlimited.
FROM:	Distribution authorized to US Government Agencies only; Export Control; 1 Jun 1956. Other requests shall be referred to Defense Atomic Support Agency, Washington, DC 20301.
AUTHORITY	
	C to U and ST-A per DNA ltr dtd 6 Jun 1980

E X C L U D E D

FROM GENERAL CLASSIFICATION SCHEDULE
IN ACCORDANCE WITH
INFORMATION SECURITY PROGRAM REGULATION

DATED - JULY 1972

DOD 5000.1R & EXECUTIVE ORDER 11652
(EXECUTIVE ORDER 10501 AMENDED)

BY

Defense Documentation Center
Defense Supply Agency
Cameron Station
Alexandria, Virginia 22314

DEC 1972

SECURITY MARKING

The classified or limited status of this report applies to each page, unless otherwise marked.
Separate page printouts MUST be marked accordingly.

"This document contains information affecting the National Defense of the United States within the meaning of the Espionage Laws, Title 18, U. S. C., Section 793 and 794. Its transmission or the revelation of its contents in any manner to an unauthorized person is prohibited by law."

EXCLUDED FROM AUTOMATIC
REGRADING; DOD DIR 5200.10
DOES NOT APPLY

" ONE HALF ORIGINAL SIZE " **attachment A**

CONFIDENTIAL

WT-1021
(Supersedes ITR-1070)

Copy No. ~~75~~ A

Operation WIGWAM

May 1955

Classification cancelled (or changed to ______)
by authority of 325
by J E Meredith TISOR date 8-23-62

Project 3.1 (Parts I and II)

LETHAL RANGE OF WIGWAM TARGETS BASED ON HULL RESPONSE AND APPLIED PRESSURE MEASUREMENTS

Issuance Date: July 10, 1957

~~FORMERLY RESTRICTED DATA~~
~~Handle as Restricted Data in foreign dissemination~~, Section 144b, Atomic Energy Act of 1954.

This material contains information affecting the national defense of the United States within the meaning of the espionage laws Title 18, U. S. C., Secs. 793 and 794, the transmission or revelation of which in any manner to an unauthorized person is prohibited by law.

PR#9137

COMMANDER TASK GROUP 7.3

571230(F)

CONFIDENTIAL

15559

If this report is no longer needed, return it to
AEC Technical Information Service Extension
P. O. Box 401
Oak Ridge, Tennessee

WT-1021
(Supersedes ITR-1070)

This document consists of 90 pages
No. [redacted] of 210 copies, Series A

Report to the Scientific Director

LETHAL RANGE OF WIGWAM TARGETS BASED ON HULL RESPONSE AND APPLIED PRESSURE MEASUREMENTS

By

G. Chertock
A. E. Hirsch
R. W. Mayo
T. F. Ogilvie

Approved by: G. CHERTOCK
Project Officer
Project 3.1

Approved by: A. B. FOCKE
Scientific Director
Operation Wigwam

Approved by: CDR D. R. SAVEKER, USN
Director, Program III

David Taylor Model Basin
Washington 7, D. C.
June 1956

ABSTRACT

The external pressures applied to the three SQUAW targets in Operation Wigwam were measured with pressure gages, and the deformations of the hull were measured with strain and displacement gages.

The results indicate that SQUAW-12 was at a horizontal range of 5150 ft and a depth of 290 ft; the peak shock pressure at the hull was about 850 psi, and the target was destroyed, probably within 10 msec.

SQUAW-13 was at a horizontal range of 7200 ft and a depth of 260 ft; the peak dynamic pressure at the hull was about 615 psi, and the hull was probably near collapse but did not rupture.

It is estimated that the lethal horizontal range of the SQUAW target under the Wigwam test conditions is about 7000 ft for a depth of 250 ft and about 4500 ft for a depth of 70 ft.

Finally, a general formula is proposed which gives conditions for lethal attack by an atomic depth charge against a full-scale submarine.

ACKNOWLEDGMENTS

We are indebted to CDR R. C. Gooding, USN, H. L. Rich, and Dr. W. J. Sette of the David Taylor Model Basin staff for their assistance in initiating the project and procuring instruments during the early stages. F. L. Roberson has been a full-time member of the project personnel and is particularly responsible for installation of many of the gages in a highly efficient manner. We are indebted to CDR A. F. Hancock, USN, for making the calculations of the static collapse pressure and for fruitful discussions of the collapse mechanism.

A. Cargyle, C. T. Johnson, and J. N. Shellabarger, all of the Navy Electronics Laboratory, and E. O. Arnold of the Naval Repair Facility supervised the installation of the instrument trailers in the barges or assisted with the operations at San Diego in many ways. F. J. Friel of the Underwater Explosions Research Division arranged the procurement and installation of the large instrument cables.

Finally, we are indebted to CDR D. R. Saveker, USN, for his efficient organization and for his continual advice and cooperation in this project.

CONTENTS

CONTENTS (Continued)

ILLUSTRATIONS

TABLES

Page

CHAPTER 1

INTRODUCTION

Objectives. A major objective of Operation Wigwam was to determine the lethal range for an atomic depth charge against a typical submarine target. This knowledge is of obvious military importance as a guide to proper tactics in using the weapon against enemy submarines and also in protecting our own shipping against such attack.

Under Project 3.1, measurements were made of the response of the pressure hulls of three submarine targets to the attack. Primarily the measurements were intended as one basis for lethal-range estimates. For this purpose it was planned that the measurements would supplement (1) a detailed examination of the damage after the test and (2) high-speed photographs of the damage taken during the test. In addition, it was planned that the measurements would verify, or perhaps elaborate, the theoretical concepts of the damage mechanism which had been formulated in the past. Some knowledge of this damage mechanism is necessary in order to extrapolate any single measurement of the lethal range to other targets or other conditions of attack.

CHAPTER 2

BACKGROUND AND PREVIOUS WORK

2.1 INTRODUCTION

The background for this project has been a long series of experimental and analytical studies directed at estimating the lethal range of an atomic weapon against a submarine. In early analyses of the problem it was customary to argue that the pressure wave from an atomic weapon has a small gradient over the dimensions of the submarine and a small decay during the time of deformation of the target. Hence the damage should be the same as though the pressure were applied uniformly and statically; and the lethal range should occur where the peak total pressure, shock-wave plus ambient hydrostatic pressure, reaches the static collapse pressure of the submarine. This argument, of course, does not apply to test conditions where either the weapon or the target is so shallow that the shock pressure is cut off by surface reflection before it is fully effective.

There are many other tacit assumptions in the argument which were discussed in the subsequent work. We shall survey this work and consider in particular how the experimental measurements and theoretical predictions of the lethal pressure compare with the static collapse pressure.

2.2 CROSSROADS TEST

The Operation Crossroads Baker test provided the first relevant data. In this test the submarines Pilotfish, Skipjack, and Apogon were lethally damaged by pressures that were estimated to be at least twice as large as the static collapse pressures. The estimated durations of the pressure wave were 4 to 6 msec, which is probably comparable with the time necessary to produce the deformation. Three other submarines, the Sea Raven, Dentuda, and Tuna, were not damaged structurally, although they were exposed to peak pressures which were presumed to range from 350 to 450 psi for durations from 2 to 4.4 msec. These pressures are slightly lower than the expected static collapse pressure of about 500 psi, and the durations are smaller than the probable collapse times. The applied pressures at these targets are not known with any great precision because the pressure-time measurements were not completely successful. In summary, the damage results suggest only that, for a pressure wave with durations from 3 to 6 msec, the total applied pressures must exceed 1 to 2 times the static collapse pressure before lethal damage occurs.

2.3 UERL MODEL TESTS

An early series of damage tests on models was conducted by the Underwater Explosives Research Laboratory (UERL) at Woods Hole Oceanographic Institution.[1] The targets were cylindrical steel shells, internally stiffened, and designed to approximate $\frac{1}{23}$-scale models of submarine pressure hulls. Some of the charges were spherical in shape, and these ranged from 0.05 to 300 lb of TNT. There were also tapered charges, which were designed to give relatively constant step-pressure waves for relatively long times. The test results showed that, for spherical charges where the duration of the shock pressure was presumably smaller than the structural response times, the lethal range occurred at almost constant values of the parameter $W^{1/2}/d$, W being the weight of the charge. For the charges with long durations, "lethal damage first occurred when the peak total pressure was not more than 20 per cent in excess of the static collapse pressure."[1] The last result could not be stated any more precisely because the tapered charge did not produce ideal flat-topped pressure waves, and the equivalent step pressure was ambiguous by about 20 per cent.

2.4 BRITISH TESTS

A similar series of damage tests was conducted by the British on $\frac{1}{50}$-scale models of surface ships and submarines.[2] The charge size was 300 lb of TNT, and the test depths ranged up to 100 ft. For submarines it was concluded that the lethal range of nominal atomic weapons is on the order of 1 to 2 miles. The results were too crude to justify a more precise conclusion.

An important British test program against full-scale S class submarines and X craft (miniature submarines) was intended primarily to determine the lethal range under attack by conventional chemical charges, not atomic weapons.[3] The charges ranged from 8 to 650 lb of Torpex at depths up to two-thirds of the collapse depth, although most of the tests were at shallow depths. It was found that most of the results could be fitted to a Hogg or Butterworth type formula which relates the degree of damage to the incident energy flux. The lethal range was given by[4]

$$D = 1.15 \sqrt{W/t} \tag{2.1}$$

where D is the range in feet, W is the charge weight in pounds of TNT, and t is the hull thickness in inches. This empirical formula applies to all tests except those with very small charges close to the hull. It was based on data with localized charges at shallow depths. For atomic bomb attack, and for submarines that are 250 to 500 ft deep, it was estimated that the ranges given by the formula should be increased by about 25 per cent.

2.5 ALIAS REPORT

A review and an analysis of available data were made by W. Mostow for the Alias Report.[5] He calculated the deformation of the submarine shell by a one-dimensional theory used in analyzing the deformation of diaphragms by underwater explosions. The results indicated that, for conditions where cutoff was not a factor, the inertial overshoot of the motion was negligible. Hence the condition for failure is that the peak total pressure should exceed the "static" collapse pressure that is calculated using the dynamic yield strength of the plating instead of the static yield strength. For shallow targets or weapons, where cutoff may be a factor, the required peak pressure was assumed to increase by the factor $\{[1 - (T/T_c)]^2\}^{-1}$, where T is the cutoff time and T_c is an arbitrarily assumed response time of the structure.

2.6 EXCESS IMPULSE

For pressures applied over a long time, a sufficient (and probably necessary) condition for lethality is that the applied pressure exceed the static collapse pressure. For more transient pressures this condition is no longer sufficient because the plastic damage may not accumulate to complete collapse before the pressure is reduced. A simple formula to fit these facts was first suggested by Bryant at the Underwater Explosion Conference of 1950. He proposed, as an empirical formula, for those cases where damage is caused by the bubble-pulse pressures, that the amount of plastic damage done to a given type of submarine depends only on the impulse of the excess of the applied pressure over the static collapse pressure, i.e., on $\int(P + P_0 - P_c)\,dt$, where P is the explosion pressure, P_0 is the ambient hydrostatic pressure, P_c is the static collapse pressure, and the integral is taken over the time interval during which the total pressure exceeds the static collapse pressure. Bryant first estimated, on the basis of the British full-scale tests, that the excess impulse must exceed 2.3 psi-sec for lethal damage.[6] After a more detailed analysis of the damage process,[4] the critical value was estimated to be about 5 psi-sec for shallow submarines and about 3 psi-sec at about half the collapse depth. It was suggested that this excess-impulse criterion should apply not only to bubble-pulse pressures but also to shock-wave pressures and even in the region of surface cutoff. However, in later discussion, at the Underwater Explosion Conference in 1955, Bryant indicated that his most recent analysis of the experimental data had shown that the excess impulse required for collapse is negligible in those cases where the damage is due to the bubble pulse.

The growth of plastic damage in the submarine shell was later discussed in a mathematical analysis by Schauer.[7] He assumed a simplified model target in which the work done on the target in the elastic range is negligible, the plastic resistance depends only on the change of volume of the shell, the damping is proportional to the rate of change of volume, and the applied pressure is the same as the incident pressure. Then, for an arbitrary range in resistance functions and applied pressures, it was found that the lethal range varies with charge weight as W^n, where n is in the range $\frac{1}{3}$ to $\frac{2}{3}$. If the plastic resistance remains constant and if inertial forces are negligible compared with damping forces, then the plastic damage becomes proportional to the impulse of the excess pressure in agreement with Bryant's theory.

2.7 MINDLIN-BLEICH ANALYSIS

Another review of the data and an additional mathematical analysis were made by Mindlin and Bleich for the report of the Pelican Committee.[8] They concluded that, under conditions where surface cutoff was not a factor, the critical lethal range would occur where the total peak pressure was somewhere between 116 and 160 per cent of the static collapse pressure.

The lower limit was calculated to be the total peak pressure for which the average circumferential strain in the plating reaches the yield strain. This was based on a mathematical solution for the motion of a uniform elastic cylindrical shell that is exposed to a transverse, acoustic, step shock wave. The mathematical solution included the effects of the refracted pressure wave and the radiation pressures and analyzed the translational and elastic motions of the shell as a superposition of various orthogonal modes of motion.

It was argued that plastic damage in a modern submarine (under either atomic bomb attack or static pressure loading) is initiated when the circumferential strain in the plating reaches the yield strain, and the mode by which it does so is analogous to the dilatational (hoop) mode response of the uniform mathematical model. The excess of 16 per cent over the static collapse pressure was estimated to compensate for the combined effects of radiation damping of the dilatational mode and exponential decay of the applied pressure during the gradual envelopment of the submarine. The estimate was based on an approximation to the mathematical solution which was shown to be adequate at the beginning of the motion and in the final stages but which was not verified for the critical time at which the strain reached its peak value. It was recognized that more complex modes of motion, and not only the dilatational mode, might contribute to the circumferential strain and cause the yield strain to be reached at a lower pressure. However, it was argued that this effect would be somewhat offset by the increase in the yield strength due to the high strain rate.

The upper pressure limit in the critical pressure range was calculated to be the pressure for which the stresses reached the strain-hardening range. It was estimated that at this point the steel becomes brittle and failure is unavoidable.

2.8 INTERACTION OF TARGET MOTION AND PRESSURE WAVE

The mathematical problem of the interaction between a transverse shock wave and a uniform cylindrical shell was also solved by Carrier in the form of a Fourier integral without numerical results.[9] The same method was used to solve for the interaction between a spherical shell and a step shock wave, for which numerical results were obtained without approximation.[10] In this case the response in the dilatational mode was not overdamped, but the peak response overshot the equivalent static response by 11 per cent. This result is the only relatively exact solution of a problem which gives a good indication of the initial interaction of a submarine target and a shock wave incident in the longitudinal direction.

The response of a cylindrical shell to a transverse exponential shock wave was calculated from a Fourier integral by Sette et al.[11] They found that the mathematical approximation of Mindlin and Bleich overemphasized the damping of the dilatational mode and that their lower critical pressure estimate of 116 per cent of the static collapse pressure should therefore be reduced by about 10 per cent.

They also calculated the response when the pressure wave propagates in the axial direction along the hull.[12] In this case the proper boundary conditions and initial conditions are uncertain. The conditions used in the calculation were arbitrary approximations whose validity is correspondingly uncertain. Similar solutions for this case were given by Bleich[13] and by Carrier,[14] with similar approximations to the boundary conditions. The final results showed a 15 per cent inertial overshoot in the response for the Lax calculation[12] and very slight overdamping of the response for the Bleich calculation.[13]

2.9 UERD MODEL TESTS

There were many model tests conducted by the Underwater Explosions Research Division (UERD) of the Norfolk Naval Shipyard in which an attempt was made to determine the lethal range for atomic bomb attack by extrapolation of lethal ranges measured with smaller charges charges.[15,16] The targets were about $\frac{1}{8}$ scale, and the charge size varied from 1 to 10,000 lb of HBX-1. On an energy basis, the largest charge scaled up to about 1.8 kt of TNT. The results showed that the damage mechanism was not the same for all charge weights. In fact, for the larger charge in the later tests, it was concluded that actual failure was caused by the bubble-pulse loading and not the shock wave. However, in both the earlier and later tests, they concluded that the lethal range varies about as $W^{1/2}$, although the proportionality constant was different for the different tests, perhaps because of a difference in the stiffener design. The final conclusion, obtained by extrapolating the results to 20 kt of TNT, was that, for a full-scale submarine of equivalent strength, the lethal radius was between 7100 and 9000 ft when the target was 500 ft deep. If this result is interpreted in terms of the static collapse pressure, it implies that the peak total pressure for lethal damage is from 1.5 to 1.9 times the static collapse pressure.

It seems clear that for large enough charge weights the lethal radius cannot vary as $W^{1/2}$ in a free field. For this would mean that for large enough charge weights the critical peak pressure could be made indefinitely smaller than the static collapse pressure. Of course, in a bounded medium with a surface present, it may possibly happen that other causes, such as the changing duration to cutoff, may conspire to keep the lethal range varying roughly as $W^{1/2}$. In any case the limit within which it is proper to extrapolate the range as $W^{1/2}$ is not known and may well be smaller than 20 kt of TNT.

The Papoose project of UERD was a major attempt to determine the lethal range by means of scaled tests.[17] The Papoose target was a $\frac{1}{5.3}$-scale model of the SQUAW target to be used in Wigwam. The charges were shaped, tapered charges, 22 ft long, containing about 3000 lb of HBX. They were intended to produce a shock wave at the target which was $\frac{1}{5.3}$ scale of that from 32 kt of TNT. The measurements included free-field pressure, applied pressure, hull displacement, hull strain, and target velocities. Four shots, each with a separate target, were found sufficient to bracket the lethal range of Papoose within 5 per cent.

It was concluded from the test results that a full-scale Papoose would fail where the peak total pressure was 910 psi ±5 per cent, or about 1.6 times the static collapse pressure. However, the lethal range of the SQUAW itself was considered more uncertain, and this was predicted to be somewhere in the range from 920 to 1100 psi, "probably" 960 psi.

The Papoose measurements demonstrated the importance of the sustained pressure durations that are necessary before plastic damage can accumulate to collapse. In the model, failure apparently occurred by a general instability of the crown structure. The instability was triggered only after the frame deformations had reached about $\frac{2}{3}$ of the hull thickness; this process required about 4 msec, which is comparable with the cutoff time and the decay time of the incident pressure.

A major difficulty in these tests, as in all tests employing shaped charges to get long-duration shock waves, is that the incident pressure wave in the first few milliseconds and also in the tail of the shock wave does not resemble an exponential shock which is cut off by surface reflection. The first two milliseconds probably represent a significant fraction of the structural response time. The tail of the shock wave may have significant pressure when compared with the residual collapse pressure of a damaged submarine target. Hence the magnitude of the equivalent exponential wave is ambiguous.

2.10 DTMB MODEL TESTS

The David Taylor Model Basin (DTMB) conducted two extensive series of model tests of atomic bomb attack. In the first series the targets were stiffened cylinders which were simplified $\frac{1}{26}$-scale models of an SS563 class submarine hull.[18] The lengths were either $2\frac{1}{2}$ or $12\frac{1}{2}$ times the diameter in order to check the effect of length. The mild steel used in the shell was heat-treated to give a yield strength comparable with the prototype. The charge size was 1570 lb of HBX-2, which scales up to 20 kt of TNT, and the tests were made over a wide range of depths reaching 1000 ft.

It was concluded from these tests that lethal damage occurred when the peak total pressure exceeded 1.38 to 1.55 times the static collapse pressure. On the basis of rather sparse data, it was tentatively concluded that the numerical factor was not sensitive to the length or orientation of the target, the presence of internal masses, or the ambient hydrostatic pressure level. The factor did seem to depend on the dynamic stress-strain characteristics of the shell material. In particular, it was concluded that the delayed-yield characteristics of the steel may be important in raising the critical pressure for these models.

The report also included a discussion of the mechanism by which plastic damage to the targets continues during collapse. The analysis was based on some measurements, made during static collapse tests, of the residual strength of the models as a function of their change in volume after the static collapse pressure had been exceeded. It was assumed that the residual strength in the dynamic tests is a function of only the mean hoop strain and that this could be related to the change in volume. This analysis predicted that, in the explosion tests, the critical total pressure should be sensitive to the depth of the target, but this prediction was not supported by the test results.

For the second series of tests,[19] the targets were similar in design to the stiffened cylinders of the first series, but there were models of four different kinds of steel and of aluminum alloy in order to study more carefully the effects of the dynamic properties of the shell material. The target depths were again varied up to 1000 ft. The charges were 5400 lb of HBX-1, which scaled up to 31 kt of TNT. Incident pressures, strains, the shock motions were all measured in some of the tests.

It was concluded that the peak total pressure necessary for lethal damage of these models ranged from 1.0 to 2.4 times the static collapse pressure, depending on the dynamic properties of the shell material. The observed mode of collapse was by shell yield in all cases, despite the fact that in the static collapse tests the aluminum alloy and the STS models failed by over-all instability. It was found possible to calculate all the measured collapse pressures within 12 per cent by a simplified elastic analysis of the response mechanism plus an assumed yield criterion. This analysis assumed that the elastic response of the target was the same as in the approximate analysis of reference 12, and that complete failure would occur when the stress intensity in the shell reached a critical value that depended on the length of time during which the stress intensity had exceeded the static yield stress of the shell material. The dynamic yield stress and delayed yield data were obtained from independent laboratory measurements. No allowance was made for any excess applied pressure to ensure that yielding would continue on to collapse. This same analytic method was then used to predict the critical value for the peak total pressure of the SQUAW target under Wigwam conditions as 880 psi ± 10 per cent. This prediction incorporates an adjustment of 5 per cent to take care of what appeared to be a systematic difference between the calculated and measured values.

2.11 NEL MODEL TESTS

A final series of model tests prior to Wigwam was conducted by the Navy Electronics Laboratory (NEL).[20] The targets were stiffened cylinders which were approximately $\frac{1}{60}$ scale of the pressure hull of the SQUAW. A major difference in the design was the use of separately supported end caps for the cylinders which could not transmit axial stress to the shell. The charges were 300 lb of TNT, which scaled up to 31 kt of TNT. Tests were made at depths up to 1500 ft, which was the nominal collapse depth. In each test the lethal range was bracketed by using seven targets at different ranges.

The test results showed a marked dependence of the peak total collapse pressure on the depth of the target. When the targets were only 100 ft deep, the peak total pressure required for lethal damage was 2.1 times the static collapse pressure. This ratio decreased slowly to 1.4 as the target depth increased to 90 per cent of nominal collapse depth. It was recognized that, with the mild steel used for the shell and the relatively small scale of the target, delayed yield effects might have a large influence on the collapse pressures, but no attempt was made to calculate this effect. However, an analysis was made to determine whether the data could be fitted to an excess-impulse criterion of damage. It was found that the excess impulse required for failure remains constant with depth at 0.18 psi-sec. This scales up to 10.6 psi-sec for a full-scale SQUAW, as compared with 1.7 psi-sec (as reference 20 suggests) for a full-scale submarine.

2.12 DYNAMIC SHELL THEORY

The analysis by a group from the Polytechnic Institute of Brooklyn was another attempt to calculate the lethal range by means of a stress analysis of the shell.[21] The shell was assumed to be exposed to a uniform pressure field, and the elastic response mode was assumed to be the same as that calculated for hydrostatic loading. The dynamic pressure was taken as a simple rectangular step whose duration was equal to the cutoff time and whose amplitude was equal to the mean shock-wave pressure averaged over this time. Also the radiation pressure was taken arbitrarily as ρc (acoustic impedance of water) times the radial velocity of the shell. When the maximum circumferential stress in the shell reached the static yield stress of the steel, then failure would be "initiated."

With these assumptions, inertial effects were found to be negligible for the Wigwam or Papoose conditions, and it was concluded that the critical total pressure, averaged over the duration of the pressure wave, is within 5 per cent of the static collapse pressure. However, the peak total pressure is about 25 per cent larger than the time average of the total pressure.

The analysis included a relatively sophisticated calculation of the static collapse pressure based on a harmonic analysis of the initial out-of-roundness of the hull. Even for this static calculation, the predicted collapse pressure was very sensitive (over a range of 1.5 to 1) to small refinements in the calculation, equivalent to emphasizing different modes of out-of-roundness.

A group from the University of Illinois has also reported an analysis and numerical procedure for computing the response of a submarine to end-on incidence of a shock wave.[22] The method is to replace the submarine structure by a ring of concentrated masses connected by weightless links. Inelastic action and dynamic buckling were included, and the resulting non-linear equations were solved by numerical integration on the Illiac digital computer. The relief pressures due to the motion of the shell were either ignored or approximated by terms proportional to the radial velocity. The computations were made for a wide range in structural parameters and applied pressures which approximated the Wigwam and Papoose conditions.

It is very difficult to assess the reliability of the approximations and hence the significance of the prediction. It seems reasonable that the results are important because they demonstrate what effects might be significant in dynamic tests of even simple models of complex structures. It was found in the calculations that very large compressive strains are not a sufficient criterion for collapse, i.e., for deformations leading to buckling. There was a large difference between the pressure function that barely causes inelastic action and the critical pressure function required for buckling. It was also concluded that the approximate method of treating the relief pressures was not satisfactory because more reasonable critical pressures were computed when the relief pressure was ignored.

2.13 FINAL ESTIMATES OF LETHAL RANGE

A final estimate for the total collapse pressure of the SQUAW, under the Wigwam test conditions, was submitted by each of the activities at a planning conference in March 1955.[23] These predictions are listed in Table 2.1.

Table 2.1—PREDICTED VALUES FOR TOTAL PEAK PRESSURE FOR COLLAPSE OF SQUAW IN WIGWAM TEST

Author	Total peak pressure, psi	Assumed yield stress, psi	
		Dynamic	Static
Bleich (Columbia University)	760	59,000	52,000
Hoff et al. (Polytechnic Institute of Brooklyn)	810	60,000	52,500
Carrier (Brown University)	840		52,000
Newmark et al. (University of Illinois)	860	{56,000 64,000	{52,000 57,000
Gooding et al. (DTMB)	880	70,000	59,000
Keil (UERD)	950	58,000	58,000

There is a divergence from the mean of ±11 per cent in the predictions. We believe that this divergence is actually smaller than the uncertainties which still remained at that time in the various theories and in the interpretation of model-test results. There is no rigorous analysis of the interaction of the complex submarine structure with an incident pressure wave. The cases that have been analyzed make it plausible that in practical cases the effective pressure at the shell and the elastic response of the target are both within about 10 per cent of what would occur if the target were loaded statically. The details of the yield and collapse process are more uncertain. In complex structures, it appears likely that the occurrence of yielding is not tantamount to complete collapse. There is no real theoretical evidence that inertial effects are important in the yield process; likewise there is no theoretical evidence that the mode of failure in practical full-scale cases is different from the static mode of failure. However, as will be discussed in the next chapter, the conditions for static failure are uncertain by perhaps 10 per cent or so. Also, the significant dynamic yield properties of the steel are uncertain by about 10 per cent.

The various model tests have narrowed the range of uncertainty, but not as much as would appear by a direct comparison of the DTMB and UERD predictions, which were presumably most directly based on model-scale results. For, even if the same effective yield stress, say 60,000 psi, had been employed in both predictions, the DTMB prediction would have been 750 psi for collapse and the UERD prediction would have been 980 psi. There is a considerable difference between the two values, apparently due to different methods of interpreting their model-scale results. The other predictions listed in Table 2.1 are nominally based on theory, but they all have been tied, more or less according to the interpretations of the authors, to the experimental results in the model tests.

It might be emphasized that both major series of model tests were effective, and deficient, in different ways. The Papoose target was a very good model of the SQUAW with most of the significant detail; the motions should scale if the applied pressure scales. However, the shaped charges used did not reproduce the pressure history well, and the interpretation of the results is not straightforward. In the DTMB model tests, the pressure wave was probably scaled in a more adequate manner, but the smaller scale of the model enhanced strain rate and delayed yield effects, and the structure was so simplified that some significant motions may have been lost.

REFERENCES

1. J. C. Decius and W. Schultz, Damage to Thin Cylindrical Shells, IV, NAVORD Report 411, 21 October 1947.
2. J. H. Powell and W. D. Hart, The Effects Produced by the Explosion of Shallow Charges in Deep Water with Particular Reference to the Atom Bomb, NCRE Report R.147 (Undex 252), March 1950.
3. Summary of the Results of Trials Undertaken by Ship Target Trials Subcommittee 1, NCRE Report R.129, 1950.
4. Underwater Explosion Phenomena, Foreign Weapon Effects Report FWE-3, 16 July 1954.
5. Project Alias, NOL Report 1158, October 1951.
6. A. R. Bryant, The Importance of Bubble Pulsation Effects in Underwater Explosion Damage, NCRE Report R.276A, October 1953.
7. H. M. Schauer, On the Estimation of the Lethal Standoff of Cylindrical Shells from Large Explosion Charges, UERD Report 1-54, January 1954.
8. The Pelican Report, Armed Forces Special Weapons Project, April 1952.
9. G. F. Carrier, The Interaction of an Acoustic Wave and an Elastic Cylindrical Shell, Brown University Report B11-4/13, October 1951.
10. P. Mann, The Interaction of an Acoustic Wave and an Elastic Spherical Shell, Brown University Report B11-11/34, February 1953.
11. W. J. Sette, J. A. Lax, and R. C. Gooding, The Calculated Response of a Submerged Cylindrical Shell to an Exponential Pressure Pulse, Fifth Symposium on Progress in Underwater Explosion Research, NavShips 250-423-22, January 1953.
12. J. A. Lax, W. J. Sette, and R. C. Gooding, Sixth Conference on Progress in Underwater Explosion Research, November 1953, NavShips 250-423-26, Report 1955-1.
13. H. H. Bleich, Sixth Conference on Progress in Underwater Explosion Research, November 1953, NavShips 250-423-26, Report 1955-1.
14. G. F. Carrier, The Response of a Submerged Cylindrical Shell to an Axially Propagating Acoustic Wave, Brown University Report B11-19/7, October 1953.
15. A. H. Keil, R. C. Gooding, and H. R. Jordon, Preliminary Investigations on the Lethal Radius of the Atomic Bomb for Submarines, UERD Report 8-52, AFSWP-254, July 1952.
16. A. H. Keil, Lethal Radius of the Atomic Bomb for Submarines, UERD Report F-17-53, May 1953.

17. A. H. Keil et al., Project Papoose, UERD Report 18-54, May 1955.
18. W. J. Sette and R. C. Gooding, Damage to Stiffened Cylinders Under Scaled A-bomb Attack in Water, DTMB Report C-616, May 1954.
19. R. C. Gooding, G. Elmer, and W. J. Sette, A Second Investigation on Damage to Stiffened Cylinders Under Scaled Atomic Bomb Attack, DTMB Report C-680, July 1955.
20. C. E. Murphey and C. T. Johnson, Target Response Studies Using High Explosives, NEL Report 637, December 1955.
21. F. V. Pohle et al., Determination of Standoff Distances for Papoose and SQUAW Models Under End-on Attack, PIBAL Report 286, March 1955.
22. J. A. Brooks, Simplified Analysis of a Submarine Subjected to End-on-incidence of a Shock Wave, University of Illinois Structural Research Studies, No. 93, February 1955.
23. A. B. Focke, Interim Summary Report of the Scientific Director of Operation Wigwam, Operation Wigwam Report ITR-1053, May 1955.

CHAPTER 3

SQUAW TARGETS

3.1 DESCRIPTION OF TARGETS

The three submarine targets were specifically constructed for the Wigwam test at the Long Beach Naval Shipyard. The details are described in the report[1] of Project 3.8; a summary description is given here.

The SQUAW target is approximately a $^4/_5$-scale model of the SS567 class submarine in section except that the SQUAW is internally framed. There are only four compartments, and thus a SQUAW is much shorter than the prototype. The significant features are:

Diameter of pressure hull (inside), 14.4 ft
Length of pressure hull, 121.5 ft
Hull plating, 1-in. HTS
Frame spacing, center section, 29 in.
Displacement submerged, 704 tons

Figure 3.1 shows some details of the SQUAW design.

The two center cylindrical compartments are attached to the conical end compartments at the bulkheads and utilize an extraheavy tapered ring as a connecting piece. These conical ends are stronger than the center test compartments because the plating is the same 1-in. HTS, but the stiffener spacing has been decreased. The conical ends are terminated with 1-in.-thick hemispherical STS caps. There are two access trunks, one into each end compartment.

There were 10 ballast tanks outside the pressure hull and along the length of the target. They covered the pressure hull up to about 32 deg port and starboard of the crown. The keel was a vertical stiffened plate between the inner and outer hulls. Below the keel there was suspended a long lead ballast weight which provided an additional negative buoyancy of 18 tons.

In the engine compartment large blocks of steel were mounted to simulate engines and generators. These blocks were mounted on foundations similar to those of the prototype. There were two motor loads and three engine-generator loads. One of the latter was shock mounted on its foundations, whereas the other units were bolted directly to the foundations. The battery compartments were fitted with concrete blocks weighing 400 lb each. These were held in place by angle-iron straps bolted together and welded to the side frames.

Out-of-roundness measurements of the circularity of the pressure hull were conducted as late as practical in the construction process. These circularity readings are reported in reference 1. Additional circularity measurements were made after completion of the SQUAW with internal mass loads installed. All the measurements show a circularity of the hull within the permitted tolerance of $\pm^1/_2$ of the shell thickness.

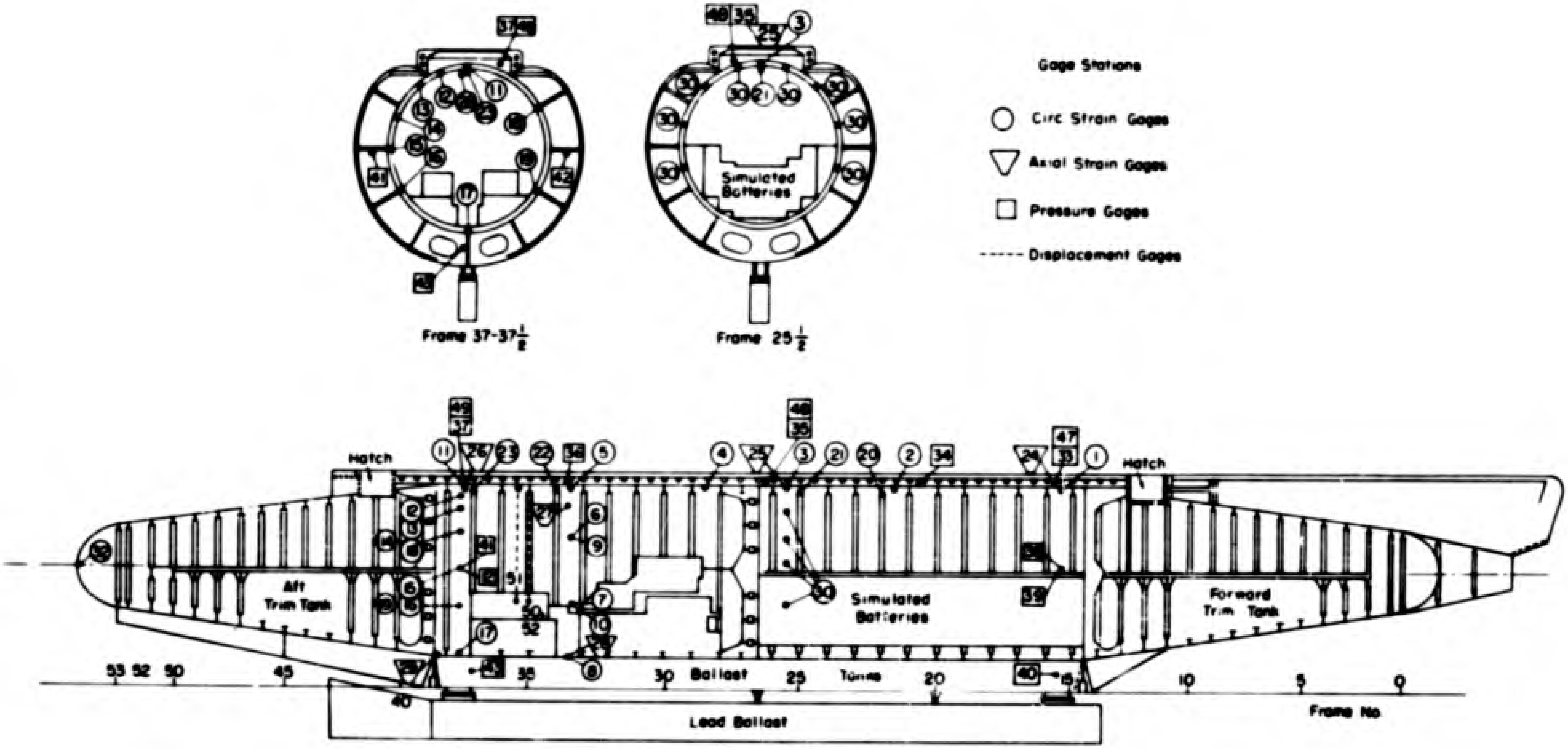

Fig. 3.1—Sections of a SQUAW, showing gage locations.

3.2 YIELD STRENGTH OF PLATING

The material used in the fabrication of the shell of the pressure hull of the SQUAW was 1-in. HTS plating. This steel was rolled by the Lukens Steel Company from special heats. Sample coupons taken from the top and bottom of each plate used were tested at the Materials Laboratory, New York Naval Shipyard. Based on the results of these static strength tests, plates were selected for the parallel-middle body of the pressure hull. A variation was found between the static yield points at the top and bottom of the plates that were used, and the plates were matched accordingly. The bottoms of plates or weaker ends were butted together on the lower longitudinal seam, and the stronger or top edges were butted together at the upper seam near the crown. This was done in an effort to strengthen the crown and compensate for the added strength given to the remainder of the hull by the outer tanks and keel structure.

After cold rolling of the body plates, coupons from each plate were tested at the Materials Laboratory, New York Naval Shipyard, for static yield strength. Specimens of the rolled plate were also tested at the California Institute of Technology and at the University of Illinois to determine the delayed-yield characteristics. Finally, specimens of the prime plate, before cold forming, were tested at the National Bureau of Standards to determine their delayed-yield characteristics.

The results of all these tests are shown in Fig. 3.2, which is a plot of the yield stress vs the delay time for yielding. Figure 3.2 also shows the values for the static yield stress as obtained by the various laboratories. It appears that the rolled plate shows a small, but real, delayed-yield effect with the yield stress depending on the delay time. However, the variation in dynamic yield strengths measured by any one laboratory is small compared with the large variation in static yield strengths measured by the different laboratories. The measured values of the static yield strength range from 52,000 to 70,000 psi. It is not clear to what extent these large variations in the results of the several laboratories are real or are due to different techniques.

3.3 INITIAL LOCKED-IN STRESS DISTRIBUTION

It is well known that the processes of fabrication may generate stress distributions which become locked into the structure and which may subsequently alter its load-bearing capacity. The initial stresses which are due to the rolling process were calculated on the assumption that the steel has a constant modulus until the stress (tension or compression) reaches the yield stress, after which the tangent modulus abruptly becomes zero.

Then the process of rolling may be thought of as taking place in two parts. First a bending moment is applied which bends the plate with some plastic action but without warping the section, i.e., the strain varies uniformly in proportion to the distance to the midsection. The stress distribution due to this moment is shown by the dashed line in Fig. 3.3. Note that the stresses are equal to the yield stress except in a narrow band at the center thickness. Second, the bending moment is allowed to relax to zero, with the plate behaving elastically but without warping the section. The bending moment and resultant of the final stress distribution both vanish, but stresses remain locked in as shown in Fig. 3.3. At the inner face of the plate there remains a tensile stress of 26,900 psi, and at 0.39 in. inside there is a residual compressive stress of 37,600 psi. On the outer face of the plate the corresponding stresses are of opposite sign. These values were calculated assuming a yield stress of 56,000 psi; the method is standard, and the equations are given in reference 2.

3.4 STATIC COLLAPSE PRESSURE OF SQUAW

The most significant single parameter which characterizes the structure and strength of the SQUAW is probably the static collapse pressure. It would be highly desirable to measure this by direct experiment on one of the SQUAW targets. However, this has not yet been done, and it is necessary to calculate the collapse pressure on the basis of past experience and theory.

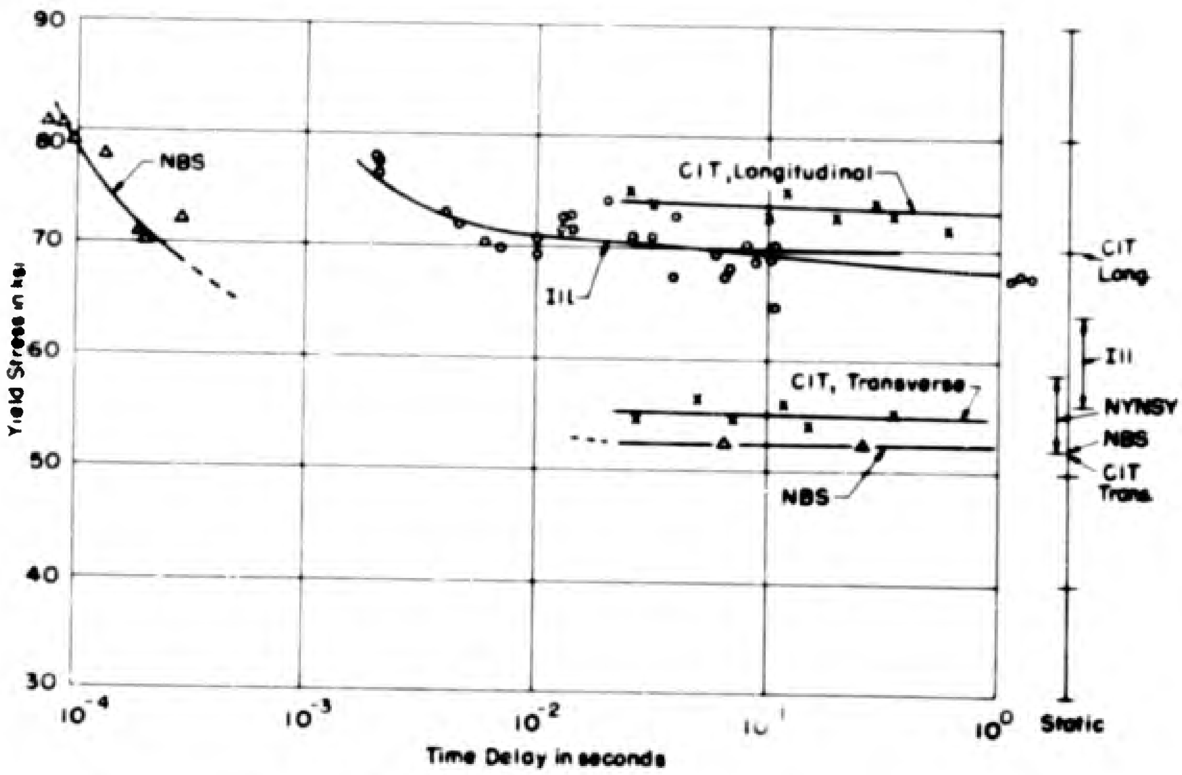

Fig. 3.2—Yield-strength and delayed-yield characteristics of hull plating.

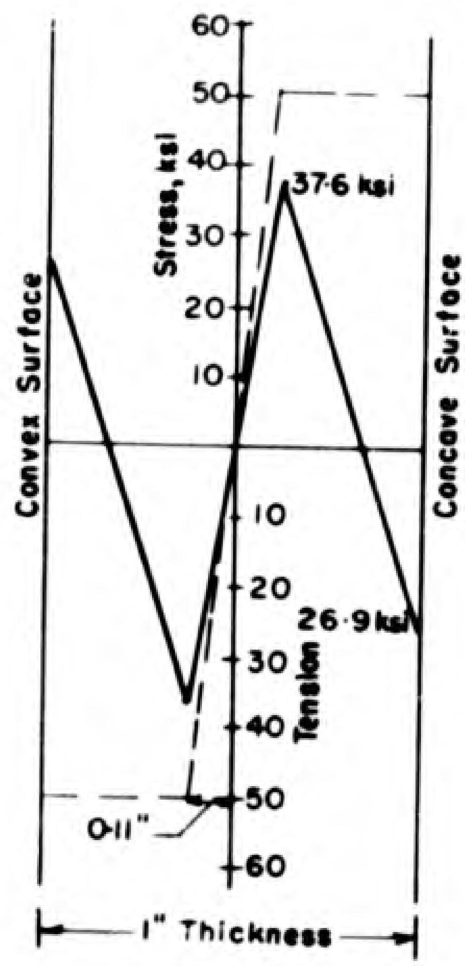

Fig. 3.3—Stresses due to cold rolling.

The static collapse pressure is some complex function of the structural design of the hull, the amount of initial out-of-roundness of the frames and shell, and the modulus of the steel as it changes with the stress. Collapse presumably occurs when the shape of the shell or frames becomes unstable and inelastic buckling ensues. If the yield strength of the steel were so high that elastic instability occurred before the yield stress was reached in the structure, then the collapse pressure would be essentially independent of the yield strength.

However, in the SQUAW, as in all practical submarines, the yield point is reached long before any "elastic" collapse can occur. When yielding begins at some point in the structure, the stress distribution is modified slightly, the deformation pattern may change, and, most important, the local modulus decreases abruptly. These changes make it possible for plastic instability to occur. There is as yet no rigorous or adequate analysis that shows how the instability pressure is modified by the decrease in modulus. Experience in full-scale tests, and in tests of scaled models, shows that the collapse pressure is only slightly higher than the pressure at which plastic yielding first begins in some part of the structure, according to nominal theory. In practice, the collapse pressure is about equal to the pressure at which the yield point is reached in the shell midway between the frames.

Accordingly, we shall calculate the pressure for yield in the frames and in the shell and shall assume that the collapse pressure is related to these yield pressures in the same manner as in a structure of similar design whose yield pressures and collapse pressure under static load have been measured.

All the yield pressures have been calculated using a value of 56,000 psi for the yield stress of the HTS steel. The pressure at which the gross average hoop stress (as calculated from the simple hoop-stress formula) reaches the yield point is 644 psi. The pressure at which the circumferential stress, averaged around the circumference of the shell, on the outside of the shell midway between the frames reaches the yield point is 655 psi. This was calculated, according to present design procedure, from the von Sanden and Gunther formula 92a.[3] At a pressure of 793 psi, the yield point is reached by the octahedral shear stress, averaged around the circumference in the midplane of the shell plating midway between the frames.

These calculations ignore the initial locked-in stresses. It is important to note that these initial stresses do not change the value for the critical pressure at which all points throughout the thickness reach the yield stress. For example, if we are considering the geometry applicable to the simple hoop-stress formula, this yield pressure must equal $(2t/D)\sigma_y$, where σ_y is the yield stress of the material and the circumferential stress is equal to the yield stress uniformly across the thickness, independent of any initial locked-in stress (t/D is the ratio of thickness to diameter). The estimates also apply only to stresses averaged about the circumference because no allowance has been made for the initial out-of-roundness of the shell. The initial eccentricities induce local bending stresses that average to zero around the circumference. However, at some points the eccentricities cause the stress to reach the yield stress sooner than at the average point. This effect for the shell can be estimated by the theories of Bodner and Berks[4] or Galletly and Bart.[5] The effect of the initial eccentricities of the frames can be estimated by the theory of Kendrick.[6] Those theories are difficult to apply rigorously. In practice, the usual methods of application tend to underestimate the collapse pressure.

It is possible to include many refinements in the calculations for yield pressures, e.g., to make allowances for different degrees of fixity and for different methods of computing the initial eccentricities of shell and frame. However, experience has not demonstrated that the experimentally measured collapse pressures correlate any better with the more refined yield pressures than with those estimated from grosser formulas such as hoop stress or von Sanden and Gunther formulas. There is some limited experience that for submarines with internal frames like the SQUAW, and with only moderate initial eccentricities, the collapse pressure tends to be about the same as the yield pressure based on the von Sanden and Gunther formula 92a.

The most direct indication of the static collapse pressure of the SQUAW should be the static collapse measurements made on two models of the Papoose. They failed in a general instability mode at 545 and 555 psi.[7] The general instability type of failure, rather than a failure of the yield type, was probably due to the initial out-of-roundness. Since, however, the initial eccentricities of the SQUAW were somewhat less than those of the Papoose, there is reasonable doubt as to whether the SQUAW would likewise collapse in a general-instability mode and at as low a pressure.

Another good indication of the static collapse pressure of the SQUAW should be the three collapse tests made on full-scale models of the SS563 hull. The models failed by yield at 640, 670, and "more than" 680 psi. However, the SS563 has external frames, and experience indicates that the collapse pressure for internally framed hulls as in the SQUAW is about 10 to 15 per cent smaller than if the frames were outside. On the other hand, the measured yield strengths of the plating in the SS563 models were 10 to 15 per cent smaller than the 56,000 psi assumed in the calculations for the SQUAW. The two effects tend to cancel, and we should thus expect the SQUAW to fail, by yield, at about the same pressure as measured on the SS563 models. No analysis has been made of the initial out-of-roundness of the SS563 models, but there is no reason to expect that these were any less than in the SQUAW.

We shall assume, for the purposes of the subsequent dynamic analysis, that the static collapse pressure of the SQUAW is 655 psi, as given by the von Sanden and Gunther formula 92a for a yield type failure. We recognize that this value is at least as ambiguous as the experimentally measured range in the yield strength of the steel and also that in fact the mode of failure may possibly be of the general-instability type and at a lower pressure.

REFERENCES

1. W. J. Ross, Design and Construction of Wigwam Targets, Operation Wigwam Report WT-1031, May 1955.
2. S. Kendrick, Analysis of Results of Static Pressure Tests of Chatham Submarine Models, NCRE Report R.218, March 1955.
3. C. Trilling, The Influence of Stiffening Rings on the Strength of Thin Cylindrical Shells Under External Pressure, Experimental Model Basin Report 396, February 1935.
4. S. R. Bodner and W. Berks, The Effects of Imperfections on the Stresses in a Circular Shell Under Hydrostatic Pressure, PIBAL Report 210, Polytechnic Institute of Brooklyn, December 1952.
5. G. D. Galletly and R. Bart, Effects of Boundary Conditions and Initial Out-of-roundness on the Strength of Thin-walled Cylinders Subject to External Hydrostatic Pressure, DTMB Report 1066, in preparation.
6. S. Kendrick, The Deformation Under External Pressure of Nearly Circular Shells with Evenly Spaced, Equal Strength, Nearly Circular Ring Frames, NCRE Report R.259, October 1953.
7. A. H. Keil et al., Project Papoose, UERD Report 18-54, May 1955.

CHAPTER 4

INSTRUMENTATION

4.1 GENERAL FEATURES

Project 3.1 consisted of measurements of the explosive loading on the SQUAWs and of the response of the SQUAW hulls to the loading. The three targets, SQUAWs 12, 13, and 29, were controlled, and the instrumentation was operated from the three barges, YFNB's 12, 13, and 29. The external pressures acting on the hulls were measured with diaphragm and piezoelectric pressure gages. The deformations of the hull plating and stiffeners were measured with strain gages and displacement gages. The signals from the gages were transmitted by electrical cables to amplifiers and recording instruments located in a truck trailer on each YFNB.

The general features of the instruments are shown in the block diagram in Fig. 4.1. There were two types of systems for amplifying and recording the gage signals: (1) multichannel cathode-ray oscillographs, with direct-coupled amplifiers, used with the piezoelectric pressure gages and about half of the strain gages; (2) carrier amplifiers and galvanometer oscillographs, used with the diaphragm pressure gages and the remaining half of the strain gages. The displacement-gage signals were recorded directly by the galvanometer oscillographs, without amplification. All channels were calibrated automatically both immediately before and after the test.

Operation of the calibration, amplifying, and recording instruments was controlled by a sequence timer, which was triggered by the radio timing signals. Power for the instruments was supplied by a battery-driven motor-generator set, and the sequence-timer motor was powered by a storage battery.

The three SQUAWs were instrumented identically. In each SQUAW there were 50 gage stations. Only 43 recording channels were provided in each trailer because it had been anticipated that some of the gages or circuits would fail prior to the test. As far as could be determined, none of the gages themselves failed at any time before the test, but there were numerous systematic failures in the external cable bundles that connected the SQUAWs with the YFNB's. These failures prevented the obtaining of complete sets of corresponding data from the three SQUAWs. Only on the YFNB-29 was it possible to use all the recording channels. On the YFNB-12 and the YFNB-13 the number of channels available at the time of the test was limited by the number of intact channels in the external cable bundle.

The gage stations that were recorded are described in Table 4.1, and the locations are shown in Fig. 3.1. On SQUAW-29 the remaining stations were in operating condition; however, on SQUAWs 12 and 13 the remaining gage stations were all inoperative because of the breaks in the external cable.

The gages were placed at locations where the model tests had shown that early damage could be expected or at locations involving simpler structures for which the response might later be subjected to theoretical analysis. It was expected that major damage would occur

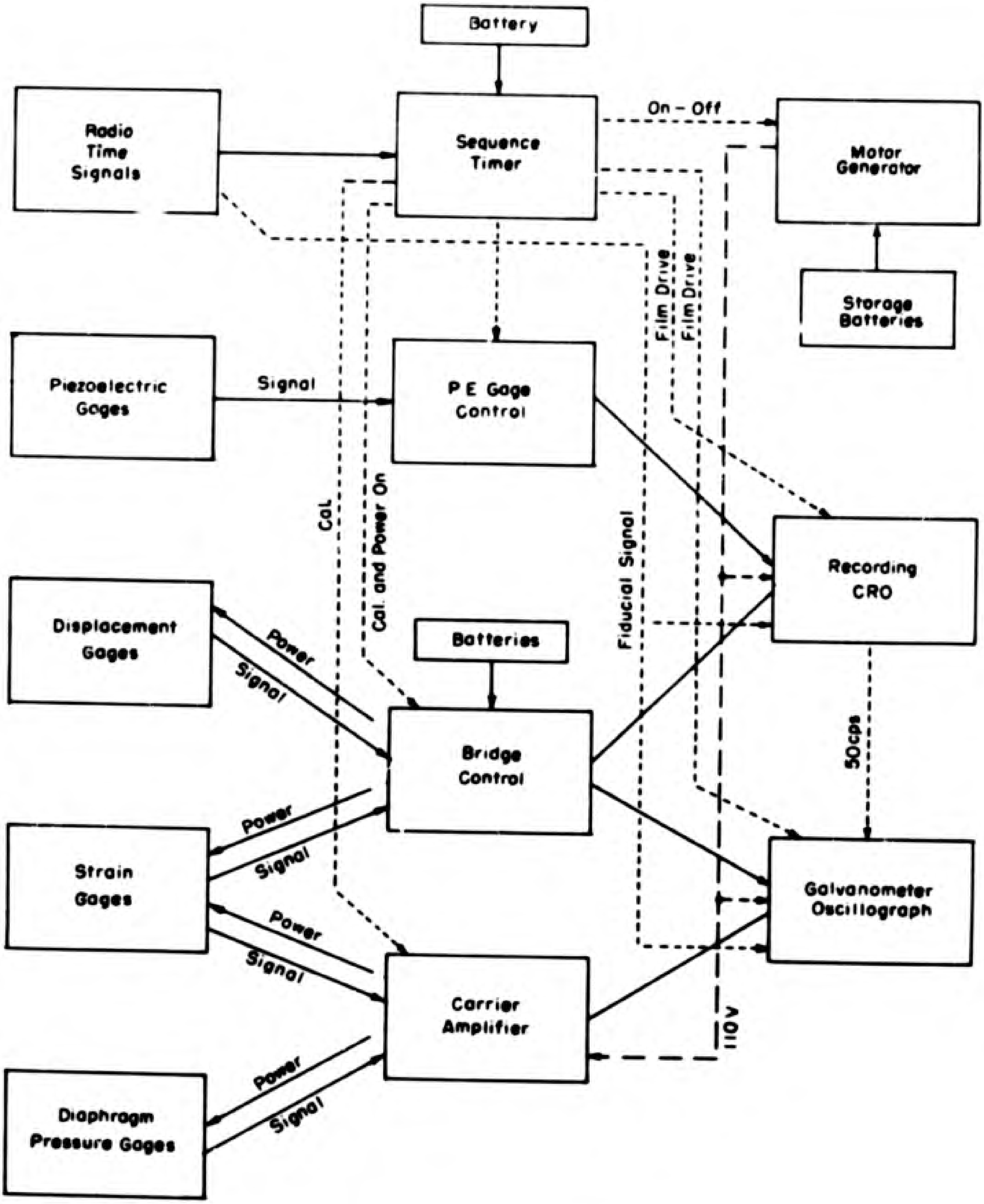

Fig. 4.1—Block diagram of instrumentation.

Table 4.1 —DESCRIPTION OF GAGE STATIONS

No.	Description	Position: Frame	Position: Angle deg	Recorded: SQUAW 12	Recorded: SQUAW 13	Recorded: SQUAW 29
01	Circumferential strain on inside hull plating	15 1/2	0	RC	RC	RC
02	Circumferential strain on inside hull plating	21 1/2	0	RO	RO	RO
03	Circumferential strain on inside hull plating	25 1/2	0	RC	RO	RO
04	Circumferential strain on inside hull plating	28 1/2	0	P	RC	RC
05	Circumferential strain on inside hull plating	33 1/2	0	RC	RC	RC
06	Circumferential strain on inside hull plating	33 1/2	60S	RC	RO	RO
07	Circumferential strain on inside hull plating	33 1/2	120S	RO	RO	RO
08	Circumferential strain on inside hull plating	33 1/2	180	RC	RC	RC
09	Circumferential strain on inside hull plating	33 1/2	60P	RC	RC	RC
10	Circumferential strain on inside hull plating	33 1/2	120P	P	P	RO
11	Circumferential strain on inside hull plating	37 1/2	0	P	RO	RO
12	Circumferential strain on inside hull plating	37 1/2	16P	RC	P	RO
13	Circumferential strain on inside hull plating	37 1/2	32P	P	P	RC
14	Circumferential strain on inside hull plating	37 1/2	60P	P	RO	RO
15	Circumferential strain on inside hull plating	37 1/2	90P	P	P	RO
16	Circumferential strain on inside hull plating	37 1/2	120P	P	RO	RO
17	Circumferential strain on inside hull plating	37 1/2	180	P	P	RC
18	Circumferential strain on inside hull plating	37 1/2	60S	P	P	RO
19	Circumferential strain on inside hull plating	37 1/2	120S	P	P	RO
20	Circumferential strain on flange of hull stiffener	22	0	RO	RO	RO
21	Circumferential strain on flange of hull stiffener	25	0	RO	RO	RO
22	Circumferential strain on flange of hull stiffener	34	0	P	P	RO
23	Circumferential strain on flange of hull stiffener	37	0	P	F	RO
24	Axial strain on hull plating	15 1/2	0	RC	RC	RC
25	Axial strain on hull plating	25 1/2	0	P	RO	RO
26	Axial strain on hull plating	37 1/2	2P	RC	RC	RC
27	Axial strain on hull plating	33 1/2	32S	P	RO	RO
28	Axial strain on hull plating	33 1/2	180	P	RC	RC
29	Axial strain on hull plating	38 1/4	180	RC	RC	RC
30	Average circumferential strain on inside hull plating; 8 active gages at ±15°, ±45°, ±75°, ±105°	25 1/2		RO	RO	RO
32	Strain on inside plating of hemispherical stern; 2 active gages at right angles			RC	RC	RC
33	Diaphragm pressure gage outside hull under walk at crown	15 1/2	0	P	P	N
34	Diaphragm pressure gage outside hull under walk at crown	20 1/2	0	P	P	N
35	Diaphragm pressure gage outside hull under walk at crown	26 1/2	0	P	P	N
36	Diaphragm pressure gage outside hull under walk at crown	33 1/2	0	P	RO	N
37	Diaphragm pressure gage outside hull under walk at crown	37 1/2	0	P	P	N
38	Diaphragm pressure gage in ballast tanks	15	90P	P	P	N
39	Diaphragm pressure gage in ballast tanks	15	90P	P	P	RO
40	Diaphragm pressure gage in ballast tanks	15	180S	P	P	RO
41	Diaphragm pressure gage in ballast tanks	37	90P	P	RO	RO
42	Diaphragm pressure gage in ballast tanks	37	90S	P	RO	N
43	Diaphragm pressure gage in ballast tanks	37	180P	RO	RO	RO
46	Dummy bridge of 4 strain gages	45		P	RC	RC
47	Piezoelectric pressure gage outside hull under walk	15 1/2	0	P	RC	RC
48*	Piezoelectric pressure gage outside hull under walk	26 1/2	0	P	P	RC*
49	Piezoelectric pressure gage outside hull under walk	37 1/2	0	P	RC	RC
50	Vertical displacement between hull stiffener and stdb motor block	35	0	P	P	RO
51	Vertical displacement between hull plating and stdb motor block	35 1/2	0	RO	RO	RO
52	Horizontal displacement between hull stiffener and stdb motor block	35	90	RO	RO	RO

NOTES:

RC - means gage recorded with CRO.
RO - means gage recorded with galvanometer oscillograph.
P - means station failed probably because of prior cable break.
N - means that gage was in good condition but not used.

All angles are measured relative to the center of the crown.
* Station 48 on SQUAW 29 was changed as described in text.

near the after end of the engine compartment. Therefore a concentration of nine strain gages was placed at frame $37\frac{1}{2}$ to measure circumferential strain at various positions on the hull plating at this single section. Another set of six gages was placed around the hull at frame $33\frac{1}{2}$, also to measure circumferential strain, because the hull at this section was not complicated by the attachment of engine or machinery mounts. Individual strain gages were installed at four other positions along the crown plating to obtain a sampling of the circumferential strain throughout the rest of the SQUAW. A set of eight gages was installed in a hoop on the plating at frame $25\frac{1}{2}$ and wired into a single recording channel. These gages were distributed over the upper 210 deg of the hull, and the circuit used for joining them was such that the signal would represent the average strain over the eight gage positions.

Four gages were installed to measure circumferential strain on the hull stiffeners. They were distributed along the crown of the SQUAW.

Six strain gages were installed to measure axial (longitudinal) strains. Three of these gages were distributed on the plating along the crown to obtain a sampling throughout the SQUAW. One was placed on the keel at frame $38\frac{1}{4}$, where maximum damage was expected. Another was placed on the keel at frame $33\frac{1}{2}$ and also one 32 deg down from the crown at frame $33\frac{1}{2}$. This last gage was at the junction of the outer shell with the pressure hull. The keel gages were expected to show axial strains that were relatively unaffected by the concurrent hoop strains.

One channel was devoted to measuring strain at the hemispherical nose at the stern. It was expected that the comparatively uncomplicated structure there would make an effective pressure gage, as well as indicate the time of arrival of the shock wave at the SQUAW.

There were three displacement gages, two to measure displacement of the hull stiffener at frame 35 and one to measure displacement of the hull plating at frame $35\frac{1}{2}$. One of the stiffener gages and the plating gage measured vertical displacements of the crown. The other stiffener gage measured horizontal displacement of one side of the SQUAW. All displacements were measured with respect to the generator blocks.

Diaphragm pressure gages were distributed along the SQUAW, five on the crown under the external walk and six within the outer shell at various positions on the sides and keel. Three piezoelectric pressure gages were spaced along the crown, under the walk, and adjacent to the diaphragm gages.

Each SQUAW was equipped with a dummy gage bridge to serve as a control on the operation of cable, amplifiers, and recorders. The dummy bridge was mounted on a block similar to those used for mounting the passive gages in the measuring channels. It was located at the terminal board in the stern compartment, and it was wired, operated, and recorded in exactly the same manner as the strain-gage bridges.

4.2 STRAIN GAGES

The strain gages used were all SR-4 type A-9; this type has a 6-in. base length and a 300-ohm resistance. A long-base gage was considered desirable since smaller gages would give signals indicating only very localized strain conditions. The A-9 gages were the longest strain gages readily available.

The strain gages were mounted in accordance with the general instructions of the manufacturer, i.e., the structure was ground smooth, abraded with fine sandpaper, and cleaned with acetone, after which the gages were attached with Duco cement and allowed to air-dry for 48 hr or more. The felt coverings supplied with the gages were removed before installation of the gages. Waterproofing was accomplished by covering the gages and the surrounding areas with Scotch Electrical Tape No. 20, cut in pieces 3 by 10 in. Waxed paper was placed between the plastic tape and the gage to prevent any possible interaction between the Duco cement and the adhesive on the tape. (Subsequent tests showed that the waxed paper was an unnecessary precaution.) A small amount of a Bostik cement (a rubber-base cement) was used to seal the joint where the gage lead wires were brought out from under the tape. Figure 4.2 shows two waterproofed strain gages on the crown at frame $25\frac{1}{2}$, measuring strains in the circumferential and axial directions.

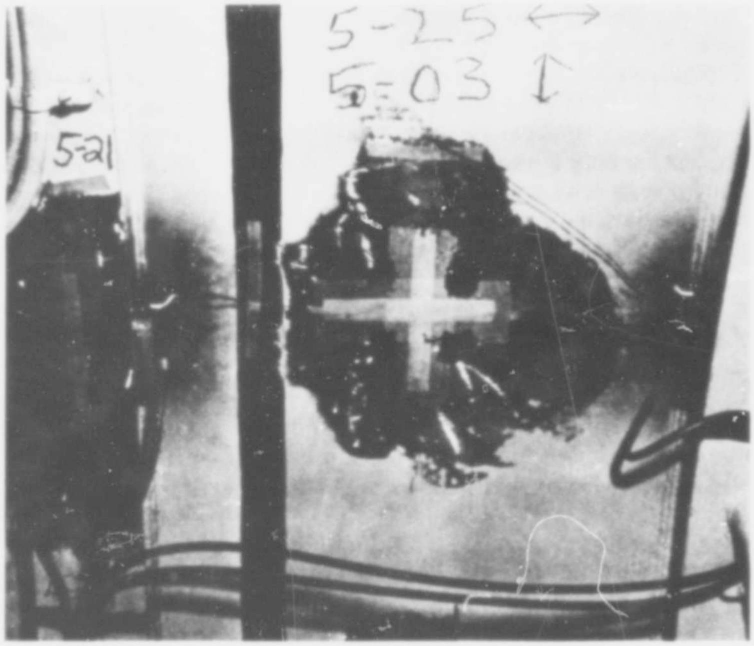

Fig. 4.2—Strain gages on the hull. Station 21 is on the inner flange of frame 25. Stations 3 and 25 are in circumferential and axial directions on the plating at frame $25\frac{1}{2}$. There are two dummy gage blocks inside the flanges of the frames.

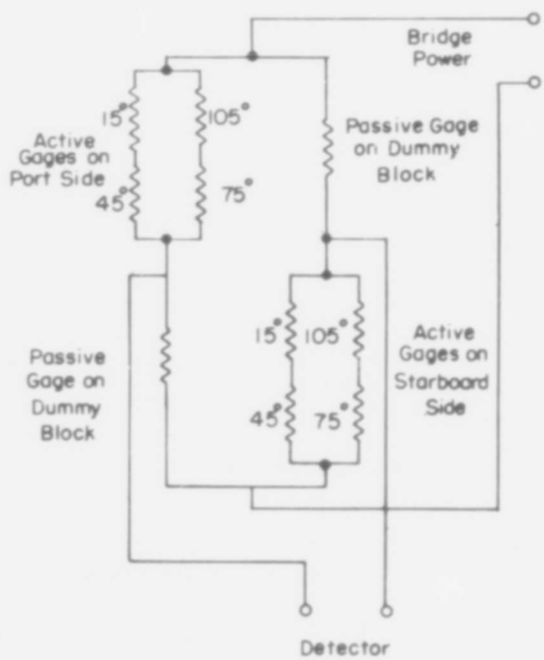

Fig. 4.3—Circuit for the gages at station 30.

This method of waterproofing was briefly tested in the laboratory. It was found that a gage so protected maintained a resistance to ground of more than 500 megohms after being immersed in water for several days.

At several gage stations it was necessary to install one gage on top of another, the two gages being at right angles to each other; see Fig. 4.2. It was assumed that the effect on the top gage of the extra layer of paper between it and the structure was negligible because the extra layer extended for only a small fraction of the gage length (about 7 per cent), and imperfect sticking of a gage near its center should have little effect on the signal.

All the strain gages were wired into four-arm bridges at the gage station. Most of the bridges contained one active gage and three passive gages, wired as a simple Wheatstone bridge. There were two exceptions in each SQUAW. Station 30 consisted of eight active gages and two dummy gages. Figure 4.3 shows the circuit for this station. It is evident from the circuit that the signal from the bridge always was proportional to the average strain over the eight gages.

Station 32 consisted of two active gages and two dummy gages. The two active gages were mounted at right angles to each other (not crossing, however) near the center of the stern hemisphere. The four gages were wired as a simple Wheatstone bridge, with the two active gages in opposite arms of the bridge. The signal in this case also represented the average strain over the active gages.

All the dummy gages were mounted on 1- by 3- by 3-in. steel blocks near the active gages, generally within 1 ft of the gage site; see Fig. 4.2. SR-4 type A-2 gages were used for dummies. The active and dummy gages were wired to form complete bridges at terminal strips attached to the steel blocks. Thus the only long leads were in the power and detector circuits and not in the bridge arms themselves. The steel blocks were resiliently mounted on studs welded to the webs of the hull stiffeners. It is believed that there was negligible probability of any signals originating from the dummy-gage block.

There is very little information available on the reliability of strai[illegible]es at high compressions and at high strain rates. At moderate compressions, up to a[illegible] per cent strains, the manufacturer's gage factor is presumably good to at least [illegible]t.[1] At the higher compressive strains measured in this test, there are no reliable [illegible]n the accuracy of the gage. However, the errors encountered in measuring large com[illegible]sive strains would tend to decrease the signal. Therefore the apparent strains measured would probably indicate lower limits on the true values.

The strain-gage circuits were calibrated by shunting a large-value precision resistor across one arm. The mechanisms for calibration and the calibration resistors were located, by necessity, at the amplifiers in the instrument trailers. An appreciable error would be introduced into the calibration if a correction were not made for the effect of the long leads from the gages to the amplifiers and calibration circuits.

It is convenient to express the effect of this calibration in terms of a bridge factor, which is a measure of the sensitivity of the bridge, for then the equations will be applicable to the other transducer bridge circuits that were used. For a strain-gage bridge, the bridge factor F is defined as the open-circuit voltage output of the bridge per unit strain and per unit voltage applied to the bridge. For a strain-gage bridge with one active strain gage

$$F = \frac{\text{gage factor}}{4} = 0.522 \text{ per unit strain}$$

since the strain gages used had a gage factor of 2.09.

Figure A.1 shows the calibration circuit with calibration resistor R_c, gage resistance R, and lead resistances R_1 through R_4. An analysis of the circuit equations (see Appendix A) shows that the signal caused by closing the calibration switch is the same as a signal caused by a strain

$$\epsilon_c = \frac{R}{4R_c F}\left(\frac{R + 2R_1}{R}\right)^2 \qquad (4.1)$$

This equation is based on the assumption that $R_1 = R_2$. It shows the effect of the line resistance explicitly by a factor which has the value unity when the line resistance is negligible. In the tests, R was approximately 300 ohms for all strain gages, and R_1 was approximately 5 ohms, and therefore the correction amounted to about 7 per cent of the signal.

4.3 DISPLACEMENT GAGES

The three displacement gages in each SQUAW were modifications of the retraction type displacement gage.[2] Figure 4.4 shows an installed displacement gage. One end of a 20-in. length of 29-gage nichrome wire was attached by a string to the point of the structure where the displacement was to be measured. The wire passed through a mercury contact which was fixed rigidly to the heavy generator blocks. The other end of the wire was held taut by rubber bands stretching to the opposite side of the SQUAW. A displacement of the hull relative to the generator block allowed the rubber bands to pull the wire through the mercury contact. The motion was measured as a resistance change by a resistance bridge circuit which was mounted on the same fixture that held the mercury contact. The circuit diagram is shown in Fig. B.1.

We can define a "bridge factor" similar to that defined for the strain-gage bridges. The change of resistance of either active arm is proportional to the displacement of the hull relative to the generator block. Then the bridge factor F, defined as the voltage output of the bridge per unit displacement per volt input to the bridge, is given by (see Appendix B):

$$F = \frac{\rho}{2R} \quad \text{per unit displacement} \tag{4.2}$$

where ρ is the resistance of the nichrome wire per unit length.

The circuit was calibrated by shunting a resistor R_c across one arm of the bridge. The displacement equivalent to this calibration resistor can be calculated, as before, to give:

$$x_c = \frac{R}{4R_cF}\left(\frac{R + 2R_1}{R}\right)^2 \tag{4.3}$$

This equation for the calibration-equivalent displacement corresponds directly to those given previously for the strain-gage bridges.

The unbalance signal of the displacement-gage bridges, due to the displacement signals, was large enough that it could be recorded directly by sensitive galvanometers without amplification. The galvanometers used, Consolidated Engineering Corporation type 338, had a frequency response that was flat to about 125 cycles/sec. The "least count" of the displacement gages was limited by the width of mercury contacts. It was estimated that the contacts contributed an uncertainty of about 0.1-in. displacement. A nominal bridge voltage of about 2 volts would give more than 0.01 in. of record deflection for a 0.1-in. hull displacement. It is considered that the minimum readable record deflection is about 0.01 in. Actually, voltages considerably higher than 2 volts were available, and thus there was ample reserve of signal on these gages.

The mercury contact initially caused some trouble, because large contact resistances built up during relatively short periods of gage inactivity. This difficulty was decreased by allowing the bridge current to flow through the contact for about 1 min before the calibration and test. It can be shown that a small contact resistance (not more than a few per cent of R_g) has only second-order effects on the records, provided that the contact resistance does not change between calibration and the test. It is also necessary that the calibration shunt not be placed across an arm adjacent to the contact resistance. (It was subsequently discovered that contact-resistance difficulties could be avoided by making both contacts to the mercury pool through nichrome wire instead of using nichrome wire and a stainless steel screw in contact with the mercury as was done in the Wigwam test.)

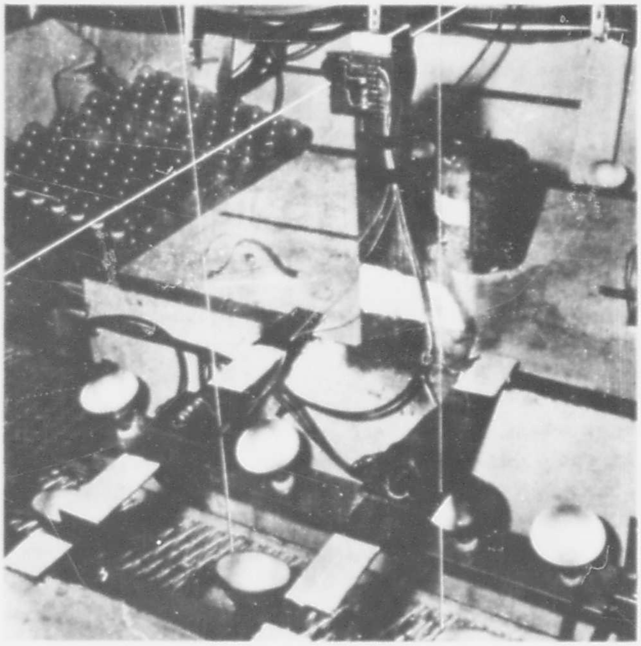

Fig. 4.4—Displacement gages between motor block and hull. The mercury contacts are mounted on the angle irons welded to the motor block. The resistance wire is stretched across the diameter of the hull.

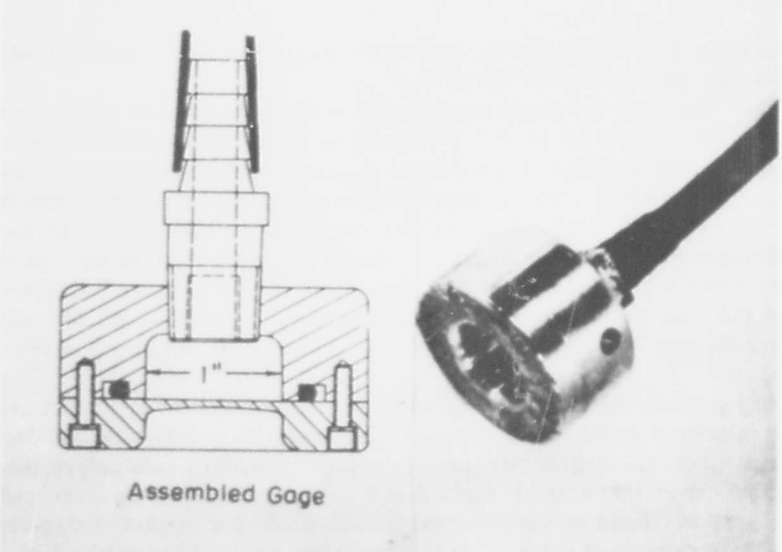

Fig. 4.5—Diaphragm pressure gage.

4.4 DIAPHRAGM PRESSURE GAGES

The diaphragm pressure gages were essentially as reported in reference 3. They will be described only briefly here.

Figure 4.5 shows a sectional drawing and a photograph of a diaphragm gage. The diaphragm is air backed, and it deflects proportionally with the total applied water pressure. A unique feature of the gage is that the diaphragm is thicker at the edges than at the center. This allows the diaphragm to experience much larger strains at the center than could a uniformly thick diaphragm of the same sensitivity without having plastic failure occur at the edges.

The diaphragms and gage bodies were fabricated from stainless steel or from Monel. Since some of the gages were immersed in salt water for three months before the test, corrosion resistance was extremely important.

One active strain gage, SR-4 type A-8, was affixed to the center of the diaphragm back. It was wired into a four-arm bridge within the gage itself. The three passive arms were also A-8 strain gages, mounted on the inside of the heavy gage body. All the strain gages were waterproofed with a thin layer of DI-J 171, a petroleum wax obtained from Astor, Boisselier & Lawrence, Ltd., of London. The four bridge terminals were connected to the leads of MCOS-4 cable. The cable was attached to the gage block by an air-hose type of fitting, which was forced into the cable under the sheath and screwed into the gage. This type of fitting was developed at DTMB for this purpose. It has proved to be much simpler and more reliable than standard stuffing tubes. A plastic resin was forced into the cable end to anchor the leads to the gage body.

Calculations and tests have shown that the acceleration response of these diaphragm gages is very low, a 100-g acceleration being required to give a signal equivalent to 1 psi. The gage is sensitive to temperature, inasmuch as the zero signal level changes. It was found in one gage that the zero shift due to ambient temperature change corresponded to a pressure change of 2 psi/°F. It is believed, however, that the pressure sensitivity of the gages is not appreciably affected by the temperature level. The natural frequency of the diaphragms in water was greater than 10,000 cycles/sec. The oscillations of the diaphragms at their natural frequencies were completely filtered out by the system that was used to amplify and record the signals.

The assembled pressure gages were given almost continuous tests until the time of their installation on the SQUAWs. Every gage was first calibrated hydrostatically in a pressure chamber at DTMB. Then all gages were subjected to at least five underwater explosions ($\frac{1}{2}$ lb of TNT at 10-ft standoff from the gages). This was followed by another hydrostatic calibration. This procedure was followed until a sufficient number of gages had been prepared and accepted. After the gages were shipped to San Diego, they were given a final hydrostatic calibration in a deadweight test chamber. After the Wigwam test, all diaphragm gages that could be checked showed negligible zero shift and less than 2 per cent change of sensitivity.

The diaphragm-gage signals were amplified by carrier amplifiers and recorded by galvanometer oscillographs. The balancing and calibrating circuits were the same as those described for the strain-gage bridges.

Once again it is convenient to define a "bridge factor," F, for the gages, i.e., the voltage output of the bridge for 1 psi pressure with 1 volt applied to the bridge. In this case, the bridge factor is an empirical quantity, obtained from the hydrostatic pressure calibrations. For the gages used in the test the bridge factor has values ranging from 0.44×10^{-6} to 1.12×10^{-6} per pound per square inch.

Any calibration shunt resistor R_c can be expressed simply in terms of the equivalent pressure which would produce the same signal. This equivalent pressure is given by

$$P_c = \frac{R}{4R_cF}\left(\frac{R + 2R_1}{R}\right)^2 \qquad (4.4)$$

The piezoelectric gages were made from tourmaline crystals, supplied by Crystal Research, Inc., Cambridge, Mass. Four sizes were used, with nominal sensitivities as follows:

$\frac{1}{2}$-in.-diameter, 4-ply, KA $\geq 8 \times 10^{-12}$ coulomb/psi
$\frac{1}{2}$-in.-diameter, 8-ply, KA $\geq 16 \times 10^{-12}$ coulomb/psi
$1\frac{1}{8}$-in.-diameter, 4-ply, KA $\geq 40 \times 10^{-12}$ coulomb/psi
$1\frac{1}{8}$-in.-diameter, 8-ply, KA $\geq 80 \times 10^{-12}$ coulomb/psi

All the crystals had been manufactured for use with a coaxial electrical cable. They were mounted on Simplex antimicrophonic coaxial cable in two ways:

1. The $\frac{1}{2}$-in.-diameter gages were mounted directly on the ends of the cables. Each cable shield was formed into two pigtails, which were soldered to the ground tabs of the gages. The center wires of the cables were soldered to the tabs of high sides of the gages.

2. The $1\frac{1}{8}$-in.-diameter gages were mounted on short pieces of heavy steel pipe, which were slotted at one end to receive the ground tabs of the gages and were tapered on the other end to fit under the cable sheath; see Fig. 4.6. The pipes connected the gage to the cable shield. The center wires were continuous through the pipes to the gages.

Several thin layers of Bostik cement No. 2292 (a rubber-base cement) were applied over the gages, metal mountings, and bare shield ends. All cavities were completely filled. The assemblies were then covered with a rubber tape of good quality. At hydrostatic pressures of 500 psi, this technique maintained the watertight integrity of the gages. Leakage resistance across all gages was at least 1000 megohms at all times before the test, although, judging from the rise time of the calibration records at test time, some of the piezoelectric channels on SQUAWs 12 and 13 may have had low resistances for unknown reasons.

There is considerable recent experience to show that the crystal manufacturer's calibration is likely to be in error as much as ±10 per cent when applied to the completed pressure gage. Therefore a series of tests was conducted to determine the KA of the mounted gages. They were placed in a hydrostatic pressure chamber and a 500-psi pressure was applied; then a diaphragm was ruptured, releasing the pressure in about 1 msec. The gages were tested in pairs in this way, each being tested several times and one gage being used throughout as a control. The signals were amplified by an a-c amplifier and recorded by a galvanometer oscillograph. The results are presented in Table 4.2.

The piezoelectric pressure gages were terminated and the amplifiers were calibrated by the circuit shown in Fig. 4.7. The 68-ohm resistor approximately matched the surge impedance of the transmission line. The 2.2-megohm resistor was used to increase the time constant of the input circuit. In the absence of a cathode follower, this method was preferable to using immense terminating capacitors, for practical reasons. Of course, it also attenuated the signal, acting as a voltage divider with the amplifier input resistance. The capacitor C_t terminated the line and attenuated the signal. The rest of the circuit served to apply a known voltage for calibration purposes in series with the terminating capacitor. The 100-ohm resistor largely determined the generator impedance of the calibration voltage source, providing a low impedance for this purpose.

When the calibration voltage is applied, the voltage across the amplifier input rises to a peak in several microseconds and then decays exponentially with the time constant $(C_t + C_2)(R' + R'')$. The values of this time constant were of the order of 1 sec. The peak calibration voltage is (see Appendix C):

$$V_c = R_g I \frac{R''}{R' + R''} \frac{C_t}{C_t + C_2} \tag{4.5}$$

where I is the steady-state current through the meter A.

If a step pressure P is applied to the pressure gage, it generates a peak voltage to the amplifier of

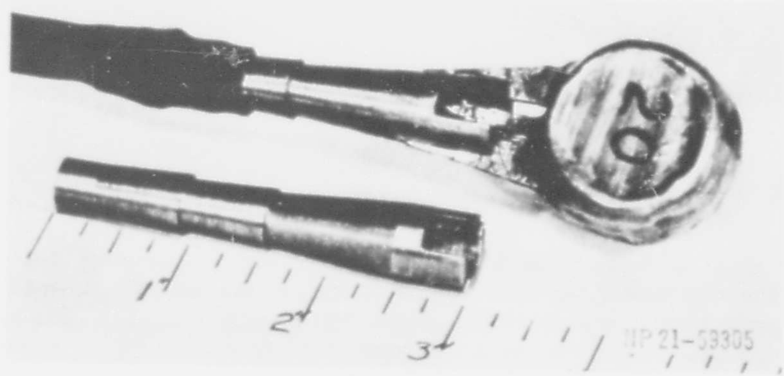

Fig. 4.6 — Piezoelectric-gage assembly.

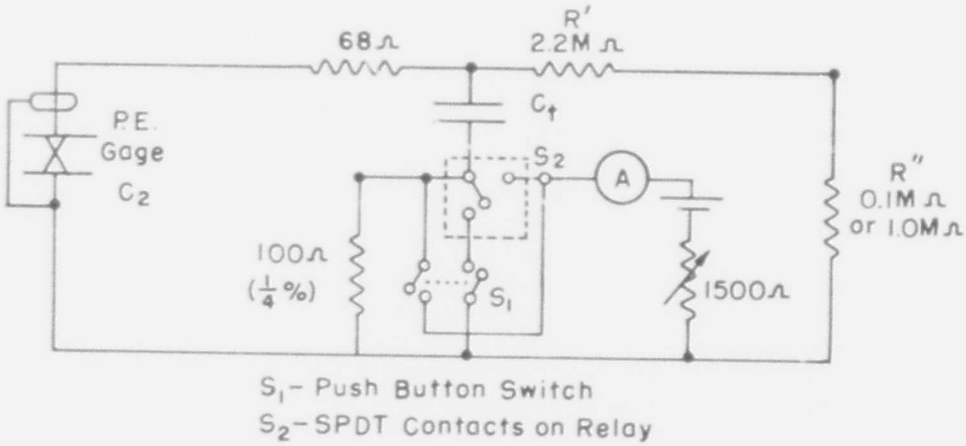

Fig. 4.7 — Calibration and termination circuit for piezoelectric gages.

Table 4.2 — CALIBRATION OF PIEZOELECTRIC GAGES

Gage	Manufacturer's calibration, $\mu\mu$coulombs/psi	DTMB calibration, $\mu\mu$coulombs/psi	No. of tests
7	8.5	8.1	4
12	16.5	17.8	3
13	16.3	17.4	4
16	43.4	40.5	4
17	41.8	41.6	4
19	81.4	82.7	4
20	84.3	78.7	44 (control)
21	84.3	81.6	17
22	84.9	80.3	4

$$V_p = \frac{KAP}{C_t + C_2} \frac{R''}{R' + R''} \tag{4.6}$$

Hence the peak signal due to the calibration current I is equivalent to the peak signal from a pressure P_c:

$$P_c = \frac{R_g I C_t}{KA} \tag{4.7}$$

The decay of the calibration signal indicates directly the time constant of the amplifier input circuit. The rise time of the calibration deflection on the record indicates the upper frequency-response limit of the amplifier system. The amplifier input circuits had time constants of approximately 1 sec. This means that the peak shock-wave signal, within 5 msec after the arrival of the shock wave, should have negligible error due to inadequate low-frequency response. Even at the cutoff time of 40 msec, the relative error should be only 7 per cent.

4.6 CABLES

From each SQUAW to the corresponding YFNB there were three large armored electrical cable bundles that were shared with the other projects of Program III. Two of these were similar, containing 36 individually shielded four-conductor cables. The third large bundle contained 54 shielded pairs. On each SQUAW, this project had the exclusive use of one of the quad bundles and shared the other quad bundle with other projects.

The cables were made by the Simplex Wire and Cable Co. and had characteristics similar to those of the antimicrophonic single- and double-conductor cables made by Simplex and used for underwater explosion measurements for several years. All surfaces within the quads had been given conducting coatings to help eliminate signals which might have originated within the cable itself when pressure was applied to it. The bundles were covered with heavy rubber sheaths that were protected by steel armor. The capacitance between any pair of wires within the quads was about 0.02×10^{-6} farad, and the capacitance between any lead and its shield was about 0.03×10^{-6} farad. The total resistance of each lead was about 5 ohms.

The main cable bundles were terminated at terminal boards in the bow compartments of the SQUAWs and in the instrument trailers aboard the YFNB's. Connections from the SQUAW terminal boards to the strain and displacement gages were made with cables similar to the external cables. The diaphragm pressure gages were connected to the terminal boards in the SQUAWs by a standard Navy cable, MCOS-4. These cables were brought into the pressure hull through double stuffing tubes in the hatches. The lengths of MCOS-4 cable varied up to 75 ft. The piezoelectric pressure gages were connected to the bow and stern terminal boards by Simplex antimicrophonic coaxial cable.

4.7 CARRIER AMPLIFIERS

Each YFNB was equipped with two 12-channel carrier amplifiers. The units were type C-3 amplifiers made by William Miller Instruments, Inc., Pasadena, Calif.

Carrier power at about 3000 cycles/sec is supplied to each channel by an individual feedback power amplifier. The availability of separate carrier power sources for each channel was considered an essential requirement, and this was the principal reason for selecting this particular amplifier for the test. If any channel shorts out, the carrier power to the other channels is not affected. The use of separate power supplies for each channel allows all connections to the bridges to be floating from ground. Also, there are no common connections between the different bridges.

All the channels in each amplifier are normally driven by a common oscillator, which supplies a low-impedance alternating voltage. In order to minimize undesirable interference between the two amplifiers in each trailer, the oscillator voltage output of one unit was used to drive all the channels of both units.

The maximum linear output of the amplifier channel is about 10 ma into a proper load. However, with large signal input, the output increases nonlinearly to as high as 20 ma. Since the galvanometers had a sensitivity of 2.3 ma/in. deflection, the linear output was ample. However, many of the galvanometers used had a sensitivity of 9.1 ma/in. deflection. Thus any deflection from these galvanometers much larger than 1 in. is in the nonlinear range of the amplifier. Therefore all channels were calibrated by shunting a series of resistors across a bridge arm and measuring the corresponding galvanometer deflections. This calibrated the whole amplifier and recording system, and calibration was carried well into the nonlinear region of the channels using the 9.1 ma/in. deflection galvanometers.

The amplifiers have a sequential calibration device in which an appropriate calibration resistor is shunted across each input bridge channel in sequence.

The amplifier turned on automatically when the power line was energized, and it remained on until the motor-generator set was turned off.

4.8 GALVANOMETER OSCILLOGRAPHS

For recording the carrier-amplifier and displacement-gage signals on the YFNB's 12 and 13, a single Consolidated Engineering Corporation (CEC) type 5-119-P4 galvanometer oscillograph was used in each barge. This instrument used a 200-ft length of 12-in.-wide type 1127 paper, running at 50 in./sec. On the YFNB-29 there were two CEC type 5-114-P4 oscillographs, each using a 125-ft length of 7-in.-wide type 1127 paper, running at 28 in./sec. The galvanometers used with the carrier-amplifier channels were CEC types 316 and 320 with a flat frequency response to 1100 and 550 cycles/sec, respectively. The displacement gages operated directly into CEC type 338 galvanometers with a flat frequency range to 125 cycles/sec.

Some difficulty was experienced with the type 114 oscillographs in that the galvanometer bulbs burned out frequently at the voltages used (about 6.0 volts). Therefore these two oscillographs were modified slightly so as to use the higher voltage bulbs that are used in the type 119 oscillographs. The latter bulbs could supply sufficient light intensity without exceeding their nominal voltage ratings. Reliability of the lamps was thus increased considerably.

The oscillograph records were developed in an automatic processor, CEC type 23-109.

4.9 RECORDING CATHODE-RAY OSCILLOGRAPH

Each instrument trailer was equipped with a multichannel cathode-ray recording system, type CR-1, made by William Miller Instruments, Inc., Pasadena, Calif. Each of these units contains 16 signal channels, all recording on 8-in.-wide film or paper. Eastman Linograph 1127 paper was used. The signals appear as traces on the faces of eight dual-gun cathode-ray tubes, whence a unique optical system rearranges them and causes them to appear on the recording paper in much the manner of a galvanometer oscillograph. The optical system reduces the signal axis by a factor of $\frac{1}{3}$ and the time axis by a factor of $\frac{1}{16}$.

The input amplifiers are direct-coupled, chopper-modulator, stabilized units. The maximum sensitivity of the whole system is 5 mv/in. deflection on the tube face. The frequency response of the amplifiers is nominally 0 to 100 kc (±1 per cent). However, at the paper speed used (50 in./sec), the highest frequency that can be resolved is about 5 kc. All amplifiers were operated at or near their maximum gain, where noise was at the limit of acceptability. Because the full frequency response was not necessary, the deflection amplifiers were adjusted so that the response at 20 kc was attenuated about 5 per cent.

On SQUAW-13 the piezoelectric pressure gages did not have sufficient sensitivity to be attenuated to the point where the time constants of the amplifier input were acceptable. Therefore, at considerable sacrifice of noise characteristics, the input grid resistors of these channels were increased from 10^8 to 10^9 ohms. In order to offset somewhat the large increase in noise that accompanied the increased input resistance, these channels were further modified to include a single-stage resistance-capacitance filter between the input amplifier and the deflection amplifier. These filters attenuated the signal about 3 db at 5 kc.

The instrument was turned on automatically when the power line was energized. The filament supply came on immediately, together with the record-drive motor. The plate supplies came on automatically after a time delay that was controlled within the instrument. The record was started automatically by the sequence timer, which actuated the proper drive clutch. The instrument was turned off by removing the power to the motor-generator set.

The records were developed in the developing tank mentioned previously.

4.10 SEQUENCE TIMER

Special sequence timers were designed for this test to perform the following functions:

1. Start motor-generator set (– 15 min).
2. Close relays supplying battery power to d-c – operated bridges (– 1 min).
3. Start paper drives (– 8 sec).
4. Initiate calibration of all gages before and after test (– 6 sec and about + 35 sec).
5. Remove battery power from d-c – operated gages (+ 38 sec).
6. Release drive clutch on cathode-ray recording system (+ 45 sec) and stop galvanometer oscillograph paper drive (+ 55 sec).
7. Stop motor-generator set (+ 60 sec).

The times of operations 5, 6, and 7 were determined largely on the basis of the length of paper available in the various recorders. It was considered desirable to allow all records to run until the paper was exhausted. The recording speeds had been determined previously on the basis of the characteristics of each instrument. The posttest calibrations were placed as near the ends of the records as was feasible.

The timer was triggered by the – 15-min, – 1-min, and – 15-sec Edgerton, Germeshausen & Grier, Inc. (EG&G), signals. Either the – 1-min signal alone or the – 15-min and – 15-sec signals in conjunction were sufficient to operate the whole sequence properly.

The timer consisted of 15 single-pole double-throw microswitches actuated by cams driven by a 12-volt d-c motor. Four of the switches were spares. Power was supplied by a 12-volt storage battery. One cycle of the timer lasted about 90 sec. The cams were 1 in. in diameter, and the design was such that the on-off times could be set with a precision of about 1 per cent of a cycle or 1 sec. The circuit for the sequence timer is shown in Fig. 4.8. Note that the circuit incorporates an auxiliary time-delay relay. This relay was started by the – 1-min EG&G signal and would replace the – 15-sec time signal if that signal should fail.

The piezoelectric pressure gages had to be calibrated by a special system. Here it was necessary to remove a short-circuiting shunt from a resistor in series with the terminating capacitor; see Fig. 4.7. When the shunt was removed, the signal trace deflected suddenly and then returned exponentially to zero. When the switch was released and the resistor was again shorted, the signal trace deflected equally in the opposite direction and then again returned exponentially to zero. The decay had a time constant of over 1 sec, and therefore several seconds would have been necessary for the trace to approach closely enough to zero. This situation was avoided by arranging a circuit that removed the calibration resistor shunt for only a very short time, about 50 msec. The shunt was provided by the normally closed contacts of a 13.2-volt relay. The relay was operated by the discharge of a capacitor previously charged to 45 volts. The size of the capacitor was selected so that the voltage decay would be proper to hold the relay for about 50 msec. Figure 4.9 shows a typical record of three calibrations obtained in this way. After the second step signal, the trace is so close to zero that only a short time need be allowed for the trace to return before the shot.

4.11 BRIDGE CONTROL UNIT

Those gage bridges which were d-c operated were provided with conventional balancing controls, calibration circuits, and power supplies as shown by the circuit in Fig. 4.10.

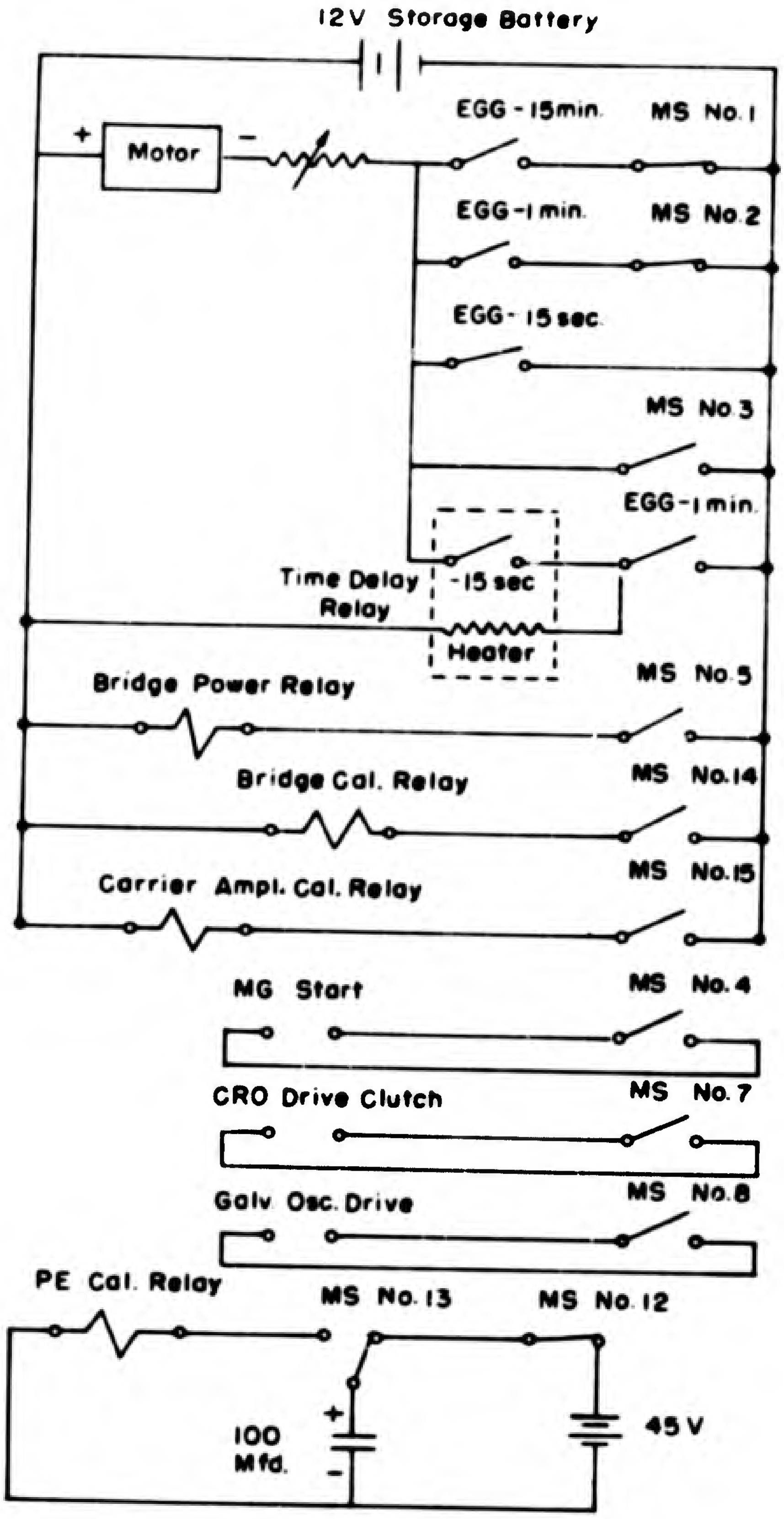

MS	Closes	Opens
1	60s	-15m+5s
2	+60s	-55s
3	-10s	+65s
4	-15m+3s	+60s
5	-57s	+38s
6	-57s	+48s
7	-8s	+45s
8	-8s	+57s
12	-57s	+40s
13	-6s	-3s
	+36s	+42s
14	-6s	-4s
	+35s	+36s
15	-6s	-4s
	+39s	+40s

Fig. 4.8—Circuit for the sequence timer.

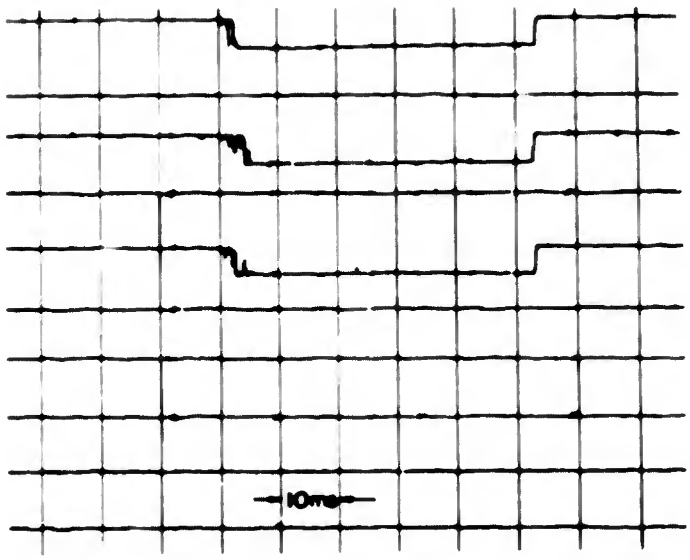

Fig. 4.9—Oscillogram showing calibration of piezoelectric channels.

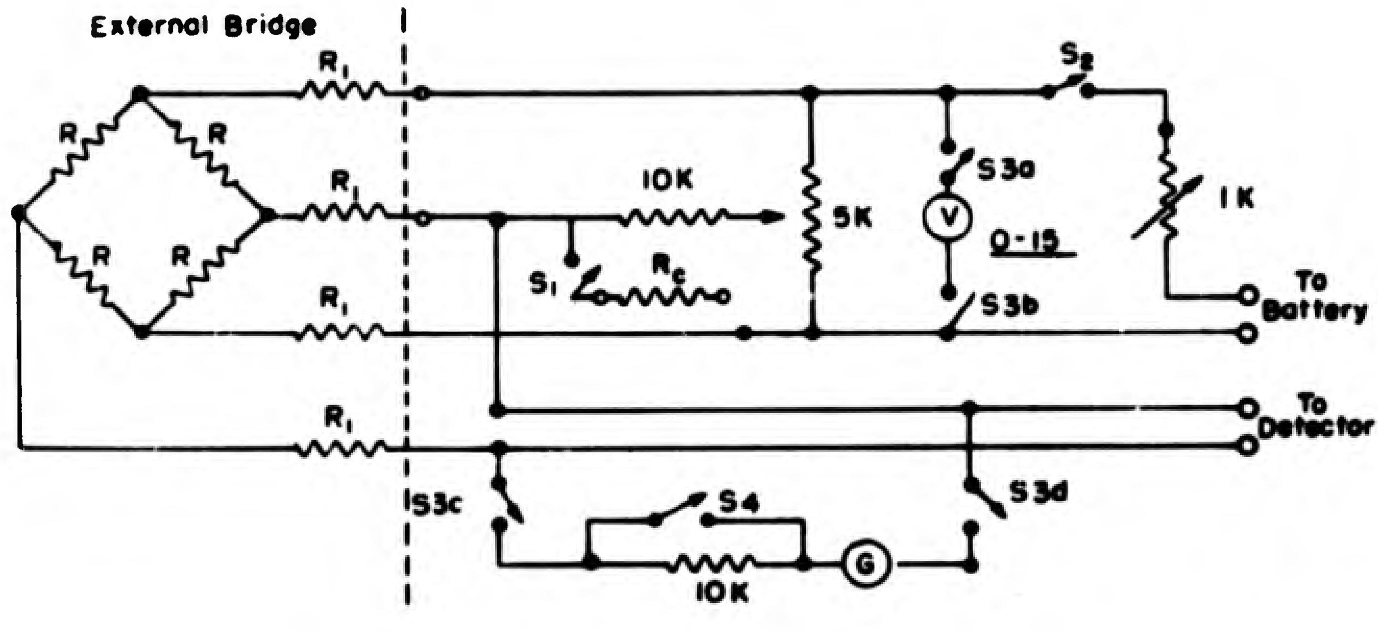

Fig. 4.10—Circuit for the gage-bridge control units.

The switch S2 (Fig. 4.10) actually consisted of two switches in parallel: (1) a manually operated toggle switch and (2) contacts of a relay, operated by the sequence timer. S1 also consisted of two switches in parallel: (1) a manually operated push-button switch, with spring return, and (2) a relay-operated contact. S3 was a nine-position meter-insertion switch. G was a microammeter used to balance the bridge initially and to monitor the amplitude of the calibration signal. The batteries for bridge power consisted of individual dry cells for each channel, located in a box adjacent to the control unit. The actual voltages applied to the bridges varied from 5 to 18 volts.

4.12 POWER SUPPLY

Line power at 115 volts, 60 cycles/sec, for all the instruments in each instrument trailer was supplied by a 10-kva motor-generator set, Navy type CAY-211182, ordinarily used for powering radar equipment. They were operated from banks of 21 6-volt storage batteries. The capacity of the batteries was sufficient to drive the motor generator for about $1\frac{1}{2}$ hr under load and with regulation satisfactory for all the instruments.

The motor-generator set was tested with loads varying from 0 to 9.2 kva. The total voltage regulation for this range of loads was about 4 volts. The average load current during the Wigwam test was only about half the maximum tested. The automatic controls for the motor-generator set included a frequency regulator, which used a resonant feedback loop to maintain the frequency between 57 and 63 cycles/sec. This range was satisfactory for the operation of all instruments.

The overspeed safety switch on the generator was shorted out before the test. The fuse in the control circuit was also shorted out. It was considered that continued operation of the motor-generator set was important enough to risk any possible damage which might happen to the equipment. The storage batteries were fused at 400 amp, and the instrument circuits were also properly fused.

The batteries and the motor-generator sets were rigidly attached to the decks of the YFNB's. The control panels, containing the starting relays and the voltage and frequency control circuits, were shock mounted on a nearby bulkhead by C-springs.

4.13 TRAILERS

All the equipment on each YFNB was mounted in a truck trailer, except the motor-generator set, its controls, and the bank of storage batteries. The trailers were modified inside and outside to make them suitable as laboratories.

Each of the trailers was equipped inside with work benches and other facilities to make them self-contained laboratories. Two sets of wiring were provided, one supplying power to the lights, instruments, and miscellaneous equipment from the ship's power, and the other supplying power to the test instruments from the motor-generator set. Each power source had its own entry, switch box, fuses or circuit breakers, wiring conduit, and outlets.

Each trailer had two 1-ton air conditioners, thermostatically controlled, and a dehumidifier. An intake and an outlet were provided for the forced ventilation of the cathode-ray recording system.

The galvanometer oscillographs were bolted directly to the tops of the carrier amplifiers, which were bolted rigidly to the trailer floors. The cathode-ray recording systems were mounted on their own shock absorbers, which had a frequency of about 15 cycles/sec. The sequence timer, bridge control units and batteries, piezoelectric-pressure-gage controls, and the 12-volt storage battery were rigidly mounted in a standard 19-in. chassis rack. The cables from the gages in the SQUAWs were terminated at terminal boards in the trailers, near the instruments. Short jumper cables connected the terminals on the boards to the appropriate instruments.

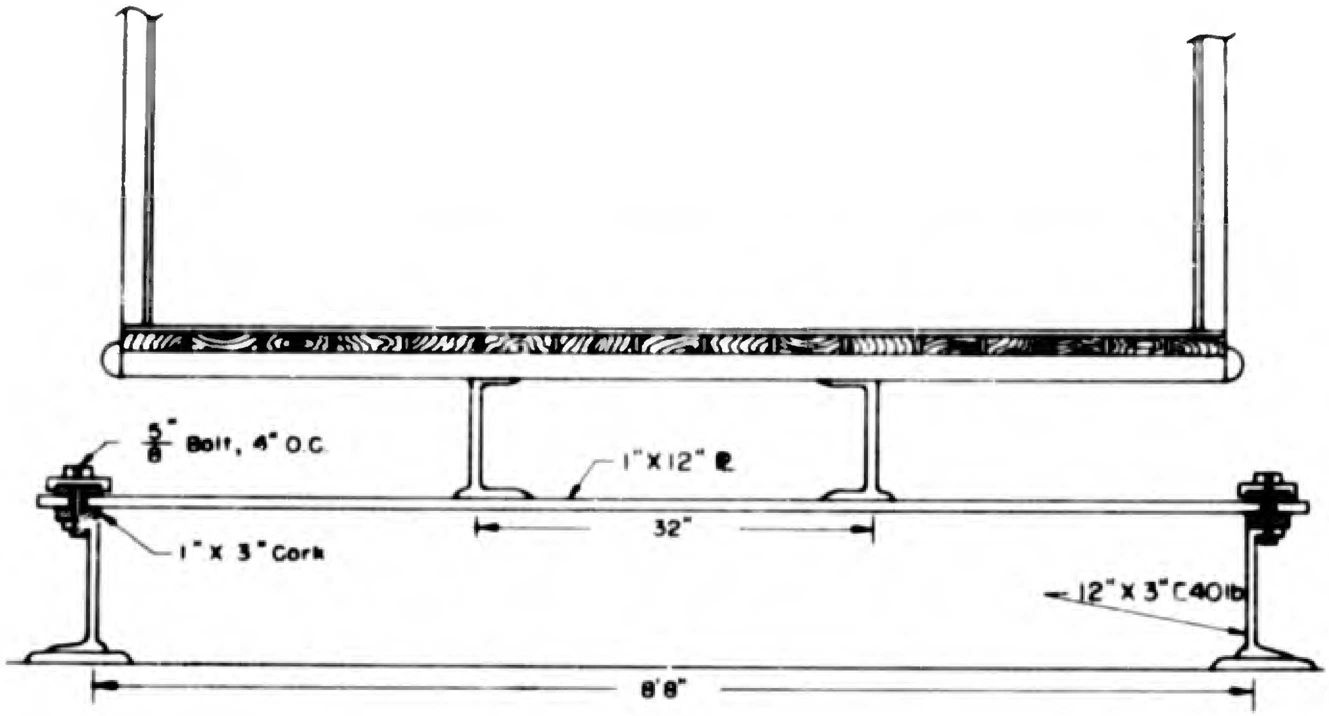

Fig. 4.11—Shock mounting for the trailers.

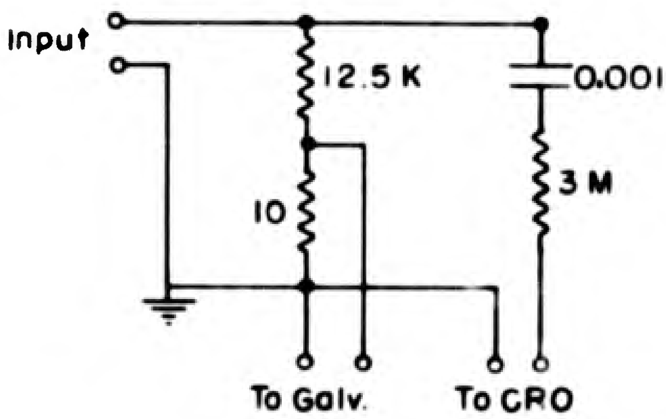

Fig. 4.12—Circuit used for distribution of the fiducial signal.

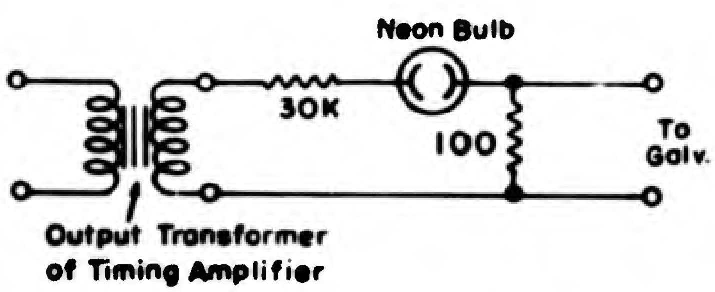

Fig. 4.13—Circuit used for distortion of the 50 cycle/sec timing trace.

The undercarriages were removed from the trailers, and special shock mountings were installed. Figure 4.11 shows a typical mounting. The natural frequency in vertical motion was about 3 cycles/sec. The mounting was expected to yield plastically on the YFNB-12 in order to absorb a considerable amount of shock motion. This prediction was confirmed after the test, when measurements indicated a permanent set of several inches at the transverse center of the mounting.

The purpose of the special mountings for the trailers was to allow a larger vertical travel. With the standard tire-and-spring undercarriage, there was a maximum possible trailer travel of about 3 in. up or down before the trailer hit either the deck above or its own stops. With the special mounting, the available travel was tripled. Several large truck tires were placed on their sides under the mountings to cushion any bottoming.

4.14 TIMING SIGNALS

A time mark was supplied by EG&G at a time specified with respect to zero time and every $\frac{1}{2}$ sec thereafter. This signal was recorded by one channel of each recording instrument. It was fed to a cathode-ray channel and a galvanometer by the circuit shown in Fig. 4.12.

The tuning-fork-controlled timing amplifier in the cathode-ray recording system was used to supply an accurate timing signal to the galvanometer oscillographs. (The latter had only a timer that depended on the line frequency. The motor-generator output frequency was not sufficiently well regulated for this purpose.) The timing amplifier had a smooth sine-wave shape, which was not a convenient pattern for use in measuring time intervals precisely, and therefore the amplifier output was fed through a neon-lamp circuit. This device provided marks in each cycle which could be used to measure time accurately. The circuit is shown in Fig. 4.13.

REFERENCES

1. W. R. Campbell, Performance Tests of Wire Strain Gages II, NACA Technical Note 978, September 1945.
2. T. A. Perls, A Retraction-type Displacement Gage, DTMB Report 651, March 1950.
3. R. W. Mayo, A New Diaphragm-type Pressure Gage for Underwater Explosion Measurements, Sixth Conference on Progress in Underwater Explosion Research, NavShips 250-423-26, Report 1955-1.

OPERATIONS

[illegible]

[illegible] YFNB-13 [illegible] SQUAW-12 [illegible]

[illegible]

[illegible] static pressure difference [illegible] between [illegible] SQUAW [illegible]. Measurements were made [illegible] on several occasions before and after the targets were lowered. However, [illegible] unbalance signals which were due to slow temperature effects [illegible] when compared with the signals due to the pressure difference.

The gauges were recovered from the barges on D+1 day. It appeared that all instruments had operated properly with one major exception. The recording paper in the [illegible] of the YFNB-13 had torn about 0.1 sec after the shock wave hit the SQUAW-12 and after the significant signals had already been recorded. Unfortunately, when the jammed paper was later removed from the magazine, this portion of the record became fogged. The reason for the failure is unknown; it does not appear to have been caused by the shock.

CHAPTER 6

TEST RESULTS

6.1 OSCILLOGRAMS

Most of the test results are contained in the oscillograms shown in Figs. 6.1 to 6.7. These show portions of the test records for an interval of about 0.2 sec and include the times at which the shock wave hits the target and the instrument barge.

Figure 6.1 is from the recording cathode-ray oscillograph on YFNB-12. On this record each pair of traces comes from a separate cathode-ray-tube face. The initial trace positions were on opposite sides of the tube near the edge, and the signal polarity was such that the expected signals were directed toward the center of the tube in order to take advantage of the full width of the tube face for each channel. Nevertheless, some signals (e.g., station 12.12) go off scale as soon as 3 msec after the shot. On this oscillogram all traces disappeared completely from the tubes within 0.1 sec after the shock.

Figure 6.3 is from the galvanometer oscillograph on the YFNB-13 and shows most of the features observed on all the records. The top trace is the signal from a precision 50 cycle/sec tuning fork; the vertical timing lines are actually 10.3 msec apart. The lowest trace is from the 2 cycle/sec fiducial time signal supplied by EG&G. The remaining signals are a mixture of strains, pressures, and displacements. The upward direction represents compressive strains, positive pressures, or inward displacements on this oscillogram. Note that all signals do not start at the same time because of the finite transit time of the pressure wave between gage stations. Also, all the signals have small negative precursors that are due to stress waves which traveled along the hull faster than the pressure wave traveled in the water outside. The pressure cutoff after about 25 msec shows up on almost all the records. On some of the traces, e.g., 13.37 and 13.16, there are violent oscillations, and these are due to prior mechanical breaks in the external cables. The noise and oscillations that occur after 0.14 sec are probably due to the effect of the shock wave on the YFNB.

Figure 6.5 shows a similar portion of the record from the SQUAW-29. The hull of this target was partly out of the water and far from the shot, and therefore pressure loading was negligible. Hence all the signals are small despite the fact that the amplifier sensitivities had been enormously increased.

6.2 SUMMARY OF DATA

Tables 6.1 to 6.3 are a summary of the immediately significant data extracted from the oscillograms. The tabulated arrival times refer in most cases to the beginning of the first compression signal and are measured from the time of detonation, which is assumed to occur at 29 msec after the first fiducial radio signal from EG&G.[1] The peak strains and pressures

(Text continues on page 56.)

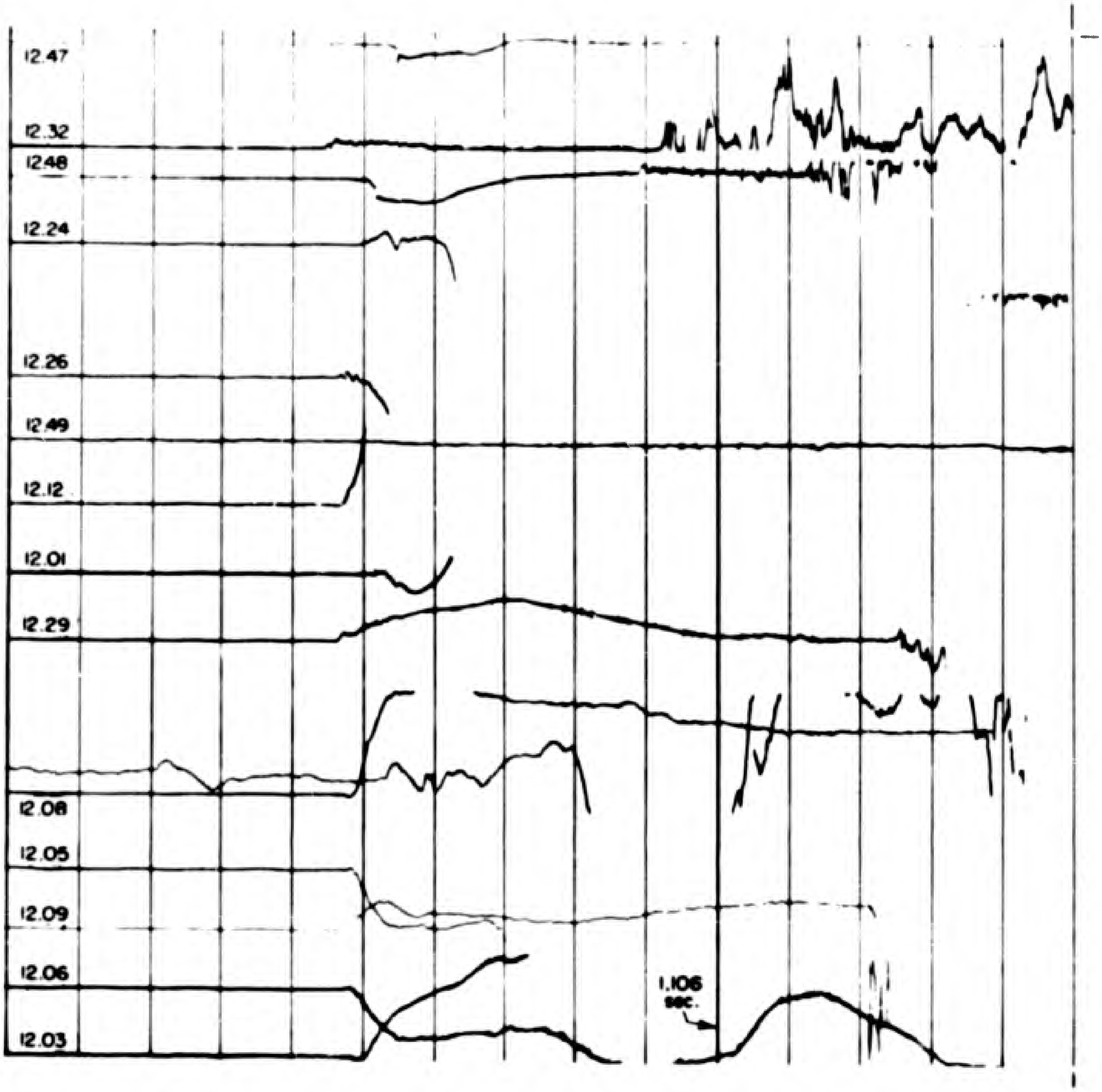

Fig. 6.1—Oscillogram from the recording cathode-ray oscillograph on YFNB-12.

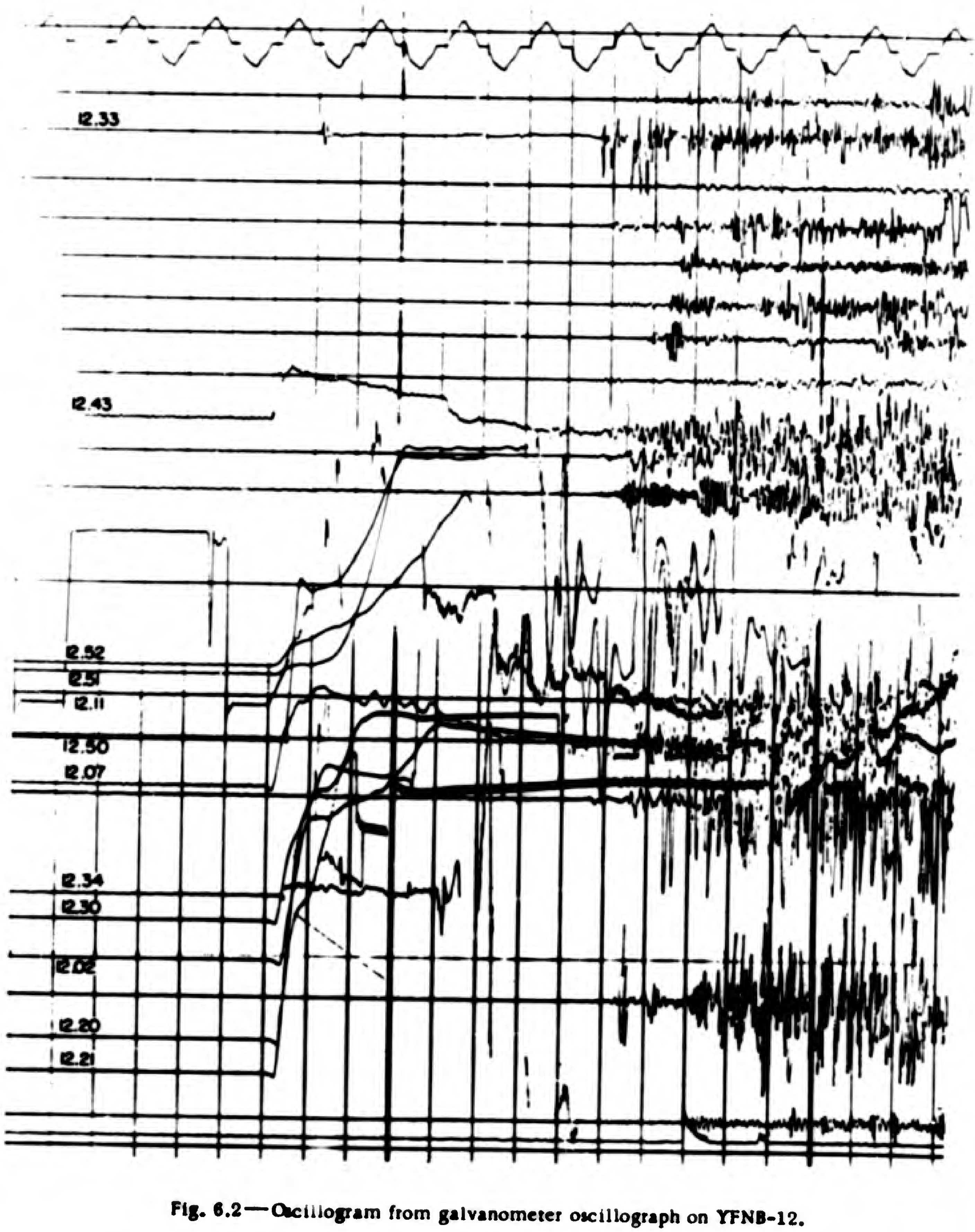

Fig. 6.2—Oscillogram from galvanometer oscillograph on YFNB-12.

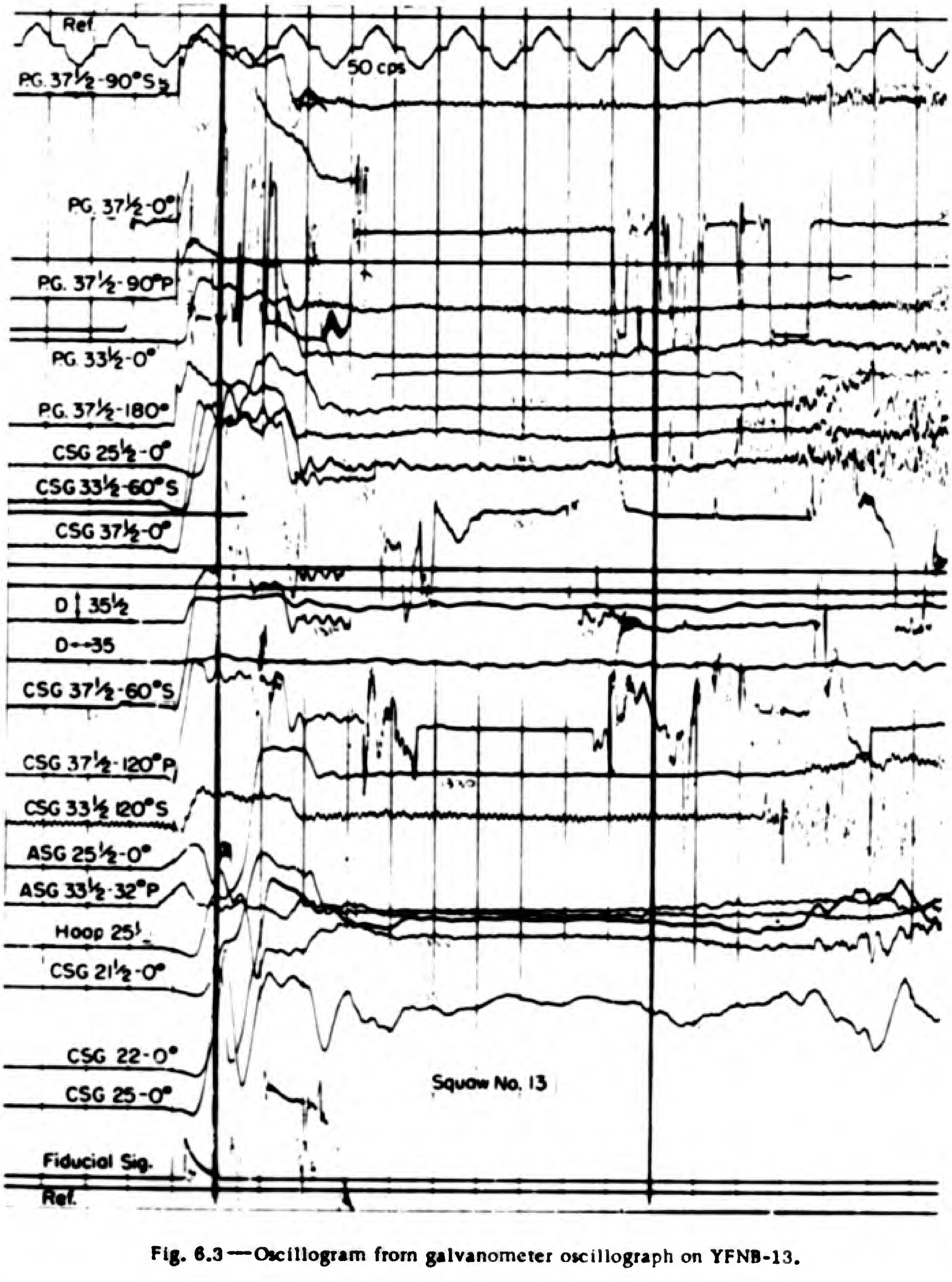

Fig. 6.3—Oscillogram from galvanometer oscillograph on YFNB-13.

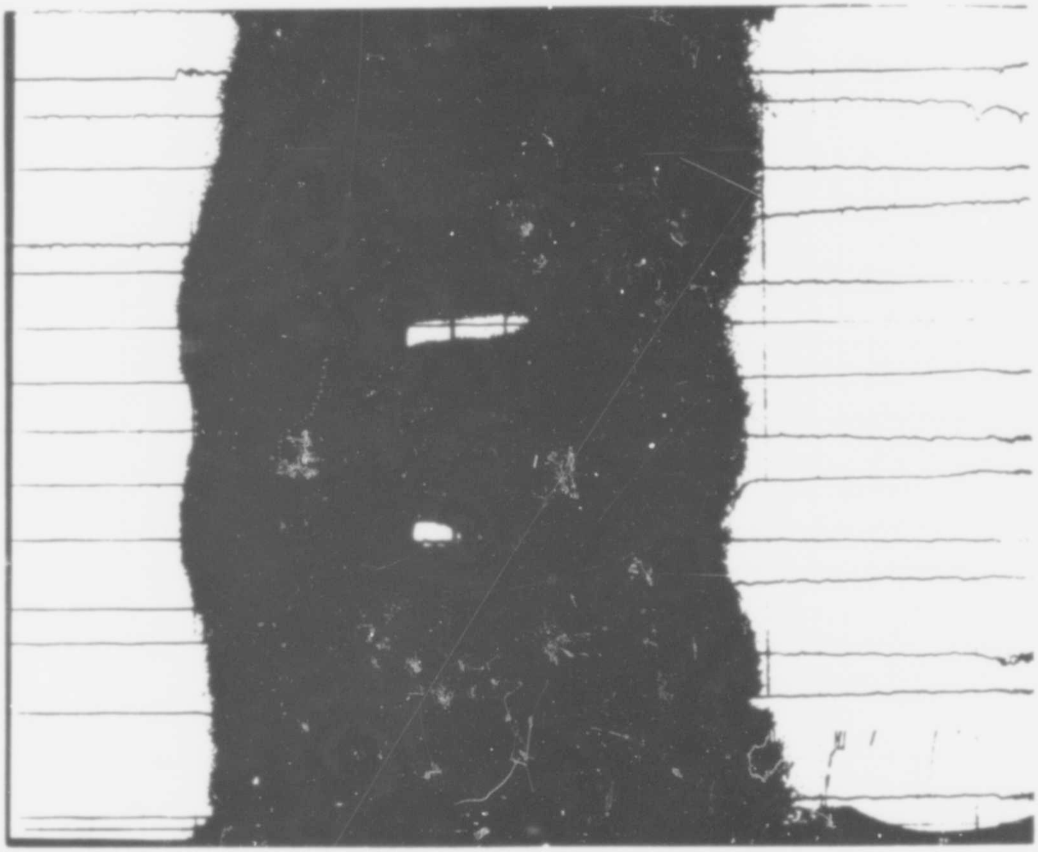

Fig. 6.4—Oscillogram from recording cathode-ray oscillograph on YFNB-13.

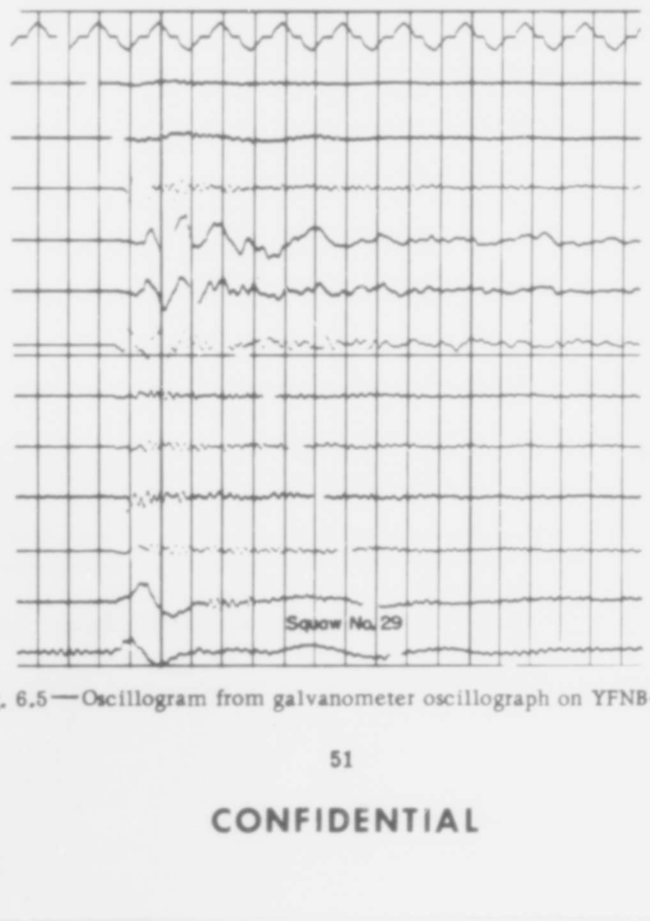

Fig. 6.5—Oscillogram from galvanometer oscillograph on YFNB-29.

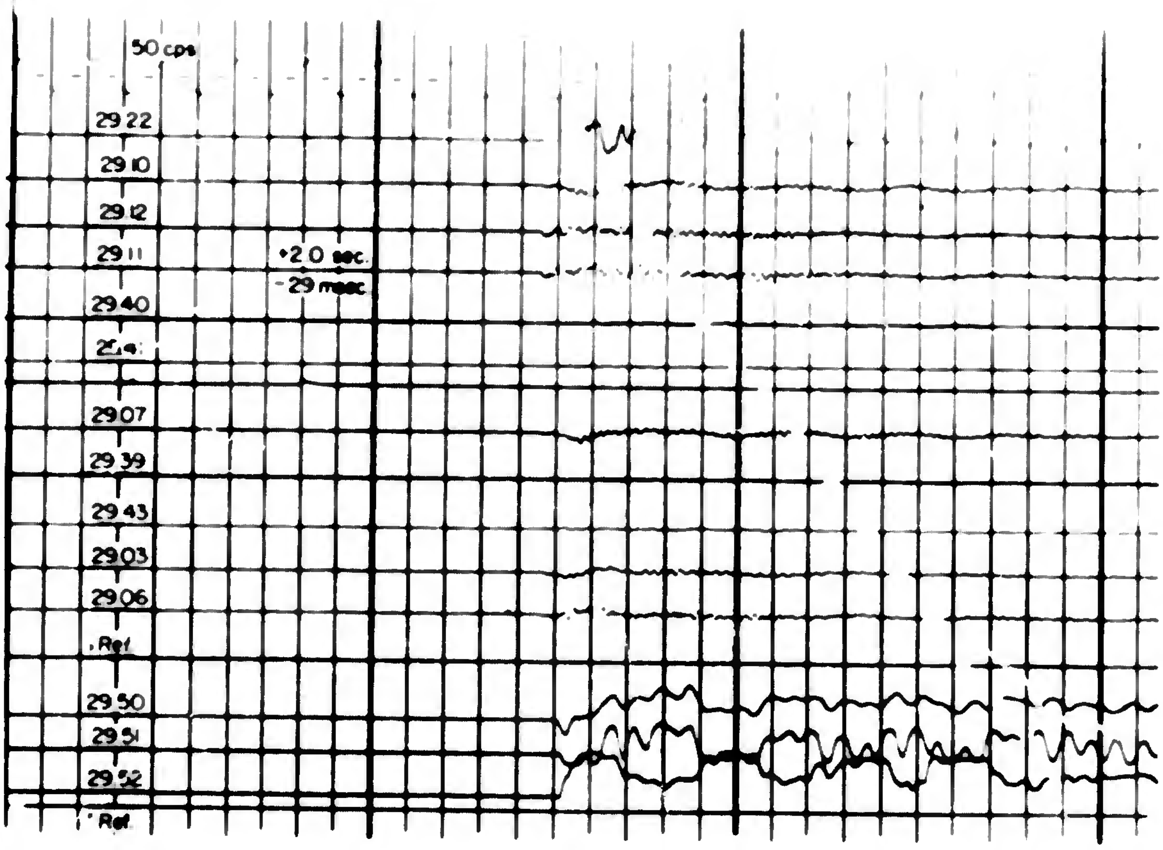

Fig. 6.6—Oscillogram from second galvanometer oscillograph on YFNB-29.

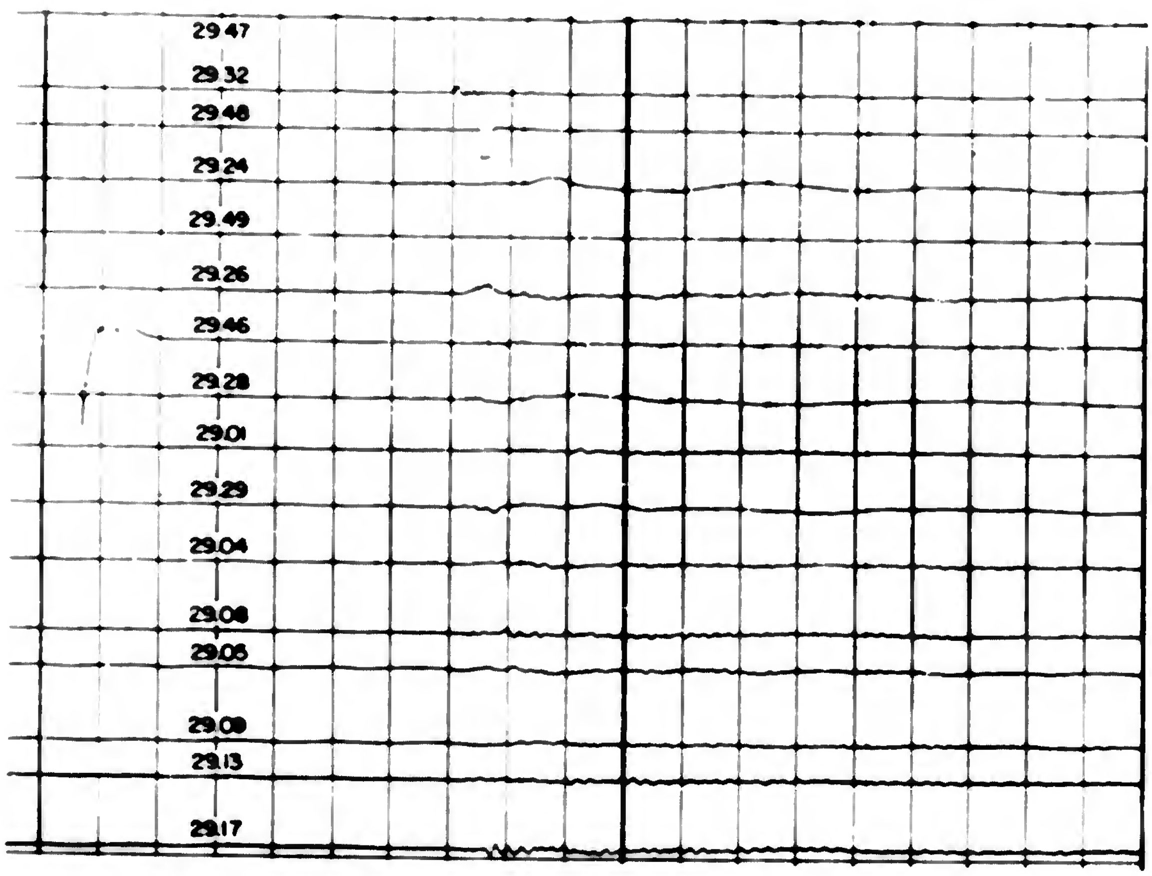

Fig. 6.7—Oscillogram from recording cathode-ray oscillograph on YFNB-29.

Table 6.1 —SUMMARY OF TEST RESULTS ON SQUAW-12

Station	Position Frame	Position Angle deg	Arrival Time sec	Maximum Strain	Time of Maximum sec	Notes	
Circumferential Strain on Plating							
12.01	15 1/2	0	1.059	1.4	1.064		
				> 1.4×10^{-3}	> 1.070	off scale	
12.02	21 1/2	0	1.058	22.0	1.098		
12.03	25 1/2	0	1.057	> 8.4	> 1.080	off scale	
12.05	33 1/2	0	1.055	> 6.4	> 1.077	off scale	
12.06	33 1/2	60S	1.055	6.4	1.096		
12.07	33 1/2	120S	1.055	3.4	1.068		
12.08	33 1/2	180	1.055	7.2	1.068		
12.09	33 1/2	60P	1.055	2.7	1.115		
12.12	37 1/2	16P	1.054	> 6.0	> 1.056	off scale	
12.30	25 1/2		1.057	7.3	1.070		
Circumferential Strain on Frames							
12.20	22	0	1.057	~70.0	1.083		
12.21	25	0	1.057	~64.0	1.076		
Axial Strain							
12.24	15 1/2	0	1.055	> 2.4 T	> 1.070	off scale	
12.26	37 1/2	0	1.053	> 2.4 T	> 1.061	off scale	
12.29	38 1/4	180	1.053	3.3	1.080		
Strain Inside Stern Cap							
12.32	53 +		1.051	0.67	1.052		
Deflection Measurements							
Station	Position Frame	Position Angle deg	Arrival Time sec	Maximum Deflection in.	Time of Maximum sec	Notes	
12.50	35	0	1.058	> 9.2	> 1.08	off scale	
12.51	35 1/2	0	1.058	> 12.3	> 1.08	off scale	
12.52	35	90	1.058	> 11.2	> 1.08	off scale	
Pressure Measurements							
Station	Position Frame	Position Angle deg	Arrival Time sec	Maximum Pressure psi	Time of Maximum sec	Duration sec	Negative Pressure Level psi
12.43	37	180P	1.054	857	1.059	0.042	-150

Table 6.2—SUMMARY OF TEST RESULTS ON SQUAW-13

Station	Position		Arrival Time sec	Maximum Strain	Time of Maximum sec	Set Strain	Time of Set	Notes
	Frame	Angle deg						
Circumferential Strain on Plating								
13.01	15 1/2	0				1.78×10^{-3}	D+1	
13.02	21 1/2	0	1.475	5.4×10^{-3}	1.490	3.4	5.2 sec	
13.03	25 1/2	0	1.475	3.6	1.480	2.0	5.2 sec	
13.04	28 1/2	0	1.473			0.3	1.6 sec	fogged
13.05	33 1/2	0	1.471	3.5	1.476	2.3	D+1	fogged
13.06	33 1/2	60S	1.470	3.4	1.481	1.4	5.2 sec	
13.07	33 1/2	120S	1.470	2.7	1.475	1.0	5.2 sec	
13.08	33 1/2	180	1.470			1.2	D+1	
						3.2		fogged
13.09	33 1/2	60P	1.470	> 3.2	> 1.480	1.4	D+1	
						1.5	1.6 sec	fogged
13.11	37 1/2	0	1.469	4.9	1.476	2.4	.05sec	
13.14	37 1/2	60P	1.469	6.2	1.476	4.1	2.4 sec	
13.16	37 1/2	120P	1.468	4.5	1.473	2.5	2.4 sec	
13.30	25 1/2		1.474	7.0	1.492	6.3	1.6 sec	
Circumferential Strain on Frames								
13.20	22	0	1.475	3.2	1.476	1.6	5.2 sec	
13.21	25	0	1.474	11.1	1.500	7.8	5.2 sec	
Axial Strain								
13.24	15 1/2	0	1.466	> 0.43	> 1.476	0.77	D+1	
						0.4	1.6 sec	fogged
13.25	25 1/2	0	1.465	3.68 T	1.488	2.2 T	5.2	
13.26	37 1/2	0	1.463	> 2.0 T	> 1.474	1.2 T	D+1	
						0.4 T	1.6	fogged
13.27	33 1/2	32P	1.465	1.0	1.470	0.2 T	5.2	
13.28	33 1/2	180	1.464	0.63	1.470	0.3		fogged
13.29	38 1/4	180	1.463	> 0.7	> 1.470	0.9		fogged
Strain Inside Stern Cap								
13.32	53 +		1.461	0.51	1.462	0	D+1	

Deflection Measurements

Station	Position		Arrival Time sec	Maximum Deflection in.	Time of Maximum	Set Deflection in.	Time of Set	Notes
	Frame	Angle deg						
13.51	35 1/2	0	1.470	2.6	1.492	2.0		Vertical
13.52	35	90	1.471	0.5	1.480	0.2		Horizontal

Pressure Measurements

Station	Position		Arrival Time sec	Maximum Pressure psi	Time of Maximum sec	Duration sec	Peak Negative psi	Notes
	Frame	Angle deg						
13.36	33 1/2	0	1.469	600	1.474	0.025	-120	0 set
13.41	37	90P	1.467	598	1.472	0.024	-100	0 set
13.42	37	90S	1.469	588	1.472	0.025	-100	0 set
13.43	37	180	1.467	635	1.470	0.024	-100	0 set
13.47	15 1/2	0	1.479	656	1.485			fogged
13.48	26 1/2	0	1.473	> 460				fogged
13.49	37 1/2	0	1.469	> 500				fogged

Table 6.3—SUMMARY OF TEST RESULTS ON SQUAW-29

Station	Position: Frame	Position: Angle deg	Arrival Time sec	Maximum Strain	Time of Maximum sec
Circumferential Strain on Plating					
29.01 to 29.19	15 to 38		2.037 to 2.041	< 75×10^{-6}	
Circumferential Strain on Frames					
29.20	22	0	2.042	195	2.062
29.21	25	0	2.040	145T	2.055
29.22	34	0	2.038	125	
29.23	37	0	2.038	135	2.054
Axial Strain					
29.24	15 1/2	0	2.048	120	2.052
29.25	25 1/2	0	2.038	14C	2.049
29.26	37 1/2	0	2.037	150	2.041
29.27	33 1/2	32P	2.037	100	2.044
29.28	33 1/2	180	2.040	100	2.058
29.29	38 1/4	180	2.037	85T	2.043
Strain Inside Stern Cap					
29.32	53 +		2.035	100	2.036
Deflection Measurements					
Station	**Position: Frame**	**Position: Angle deg**	**Arrival Time sec**	**Maximum Deflection in.**	**Zero Shift in.**
29.50	35	0	2.044	0.13	0.25
29.51	35 1/2	0	2.044	0.18	0.10
29.52	35	90	2.044	0.23	0.22
Pressure Under SQUAW					
Station	**Depth ft**		**Arrival Time sec**	**Peak Pressure psi**	**Duration sec**
29.48	25		2.039	420	0.002

tabulated are the peak values that can be read on the oscillograms. In many cases much higher strains did occur, but they were off scale. In a few cases the peak signals were obscured by fogging of the torn oscillogram, which occurred when the paper was removed from the magazine. All the tabulated strains are compressive strains unless a subscript T (meaning tension) is appended to the value. The values tabulated for the "set" strain or "set" pressure signal were read in most cases on the oscillograms at either 1.5 or 5 sec after the shock at the barge had ceased. For the cathode-ray-oscillograph channels on the YFNB-13, the set strains were measured with a Baldwin strain indicator on D + 1 day.

REFERENCE

1. M. F. Wardrol and D. C. Cochrane, Timing and Firing, Operation Wigwam Report WT-1036, May 1955.

CHAPTER 7

DISCUSSION OF TEST RESULTS

7.1 RANGE AND ATTITUDE OF TARGETS

The first quantities deduced from the records are the ranges and orientations of the SQUAW targets. These were based on the measured time of arrival of the pressure wave at the various gages and on some independent depth, roll, and pitch data reported by Project 3.6.[1] The data are summarized in Table 7.1; the calculations are described below.

The tabulated arrival times are those times at which the signals were first detected from the gages in the stern noses. These times were measured with respect to the time of detonation, which is assumed to have occurred 29 msec after the zero fiducial signal. The times are indicated to the nearest millisecond. The time scale was provided by the repetition of the fiducial signal at $\frac{1}{2}$-sec intervals and by the tuning-fork signals from the cathode-ray oscillographs. The two scales agreed to within $\frac{1}{4}$ per cent.

The angles between the longitudinal axes of the SQUAWs and the incident waves were obtained from the times of arrival of the shock wave at the various gages at different longitudinal positions. Thus, for any target, the time of arrival at a particular gage station was plotted against the distance of that station from the stern. These points lay approximately along a straight line whose slope indicated the rate at which the shock wave enveloped that SQUAW. The angle between the axis of the SQUAW and the incident wave was then arc cos c/v, where c is the sonic velocity and v is the observed velocity of the shock wave along the SQUAW. The sonic velocity was obtained from data of the Scripps Institution of Oceanography,[2] which gives the sonic velocity as a function of depth at the test site.

It is apparent from Table 7.1 that SQUAW-12 was hit nearly broadside by the shock wave (62 deg from the longitudinal axis) and that SQUAW-13 was hit nearly end-on (18 deg from the longitudinal axis).

The angle of heading is the angle formed by the horizontal projection of the axis of the SQUAW and a horizontal line extending from the SQUAW toward the weapon. The magnitude of this angle is determined uniquely by the angle of pitch, the angle between the shock wave and the SQUAW axis, and the vertical angle at which the shock wave arrives at the SQUAW. However, the sign of the angle cannot be determined from these data alone, i.e., whether the SQUAW was hit on the portside or the starboard side cannot be obtained from the calculation. The time-of-arrival data are not sufficiently precise to indicate the side of attack.

The slant range was calculated from the measured arrival time, the sound velocities,[2] and an average shock velocity determined by the Armour Research Foundation.[3] The sound velocity is a function of salinity and temperature and hence depends on the depth. The shock velocity, in addition, is a function of shock strength and thus depends on range and depth. We assume that the travel time for the shock wave between the weapon and the surface point 2000 ft above it was 0.364 sec, as reported in reference 3. If we consider the shock that travels diagonally along the

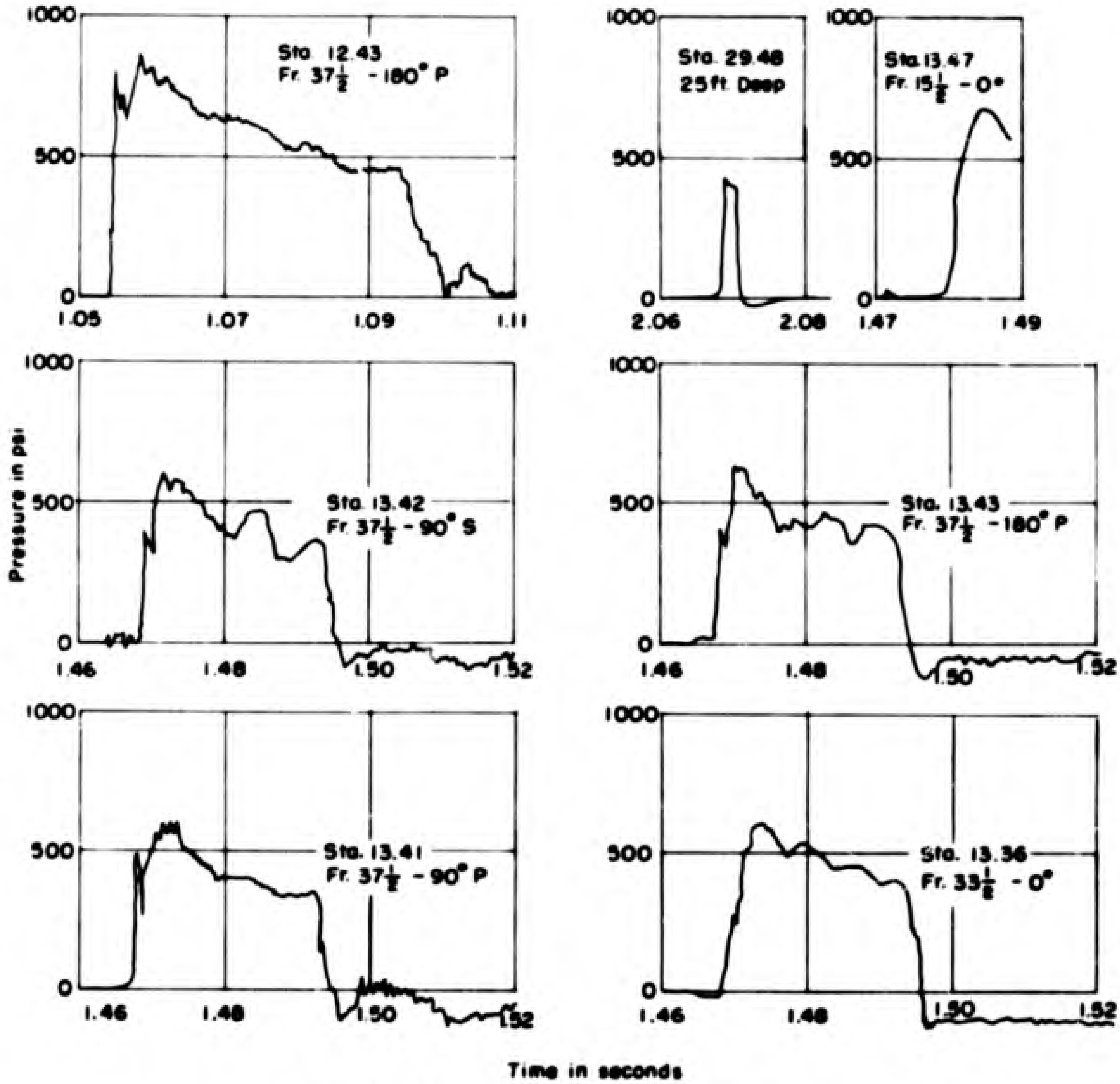

Fig. 7.1—Pressures measured at SQUAW targets.

Table 7.1—RANGE AND ATTITUDE OF SQUAWS

	SQUAW-12	SQUAW-13	SQUAW-29
Depth at midsection,[1] ft	290	260	0
Angle of pitch,[1] bow up, deg	+36	−3	
Angle of roll,[1] starboard, deg		+1	
Arrival time at stern, sec	1.050	1.460	2.035
Angle between SQUAW axis and normal to pressure wave, deg	62	18	
Angle of heading relative to weapon, deg	67	13	
Horizontal range to midsection, ft	5,150	7,200	10,000
Slant range of midsection, ft	5.420	7,410	10,200

ray to the target instead of straight up, then we assume that, in this same time interval of 0.364 sec, the 2000-ft range would be increased in the ratio of the mean sound velocity up to the depth that the shock reaches along the ray to the mean sound velocity up to the surface. Now it is easily verified that along a ray to the target an approximate range of 2000 ft would bring the shock up to about the 1500-ft level. Hence in 0.364 sec the range of this shock would be 2000 $\bar{C}_2/\bar{C}_1$, where a value of $\bar{C}_1$ = 4889 ft/sec is the mean sound velocity between the surface and the 2000-ft depth and a value of $\bar{C}_2$ = 4854 ft/sec is the mean sound velocity between the 1500-ft depth and the 2000-ft depth. In the remainder of the travel time to the target, $t - 0.364$ sec, where t is the arrival time in seconds, the shock amplitude is so low that the mean velocity equals $\bar{C}_3$ = 4893 ft/sec, which is the average sound velocity between the 250-ft depth and the 1500-ft depth. Hence the simplest formula for the slant range using these data is

$$S = 2000 \frac{\bar{C}_2}{\bar{C}_1} + (t - 0.364)\, \bar{C}_3 \tag{7.1}$$

The ranges were also calculated by tracing rays from the weapon to the targets, making appropriate stepwise corrections for the changing index of refraction with depth, and correcting the travel time of the lowest step for the increase in shock velocity over the sonic velocity. This second method gives results which are within 0.1 per cent of those obtained by Eq. 7.1.

7.2 PRESSURE MEASUREMENTS

All the pressure oscillograms have been replotted to a common scale in Fig. 7.1. There is only one measurement from the nearest target, five from the center target, and one from the distant target. Of the remaining pressure channels on SQUAWs 12 and 13, 18 failed because the cables parted prior to the test, two failed apparently due to leakage, and two records were fogged when the torn paper was removed from the magazine. On SQUAW-29 the remaining 13 pressure channels were in good operating condition, but the gages were above the surface, and there was no pressure to measure. The SQUAW-29 record shown in Fig. 7.1 is from a gage hanging in the free field 25 ft below the target.

At SQUAW-12 the one gage at the keel shows a peak applied shock pressure of 857 psi. The applied pressure on the hull is compared with the incident free-field pressure in Fig. 7.2. This incident free-field pressure is estimated to have a peak of 920 psi, a time constant of 36 msec, and a duration of 36 msec from the data of Program I.[4] The estimate is based on the free-field pressures measured in that program at the depth of the SQUAW and at the range of YFNB-12 but corrected for the range of SQUAW-12. Note that the peak applied pressure is only 7 per cent lower than the estimated peak incident pressure. Also, the duration and apparent decay time of the hull pressure are longer than those of the free-field pressure.

At SQUAW-13 the peak measured pressures at the five gages range from 585 to 656 psi with an average of 615 psi. In Fig. 7.3 these pressures are compared with the incident free-field pressure. The free-field pressure at SQUAW-13 is estimated to have a peak of 650 psi (from reference 4), a time constant of 44 msec, and a duration of 22 msec as based on the measurements of Project 1.2 near YFNB-13 and YFNB-12 and adjusted to the range and depth of SQUAW-13. The mean peak applied pressure is only 5 per cent lower than the estimated peak incident pressure. The applied pressure takes 2 to 3 msec to reach peak and decays at about the same rate as the incident pressure, but the duration again is slightly longer than that of the incident pressure. The residual pressure after cutoff is about 100 psi below hydrostatic pressure in good agreement with the assumption that prolonged cavitation occurs at zero absolute pressure. At SQUAW-29 the peak free-field pressure was 420 psi, which compares well with an estimate of 395 psi based on Project 1.2 results, particularly in view of the very large scatter in measurements near the surface at this range.

The applied pressures at the hull differ from the incident pressure wave because the latter is modified by transmission through the outer tank walls, reflection from the hull, diffraction around the hull, and radiation from the local hull motions. It is interesting, and plausible, that

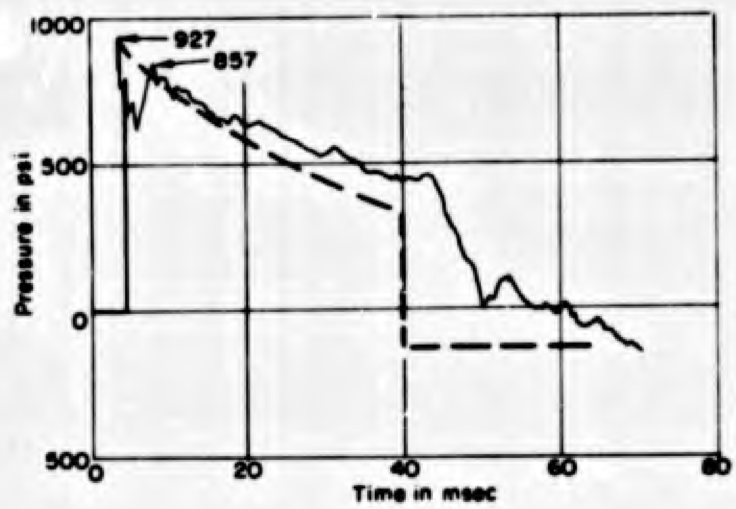

Fig. 7.2—Comparison between pressure measured at SQUAW-12 and estimated free-field pressure.

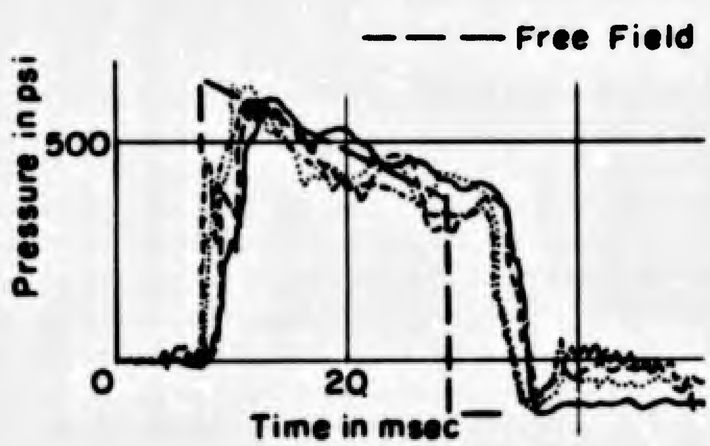

Fig. 7.3—Comparison between pressures measured at SQUAW-13 and estimated free-field pressure.

these various modifications do not change the effective pressure in any important way. For a plane pressure wave with a 22-msec decay time passing through 1-in. steel plate, with water on both sides, the peak pressure would be retarded by 0.4 msec and reduced by 1.7 per cent.[5] For the same pressure wave incident normally on 1-in. air-backed plating, the reflected pressure instantaneously doubles the effective pressure on the plate, but the motion of the plate soon relieves this pressure and the total pressure drops to zero in 0.7 msec. These calculations are not meant to apply exactly to the interaction of the pressure wave and the structure of SQUAW-13, but they do suggest that the actual interaction process, which was made up of elementary processes similar to those calculated here, could be expected to influence only the first 2 or 3 msec of the applied pressures. After the first few milliseconds, oscillations of about ± 15 per cent are still noticeable on either side of a smooth "free-field" pressure. The cause of these pressure oscillations is not known. It might also be noted that the durations measured on the pressure oscillograms are slightly larger than the expected free-field duration.

Secondary pressure pulses were observed on all the pressure gages on SQUAW-13. At 4.3 sec there was a pressure with a peak of about 70 psi, presumably due to the first bubble pulse. At 6.2 sec there appeared to be a pressure of about 60 psi, perhaps from bottom reflection, and at 6.95 sec there was a pulse with a peak of about 100 psi.

7.3 HULL RESPONSE OF SQUAW-12

The peak measured pressure at SQUAW-12, shock wave plus hydrostatic, was 984 psi, and the estimated value for the peak incident pressure plus hydrostatic was 1045 psi. In either case this pressure is substantially above the estimated static collapse pressure of 655 psi, and collapse would be expected. The strain and deflection measurements substantiate this expectation.

All the records for SQUAW-12 have been replotted to the same scales in Fig. 7.4. They show that enormous strains were reached within very short times. The largest strains appear in the records for the battery compartment where circumferential gages at the crown on frames 25 and 22 show strains of from 0.006 to 0.010 within 8 msec and up to 0.070 within 20 msec. Also, circumferential gages at the crown on the pressure-hull plating midway between stiffeners at frames 21½ and 25½ show strains of from 0.005 to 0.007 within 8 msec and to 0.022 within 30 msec. Note that the strains on the inner flanges of the frames rise much faster and reach higher values than at the plating between frames, perhaps owing to some sort of buckling. At frame 15½ on the crown plating there were both an axial and a circumferential gage. The circumferential gage showed a strain which started in compression but within 7 msec reversed and increased very rapidly in tension as it went off the screen. The axial gage at this location also went off the screen while increasing in tension very rapidly. The very high early values for the strains, the very high strain rates, the abrupt transition in the strain direction at frame 15½, and the high values for the rate at which the tensile strains at frame 15½ increase, together suggest that buckling and possible rupture of the shell of this compartment must have been assured at an early time, e.g., within 10 msec.

In the engine compartment the measured strains were smaller than those in the battery compartment but were still very large. There was very good coverage of the strain on the plating midway between stiffeners in the circumferential direction at frame 33½. Here there were five circumferential strain gages at positions of 0 deg, 60 deg port, 60 deg starboard, 120 deg starboard, and 180 deg. All these gages show that the circumferential strain in the plating at frame 33½ reached an initial stability at about 7 msec after the first loading. At this initial peak, strains varied from 0.002 to 0.0045 except at the 180-deg position, where the initial peak strain was 0.0071. The 180-deg gage was over the keel where large bending could be expected, and the large strain in proportion to the other locations in the same bay is not unreasonable. In Fig. 7.4 it can be seen that strains at frame 33½ remain in equilibrium with the pressure for about 20 msec, after which the crown gage indicates a sudden very rapid increase of compressive strain. A short time later the 60-deg-starboard gage also indicates an increase in

Station	Frame	Angle in degrees	Direction
1	15½	0	Circ.
24	15½	0	Axial
2	21½	0	Circ.
20	22	0	Circ.
21	25	0	Circ.
30	25½	—	Circ.
3	25½	0	Circ.
5	33½	0	Circ.
6	33½	60 S	Circ.
7	33½	120 S	Circ.
8	33½	180	Circ.
9	33½	60 P	Circ.
12	37½	16 P	Circ.
26	37½	0	Axial
29	38¼	0	Axial
32	—	—	—
52	35	90	↔
50	35	0	↕
51	35½	0	↕

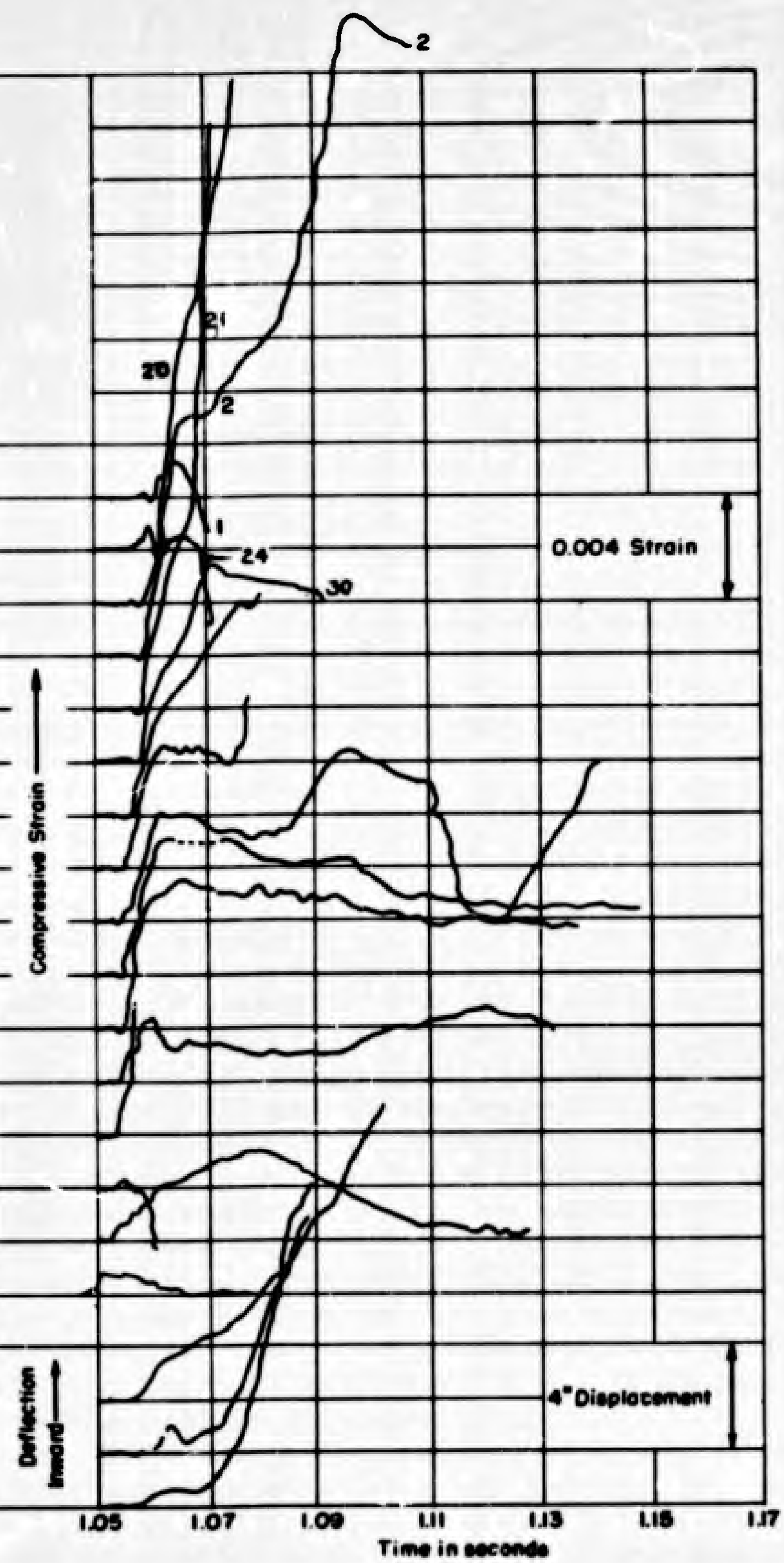

Fig. 7.4—Strains and deflections measured on SQUAW-12.

compressive strain, followed by the same trend on the 60-deg-port gage. This indicates a failure of this section which may have been initiated at this location, but it seems more likely that failure occurred elsewhere in the compartment first and then the weakening of adjacent sections caused a later failure at frame $33\frac{1}{2}$. In either case the indications are that at least at section $33\frac{1}{2}$ the applied pressure was not so overwhelming as to cause prompt failure in a hoop mode. The wide range in strains at this section, even during the early, presumably elastic, phase, demonstrate that the hull is not simply being squeezed in a uniform hoop mode but that considerable bending must be occurring in the plane of the section.

At frame $37\frac{1}{2}$ there were two strain gages, a circumferential gage at 16 deg port and an axial gage at 0 deg midway between the stiffeners. From Fig. 7.4 it is evident that strains in these principal directions were increasing very fast as the traces went off the screen. The circumferential compressive strain had reached 0.006 at 3 msec, at which time the trace went off the screen, and the axial strain at the crown had reached 0.0024 at 6 msec, when its trace went off the screen. This very high rate of increase in strain suggests that some buckling very likely occurred at this section within 10 msec.

The three displacement gages installed in SQUAW-12 showed large displacements, which reached the limits of the gages within 30 to 40 msec. Figure 7.4 shows these displacement records. The gages measuring radial motion of the crown at frames 35 and $35\frac{1}{2}$ relative to the engine show an initial hesitation for about 15 msec, after which the motion inward changes abruptly to a higher velocity. The measurement of radial motion of frame 35, 90 deg to starboard relative to the engine, shows an inward motion with an average velocity of about 20 ft/sec after the initial hesitation. The displacements of 9 to 12 in. measured at the gage limits are listed with times in Table 6.1. These large deflections can certainly be associated with a failure of this section. They indicate that not only was the crown collapsing at this point but also that at least one point at 90 deg starboard was also collapsing at a slightly slower rate. Hence it is estimated that collapse of the engine-room compartment occurred at about 1.074 sec, or about 20 msec after the pressure was applied.

It is inferred from these high strains that the target was well within the lethal range; the attack was overwhelming in the sense that, even if the applied pressures had cut off after 10 msec instead of 40 msec, the target would have been destroyed.

7.4 HULL RESPONSE OF SQUAW-13

The total peak pressure, shock plus hydrostatic, measured at SQUAW-13 was 728 psi; the peak incident pressure plus the hydrostatic pressure is estimated to be 763 psi. This is about 15 per cent higher than the estimated static collapse pressure, and the conditions are about marginal for collapse. However, the evidence of the strain measurements is conclusive that that target did not collapse, since two days after the test most of the gages that had recorded properly during the test were still operating, although there were large permanent sets of the same size as those observed 15 sec after the shot. This implies that there was negligible leaking of the pressure hull, since the strain-gage-bridge balance is very sensitive to moisture.

The strain and deflection measurements have been replotted to a common scale in Fig. 7.5. Despite the fact that the target did not collapse, the strains reached very high values that were well within the plastic range since the deformation remained after the pressure wave had passed on. At one gage on frame 25 a strain of 0.01 was reached within 20 msec. The set values of the strains were as high as 0.006 and 0.008. The measured deflection at the crown reached a peak of 2.6 in. and set at 2 in. Exclusive of these extreme gages, the peak circumferential strains were 0.003 to 0.005, and the set values were about 60 per cent of these peaks. These large values make it plausible that SQUAW-13 was close to failure. But the target did not fail, and since the peak strains and deflections occurred before the pressure was cut off, it is clear that the target survived not because of premature surface cutoff but because the pressure was too low even before cutoff.

Station	Frame	Angle in degrees	Direction
24	15½	0	Axial
2	21½	0	Circ.
20	22	0	Circ.
21	25	0	Circ.
30	25½	—	Circ.
3	25½	0	Circ.
25	25½	0	Axial
4	28½	0	Circ.
5	33½	0	Circ.
9	33½	60 P	Circ.
6	33½	60 S	Circ.
7	33½	120 S	Circ.
8	33½	180	Circ.
28	33½	180	Axial
27	33½	32 P	Axial
11	37½	0	Circ.
14	37½	60 P	Circ.
16	37½	120 P	Circ.
26	37½	0	Axial
29	38¼	180	Axial
32	—	—	—
52	35	0	
51	35½	0	

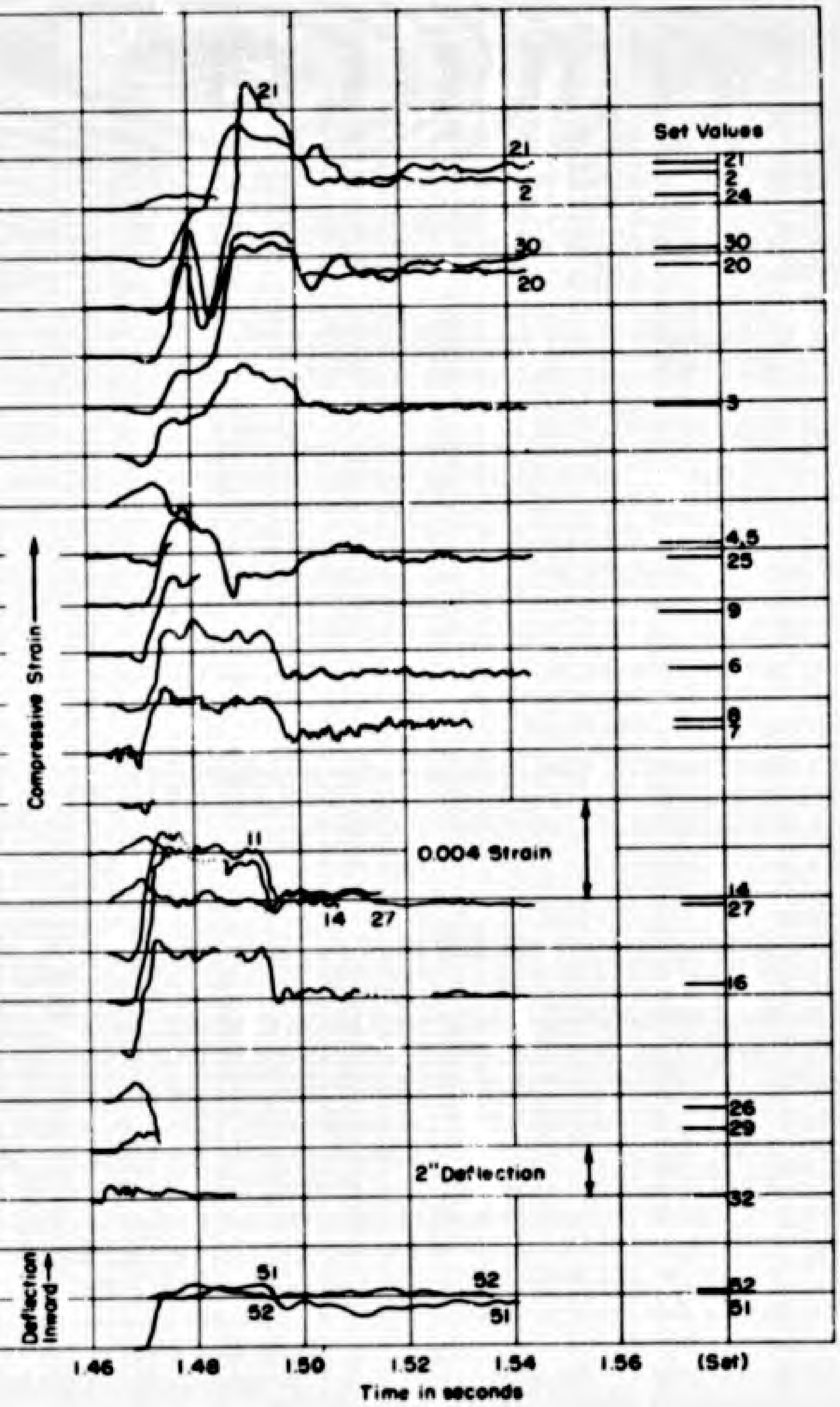

Fig. 7.5—Strains and deflections measured on SQUAW-13.

The strains measured on the plating in the engine-room compartment (stations 13.06, 13.07, 13.11, 13.14, and 13.16) give the impression of being in approximate equilibrium with the external pressures on the hull. This is shown more clearly in Fig. 7.6, where we have plotted on a time basis the average of three circumferential strain gages at frame $37\frac{1}{2}$ and also the average of three pressure gages at the same section. The average strain rises at about the same rate as the average pressure, it decays slightly as the pressure decays, and it drops off sharply as the pressure is cut off by surface reflection. This approximate equilibrium is reached in a few milliseconds and persists for the duration of the pressure pulse.

Hence we consider the deformation of the plating as a quasi-static process and compare the applied pressures and the measured response in Fig. 7.7 without explicit reference to the time. The experimental data, shown by the solid line, represent a plausible type of load-response behavior. The strains in the initial portion of the curve, up to a pressure of 112 psi, are those which were measured as the SQUAW was lowered to its test depth of 250 ft. Up to a pressure of about 650 psi, there appears to be an elastic response, thence a plastic yielding to a strain of about 0.005 with small change in pressure, and finally an unloading leaving the hull with a permanent set.

A theoretical relation between the pressure and the mean hoop strain is also shown by the dashed curve in Fig. 7.7. The rising portion of this curve represents the normally elastic regime of the hull, based on the von Sanden and Gunther equations. The upper flat portion of the theoretical curve is a regime of completely plastic flow, which is reached when the octahedral shear stress reaches a critical value of 0.47 times the yield stress. This essentially is the Hencky–von Mises yield criterion. The circumferential stress at this time is 64,000 psi, or 15 per cent larger than the assumed yield stress, and the corresponding external pressure is 790 psi. This pressure is independent of the existence of the initial locked-in stresses that are shown in Fig. 3.3. However the initial stresses do increase the values for the strains up to the yield point, and they account for the nonlinearity of the rising portion of the theoretical curve in Fig. 7.7. According to Fig. 3.3, the surface at 0.39 in. from the inner face has an initial compressive stress of 37,600 psi. Hence we can superimpose a stress of only 26,400 psi before the yield point is reached. According to the von Sanden and Gunther equations, this occurs when the applied pressure is only 325 psi, and at this pressure the theoretical response curve of Fig. 7.7 starts to become nonlinear. As the pressure increases beyond that, the plastic region spreads until at 790 psi the full thickness of the steel plating is yielding plastically. At the yield pressure the theoretical strain increment is 3.36×10^{-3} instead of 2.14×10^{-3} as would occur if there were no locked-in stresses.

The last portion of the theoretical curve represents unloading, at constant modulus, after the plastic flow.

In comparing the experimental and theoretical curves, it is well to emphasize that the experimental data are being exploited at the limit of their reliability, and the differences in the two curves may well be within the uncertainty of the experimental data. The experimental errors may be particularly large during the elastic phase and during the phase of pressure drop-off because very small time differences are involved. Also during these times the inertial effects are most important, and we should expect the strain to lag behind the pressure, as it roughly seems to do. In the regime of completely plastic flow, the hull appears to be yielding at a total pressure of 690 psi, which is 13 per cent lower than the calculated yield pressure of 790 psi. The difference might mean that the effective yield strength of the plating was 13 per cent below the 56,000 psi assumed or that there is an inertial overshoot of the plating, or it might mean that the experimental data are too sparse. The unloading portions of the two curves are of interest because the final set strains are so large, twice as large as if there had been no complete plastic flow and only the initial locked-in stress had been unloaded. The implication of this analysis is that the hull plating at this section in the engine room was yielding but did not continue on to collapse because the local pressures fell below about 660 psi.

However, this same type of analysis cannot be valid for the strain measured in the battery compartment. The strains there do not vary in approximate equilibrium with the external pressures. The circumferential strain gages on the plating at the crown and in the semihoop

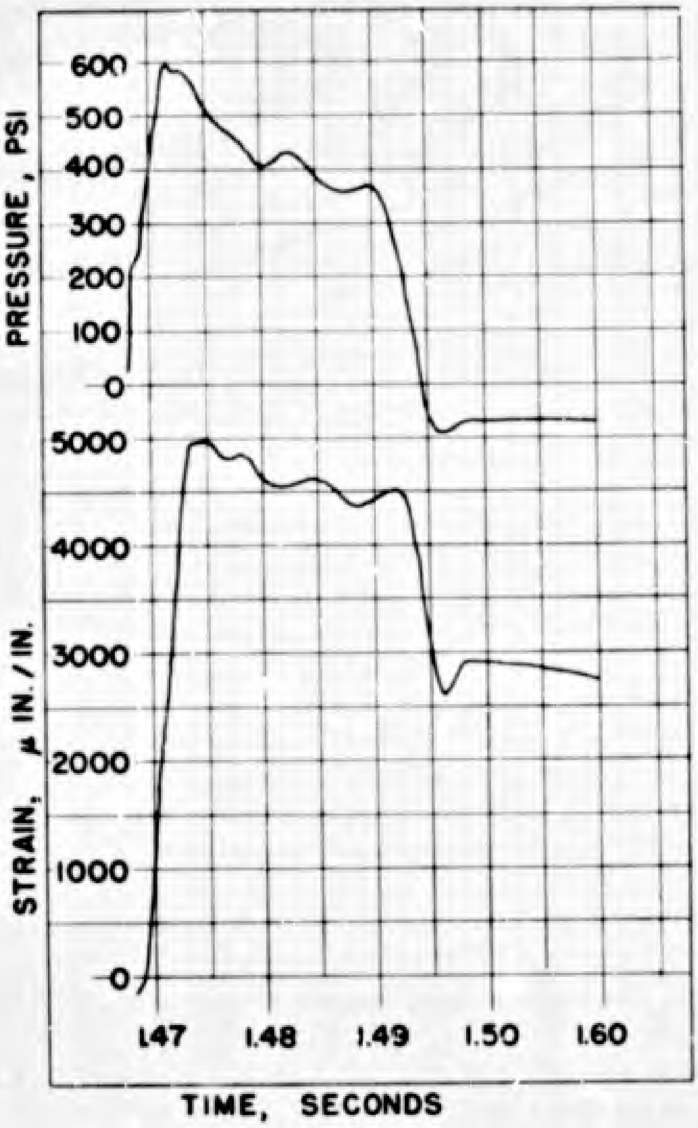

Fig. 7.6 — Applied pressures and circumferential strains averaged around circumference at frame 37½ for SQUAW-13.

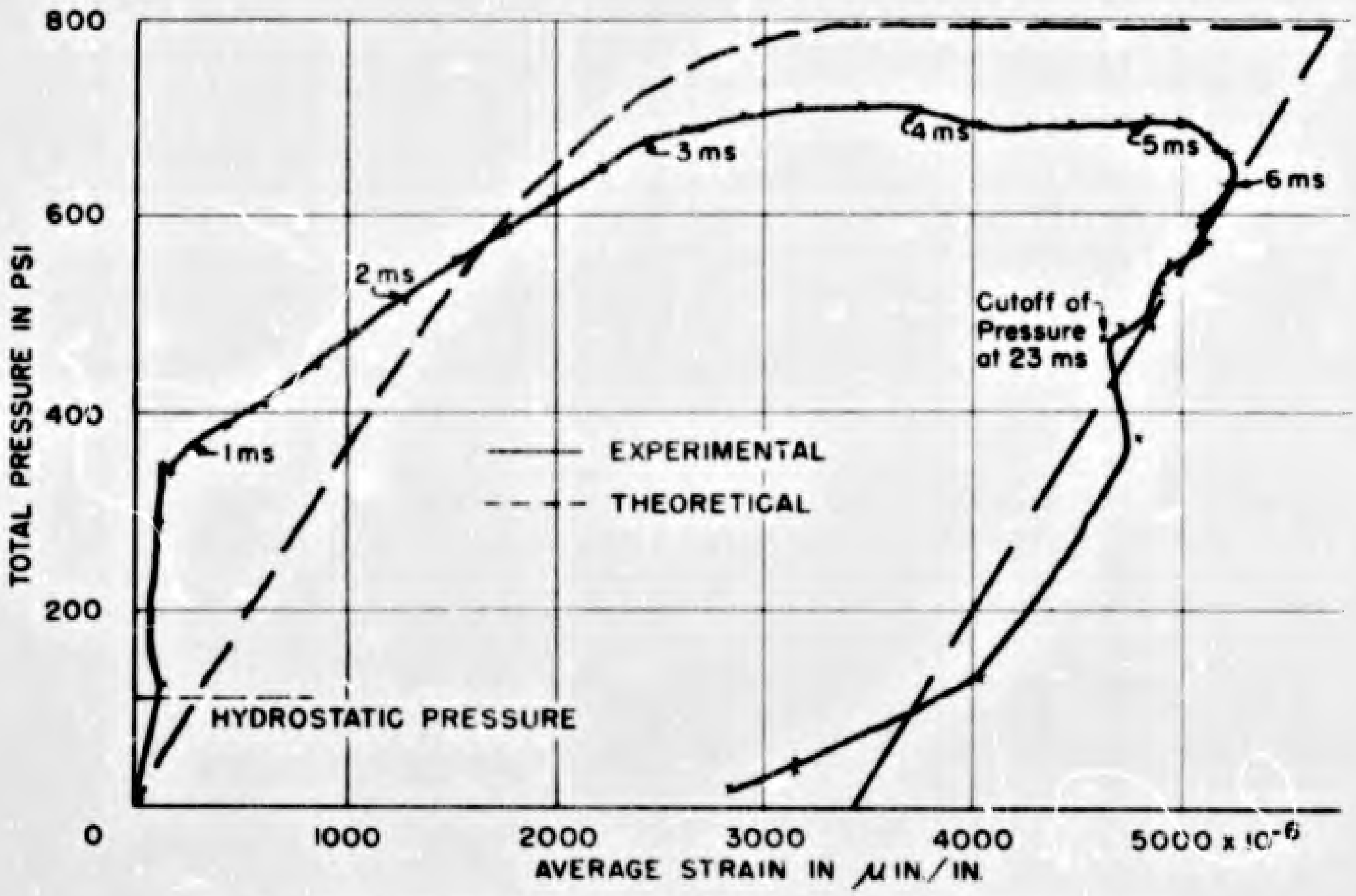

Fig. 7.7—Total pressure vs average hoop strain at frame $37\frac{1}{2}$ on SQUAW-13.

Station	Frame	Angle in degrees	Direction
24	$15\frac{1}{2}$	0	Axial
20	22	0	Circ.
21	25	0	Circ.
25	$25\frac{1}{2}$	0	Axial
27	$33\frac{1}{2}$	32 S	Axial
28	$33\frac{1}{2}$	180	Axial
23	37	0	Circ.
26	$37\frac{1}{2}$	0	Axial
29	$38\frac{1}{4}$	180	Axial
32	—	—	—
52	35	90	↔
50	35	0	↕
51	$35\frac{1}{2}$	0	↕

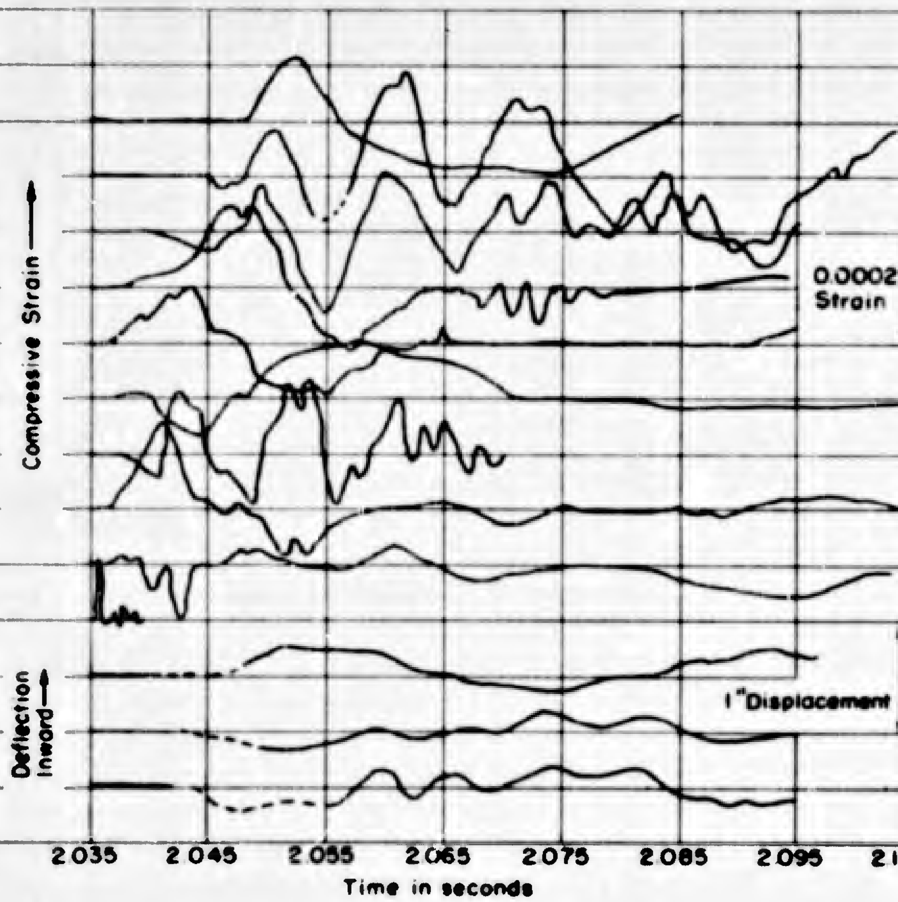

Fig. 7.8—Strains and deflections measured on SQUAW-29.

arrangement show strains that rise to an initial step within 5 msec and, after a hesitation of several milliseconds, go on to the actual peak strains recorded. The strains at the stiffeners rise faster and reach bigger values than those on the adjacent plating. There is definite evidence of an excited oscillation with a period of about 10 msec. The same oscillation occurs at these frames in SQUAW-29, and there is some indication of the abortive beginning of such an oscillation on SQUAW-12. This mode of motion, whatever it is, is important because it is responsible for the largest strains measured on SQUAW-13 and would presumably have caused collapse if the target had been a little closer to the charge. On SQUAW-12 the strains at those locations were the first to indicate failure of the structure. On SQUAW-29 these strains were likewise the largest measured.

We assume that this mode of response is essentially a dynamic mode, i.e., inertial effects are important, whereas they would be missing in a static pressure test. This mode is apparently dominant in the battery-room compartment rather than in the engine-room compartment. It may be due to some oscillation of the heavy battery masses on the frames, or it may be due to the fortuitous superposition of two longitudinal vibration modes of the SQUAW, adding up in the battery compartment but cancelling in the engine-room compartment.

Good oscillograms were obtained from only two of the axial strain gages, although the initial portion of the record and the final set strains could be measured on all. The axial strain at the crown at frame 25½ varies in the same way but in opposite phase (tension) to the circumferential strain at the same location. There is a final set tensile strain of 0.0022 in the axial direction as compared with a compressive set of 0.002 in the circumferential direction. In the other axial gages the final set strains are all less than 0.001, despite the fact that the compressive gages nearby have sets of 0.002 or greater. This again indicates that the response was probably quite complex with appreciable lobe formation.

A final set displacement of 2 in., or two plate thicknesses, was measured at the crown plating. This is about the amplitude that can be described, according to past experience, as severe but not necessarily lethal. There is only one other displacement measurement (at the side, on the frame) with which to compare this, so one cannot say whether this 2-in. deflection is a typical or an extreme measurement.

After the shock wave passed on, smaller strains were measured at all stations at about the same time as secondary pressure pulses were measured with the pressure gages. Thus at about 4.3 sec there were additional strains up to 0.0003 at most gages. At 6.3 sec there were additional strains up to perhaps 0.0002, and finally at 7.0 sec the additional strains ranged from 0.0003 to 0.0007. The deformations due to these secondary pulses appeared to be elastic, and the final set strains were not changed.

7.5 HULL RESPONSE OF SQUAW-29

It was originally hoped that the data on SQUAW-29 would display the response of the SQUAW structure under linear conditions unaffected by nonlinearities due to buckling and yielding. As it turned out, SQUAW-29 was not submerged at test time; hence the nature of the pressure loads is purely speculative, the measured strains were almost negligible (up to 150×10^{-6}), and at least there were no permanent set strains greater than the noise level of about 20×10^{-6}. The measurements have been replotted to a common scale in Fig. 7.8.

The largest strains were measured on the frames at frames 22, 25, and 27. These show a very clear oscillation at a frequency of about 100 cycles/sec. This is presumed to be the same mode that appears in strain measurements at frames 22 and 25 in SQUAW-13. The fact that the period is the same in the two targets, despite the fact that the pressure hull of SQUAW-29 is out of the water, indicates that the motion, whatever it may be, entrains a negligible mass of water. Also, the fact that these motions could be excited at all, with such small amplitudes, shows that the oscillation is not due to a buckling of the structure or to yielding at some other point.

7.6 COMPARISON OF SQUAW RESPONSES WITH MODEL TESTS

If the strain and deflection measurements on the SQUAWs, particularly on SQUAW-13, could be matched against measurements made on model tests, then the model-test results might serve as a scale on which the lethal range for the SQUAW could be interpolated.

We consider first the displacement amplitude of 2.5 in. (set of 2.0 in.) measured at the crown plating on SQUAW-13 and the amplitude of 0.5 in. (set of 0.2 in.) measured at the side framing. The DTMB model tests[6] show that, for those simplified models, a dent in the plating in excess of five to six thicknesses usually meant collapse. Also, a very small increase in pressure, perhaps 5 to 10 per cent, was required to increase the maximum damage from one plating thickness to lethal damage.

In the NEL model tests,[7] also, it was found that the maximum dent without collapse was about five to six shell thicknesses, whereas the decrease in range required to increase the damage from one thickness to collapse was about 20 per cent. The damage range before collapse in the DTMB models was smaller than in the NEL models because the former were quite sensitive to instability caused by axial stresses, whereas the latter models, because of their construction, were completely insensitive to axial forces. The SQUAW target was presumably intermediate in this respect. It is improbable that the one measurement of plating deflection on SQUAW-13 was at the point of maximum dent. Hence from these data we infer that SQUAW-13 was probably located less than 10 per cent outside the lethal range.

In the Papoose model at the lethal range, the displacements measured at the frames on the sides were about one-half of a plating thickness, which is about the same as that measured on SQUAW-13. The maximum lobe deformation depth on Papoose model B at the crown plating was two shell thicknesses, and the average was equal to one shell thickness. This model B was presumed to be 2 per cent outside its lethal range. In Papoose model A, which was presumed to be within 6 per cent outside its lethal range, the largest deflections measured at the frames were up to one-half of the shell thickness, which is the same as that measured on SQUAW-13. From these data we again infer that SQUAW-13 was probably within 10 per cent of its lethal range.

Similar conclusions can be inferred from a comparison of the strain measurements, but here it is more obvious how uncertain these conclusions must be because there are so many strain measurements on SQUAW-13 with so much scatter in the results.

In the Papoose tests the crown strain gage on the plating showed a peak strain of about 0.008 when the target was 6 per cent from its presumed lethal range and 0.014 when the target was presumed to be within 2 per cent of its lethal range. The strain gage on the side plating in the same tests showed peak strains up to 0.005 and 0.006 in the same tests, respectively. The peak strains measured on SQUAW-13 in similar locations range from 0.003 to 0.007. The DTMB model tests, both static and dynamic, showed that the mean circumferential strain on these very uniform models could reach about 0.0035 before collapse would occur. These models were machined from solid cylinders and had no locked-in stresses due to cold rolling; the analysis of Fig. 3.3 indicates that in the SQUAW there would be an additional hoop strain (inside) of 0.0012 due to cold rolling. Hence we might expect a peak hoop strain up to 0.005 before collapse is assured. This is about 70 per cent of the peak strain measured at the semi-hoop gage on SQUAW-13 at frame $25\frac{1}{2}$. It is about equal to the peak average hoop strain at frame $37\frac{1}{2}$. Again we infer that SQUAW-13 was probably within 10 per cent of its lethal range.

7.7 LETHAL RANGE OF SQUAW

We suggest that the lethal horizontal range of the Wigwam weapon to a SQUAW submarine at a depth of 250 ft be taken as the round number of 7000 ft.

This value is 3 per cent closer to the weapon than the actual range of SQUAW-13. It is thus consistent with our discussion and analysis of the SQUAW-13 data to the effect that this target was probably not more than 10 per cent farther than its lethal range. The choice of a value relatively close to the range of SQUAW-13 reflects our feeling that the lethal range for a SQUAW type target is probably best described by a probability distribution which overlaps the position of SQUAW-13. That is, we believe that many repetitions of the Wigwam test, using targets built to the same specifications as the SQUAW, would reveal a real spread in values for the lethal range.

The suggested value of 7000 ft is considered uncertain by perhaps 10 per cent in the direction of smaller ranges. It applies to targets hit end-on; but within the uncertainty and for want of better information, we assume that the direction of the shock wave is not significant.

At the suggested lethal position, the slant range is 7200 ft, and the incident pressure is estimated, from Program I data,[4] to be 660 psi with a time constant of 45 msec and a duration to cutoff of 28 msec. The peak total pressure at this point, shock wave plus hydrostatic, is estimated to be 770 psi.

It is interesting to compare the estimated critical pressure of 770 psi with the predictions listed in Table 2.1. There is a close agreement with Bleich's prediction of 760 psi. Within the adopted uncertainty of 10 per cent, there is also a possible agreement with the predictions of the Polytechnic Institute of Brooklyn group and of Carrier. It will be noted that their predictions were all based upon a static yield stress of about 52,000 psi; values reported from tests on samples from the materials from which the SQUAWs were constructed ranged from 50,000 to 70,000 psi. Since apparently all the predictions were tied to estimates of yield stress and to interpretations of the model-scale experiments, we believe that this comparison of Wigwam results with the predictions is only a weak indication of the relative merits of the various analytical methods. The deviations in the predictions may be largely due to uncertainties in interpreting the scaled experiments.

For a SQUAW target at shallower depths, where surface cutoff is a major factor, it is possible to base another estimate of the lethal range on the measurements made on SQUAW-12. From those measurements we infer that a peak total pressure of 1045 psi with a decay time of about 36 msec and a duration of about 10 msec is sufficient to damage the SQUAW lethally. We estimate that, within the uncertainty of the free-field pressure measurements, these conditions occurred in the Wigwam test at a depth of 70 ft and a horizontal range of 4500 ft, and we consider this as a second point on the lethality locus. The major uncertainty in this last estimate is due to the uncertainty in the necessity for a 10-msec duration. Since this may be off by perhaps 50 per cent, we estimate that the target depth of 70 ft for a horizontal lethal range of 4500 ft is likewise uncertain by 50 per cent.

REFERENCES

1. R. E. Converse, Jr., Depth, Trim, Heading, and Flooding of Wigwam Targets, Operation Wigwam Report WT-1030.
2. A. B. Focke, Interim Summary Report of the Scientific Director of Operation Wigwam, Operation Wigwam Report ITR-1053, May 1955.
3. F. B. Porzel, Close-in Time of Arrival of Underwater Shock Wave, Operation Wigwam Report ITR-1082, May 1955.
4. C. J. Aronson, Explosion Phenomena—Operation Wigwam, Seventh Symposium on Underwater Explosion Research, Part II, DTMB Report C-746, November 1956.
5. E. H. Kennard, Underwater Explosions—A Summary of Results, DTMB Report C-334, February 1951, Eqs. 93a and 93b.
6. R. C. Gooding, G. Elmer, and W. J. Sette, A Second Investigation on Damage to Stiffened Cylinders Under Scaled Atomic Bomb Attack, DTMB Report C-680, July 1955.
7. C. E. Murphey and C. T. Johnson, Target Response Studies Using High Explosives, NEL Report 637, December 1955.

CHAPTER 8

GENERAL EQUATION FOR LETHAL RANGE

8.1 GENERAL EQUATION

The ultimate objective of this project is the establishment of a relation for the lethal range which would be applicable for all targets and all conditions of attack. Ideally such a relation would be based on a dynamic structural theory that would take proper account of the detailed structure of the submarine and its interaction with an incident pressure wave. We cannot propose such a rigorous theory at this time; indeed we believe that it is hopeless to do so until the corresponding preliminary problem of the static collapse of submarines has been solved in a rigorous manner. However, we can suggest a simple phenomenological formula which fits most of the facts as we see them and which can be used to predict the lethal range of atomic weapons to submarines.

We shall assume that the strength of a submarine to all possible conditions of attack by atomic weapons is completely defined by only two parameters — a "static" collapse pressure P_c and a characteristic response time T_c. The applied pressure is completely specified by the ambient hydrostatic pressure P_0, together with the shock-wave pressure of amplitude P_s, decay time θ, and duration T.

Then we propose that the condition for collapse is that the peak pressure of the shock wave must satisfy the condition

$$P_s = (P_c - P_0)\,(1 + e^{-\theta/T_c})\,(1 + e^{-T/T_c}) \qquad (8.1)$$

This equation fits the two estimated lethal-range data for the SQUAW target if P_c is taken as 655 psi and if $T_c = 0.015$ sec.

The form of the equation implies that the shock-wave pressure must exceed the reserve strength of the target $(P_c - P_0)$ by an amount which depends upon the various characteristic times and which approaches zero asymptotically as both the duration and the decay time become much larger than the collapse time. Hence, for large depths and/or large charges, the required peak total pressure, shock wave plus hydrostatic, approaches the collapse pressure. In this equation T_c is an empirical constant, which is expected to vary in proportion to the scale of the submarine so long as the structure remains similar and the strain-rate effects are not appreciable. Thus, since the value $T_c = 0.015$ sec seems to fit the data for the SQUAW, $T_c = 0.018$ sec should be applicable to an SS563 class submarine.

Of course, there are many possible equations, with two parameters to specify the submarine, which have the same limiting properties as Eq. 8.1 and which fit the lethal-range estimates within the uncertainty of these estimates. For example, an excess-impulse criterion has the proper limiting behavior. It requires two parameters, the static collapse pressure and the excess impulse. However, it does not fit the two previous estimates for the lethal range of the SQUAW. Thus, for the lethal point at the 250-ft depth, the excess impulse is estimated to be 0.44 psi-sec, whereas, for the lethal point at the 70-ft depth, the excess impulse is estimated to be 2.6 psi-sec. However, the various estimates of lethal range, static collapse pressure, and excess impulse might all be readjusted within their possible errors to make the estimates fit the equation. This would be justified only if the excess-impulse criterion had some rigorous theoretical basis instead of being simply a plausible relation like the simpler relation given above.

The measurements on SQUAW-13 suggest that there were at least two different response modes which might have caused collapse if the target were closer in. It is possible that subsequent research will show that there are many possible collapse modes, each with an equivalent static collapse pressure P_c and a different characteristic time T_c, and their relative importance may depend upon random differences in otherwise similar submarines or perhaps on the direction or pattern of the incident pressure wave. In that case an equation of the type given may still be valid if P_c, T_c, and P_s are interpreted as the most probable values that apply to the various possibilities rather than as the specific values that apply to each possibility.

Equation 8.1 is meant to apply to full-scale targets where strain-rate effects and delayed-yield effects are probably not very significant. Otherwise it is clear that an equation with only two target parameters may not be adequate. The simplest solution is to add another factor to the equation to take care of such effects in the dynamic strength of the steel; for example,

$$P_s = (kP_c - P_0)\,(1 + e^{-\theta/T_c})\,(1 + e^{-T/T_c}) \tag{8.2}$$

where k is the ratio of the dynamic and static yield strengths at the expected loading conditions. This equation has three parameters which can be picked with some degree of arbitrariness, and it seems intuitively clear that it can be made to fit the DTMB model tests and the NEL model tests within their experimental uncertainties. However, the equation now no longer applies right up to the collapse depth. It might also appear logical to add another parameter, perhaps as an additional term to T_c, to take care of delayed-yield effects. However, this would increase the number of adjustable parameters to four, which seems too many in view of the probable scatter in the experimental data.

These equations should not be expected to apply, except fortuitously, to attacks by conventional chemical charges against local sections of the targets. In that case the available evidence indicates that lethal damage is often due to whipping or to the local action of the bubble pressures, and there is no evidence that this type of damage is related in any simple way to the static collapse pressure. The equations likewise should not be expected to apply if the target is at such a shallow depth (for example, less than 50 ft) that the duration of the shock wave is comparable with the transit time of the pressure wave across the width of the submarine.

8.2 BOUNDARY OF LETHAL-DAMAGE REGION

Equation 8.1 can be used to calculate the boundary of the lethal-damage region for the SQUAW target under Wigwam test conditions (see Fig. 8.1).

The solid-line curve in Fig. 8.1 applies down to the 300-ft depth. It was calculated using the experimental free-field pressures, the durations, and the decay constants reported by Project 1.2.[1] In this region the pressures tend to be slightly lower than for 20 kt of TNT, the decay times slightly higher, and the durations about 20 per cent lower, all probably because of the nonhomogeneous thermal structure of the ocean. At depths from 300 to 600 ft, the free-field measurements indicate an anomalous pocket of high pressure which is not mapped too well. It is possible that the lethality region is not simply connected in this neighborhood, and we have sketched in the boundary in an approximate way by a dashed line. Below the 700-ft depth the pressures presumably are close to those calculated for 20 kt of TNT in homogeneous water, and these pressures were used to calculate the dashed portion of the curve.

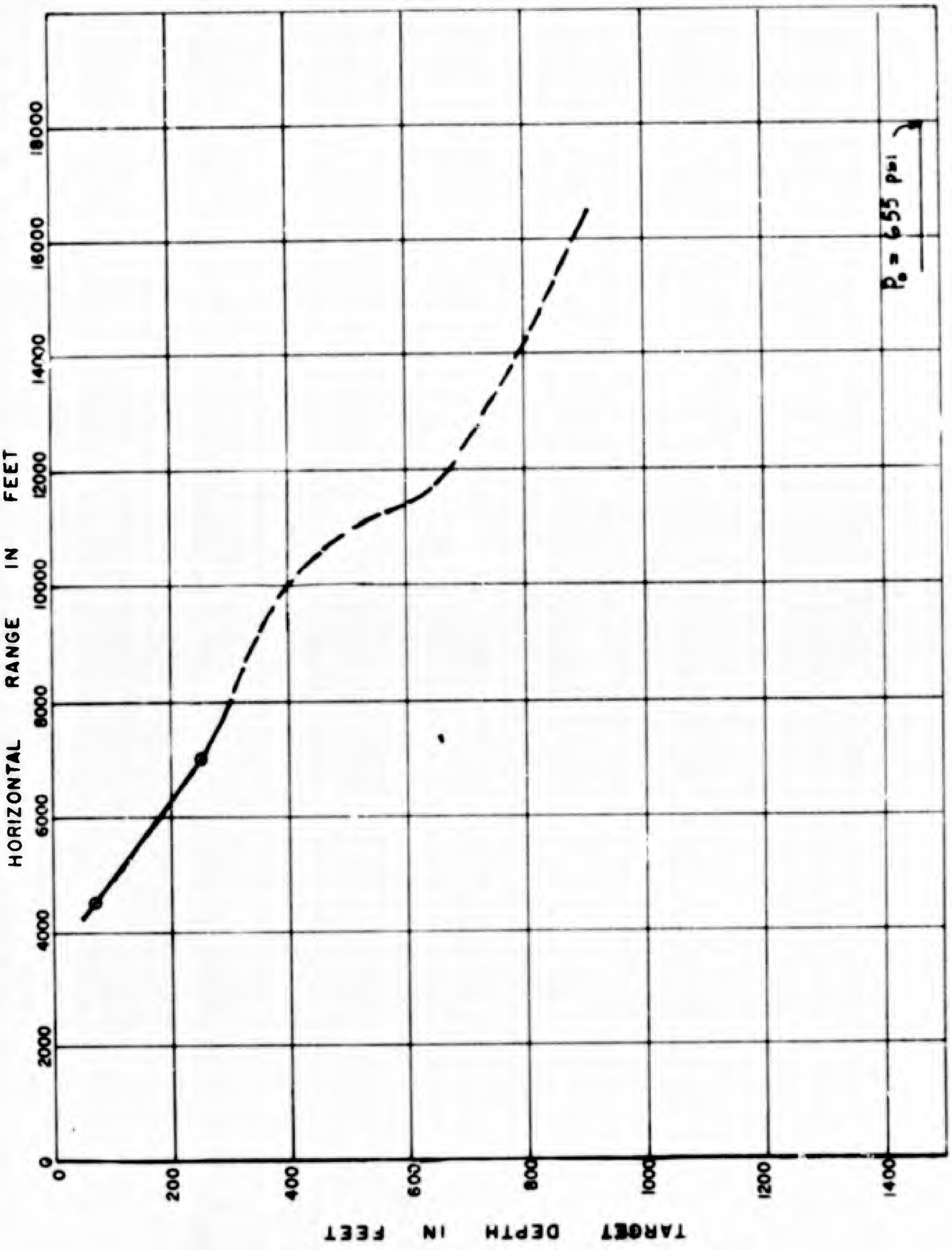

Fig. 8.1 —Boundary of lethal-damage region for a SQUAW under Wigwam test conditions.

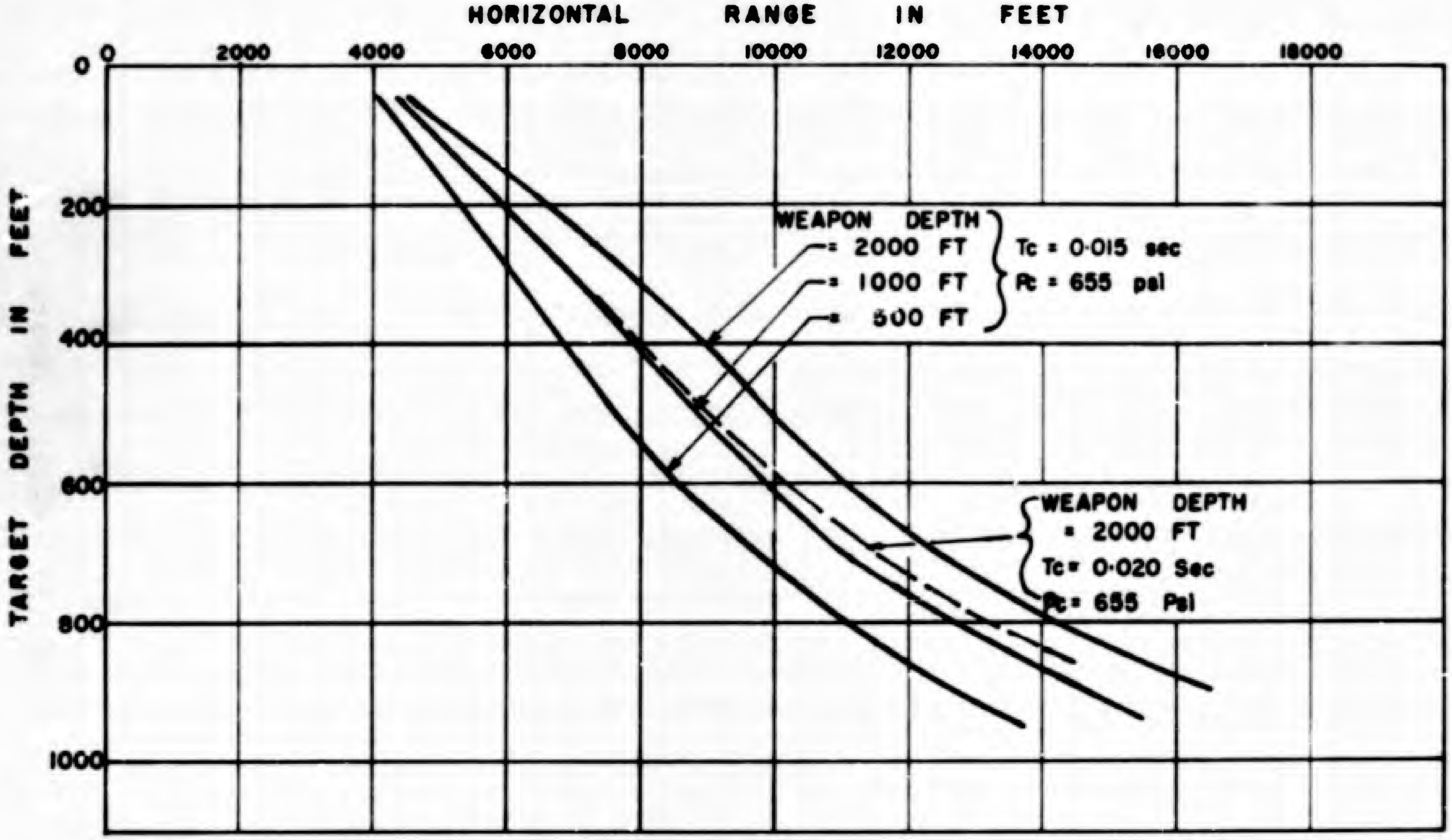

Fig. 8.2—Boundary of lethal-damage region for 40 × 10⁴ lb of TNT in homogeneous water with weapon at specified depth and submarine target as specified.

In Fig. 8.2 there are several lethality curves that result from applying Eq. 8.1 to homogeneous water. The weapon is assumed to be equivalent to 20 kt of TNT fired at depths of 500, 1000, and 2000 ft, and the target is assumed to have a collapse pressure of 655 psi and a T_c of either 15 or 20 msec.

An interesting feature of the lethality curve is that it passes only 100 ft below the location of SQUAW-13 but is 400 ft away horizontally. The exact numbers may, of course, be uncertain, but we believe that this general characteristic of the curve, namely, that the lethal range is very sensitive to depth at the shallower depths, is almost certain and quite important. The sensitivity to depth is partially due to the increase in hydrostatic pressure and to the possible focusing action of the thermal structure of the ocean, but, more importantly, to the increase in duration of the shock wave with depth. It is important because it suggests that the proper tactic, for a submarine skipper who expects to be attacked by an atomic depth charge, may be not to run away but to get to the surface as quickly as possible.

REFERENCE

1. C. J. Aronson, Explosion Phenomena—Operation Wigwam, Seventh Symposium on Underwater Explosion Research, Part II, DTMB Report C-746, November 1956.

CHAPTER 9

CONCLUSIONS

1. SQUAW-12, at a slant range of 5400 ft, was hit nearly broadside by the shock wave, with a peak dynamic pressure at the hull of about 860 psi. The target was destroyed, probably within 10 msec.

2. SQUAW-13, at a slant range of 7400 ft, was hit almost end-on by the shock wave, with a peak dynamic pressure at the hull of about 615 psi. The submarine was severely damaged but did not collapse.

3. The peak dynamic pressures acting on the hull are within 10 per cent of the peak pressure of the incident pressure wave.

4. It is estimated that the horizontal lethal range of the Wigwam weapon to a SQUAW submarine at a depth of 250 ft is about 7000 ft. This estimate is considered uncertain by perhaps 10 per cent in the direction of smaller ranges.

5. It is estimated that the horizontal lethal range of the Wigwam weapon to a SQUAW submarine at a depth of 70 ft is about 4500 ft. This estimate is considered uncertain by perhaps 50 per cent in depth.

6. The peak shock-wave pressure, from an underwater atomic weapon, which is required to damage a submarine lethally, may be given by

$$P_s = (P_c - P_0)\,(1 + e^{-\theta/T_c})\,(1 + e^{-T/T_c})$$

where P_c is the static collapse pressure of the submarine, P_0 is the ambient hydrostatic pressure, T_c is a characteristic collapse time for the submarine, and θ and T are the decay time and duration of the incident pressure wave, respectively. For an SS563 class submarine, P_c = 640 psi and T_c = 0.018 sec. This equation is a phenomenological relation which fits the estimates for the lethal range of the SQUAW and which is certainly no more reliable than these estimates.

CHAPTER 10

RECOMMENDATIONS

There were at least two major problems in the interpretation of the data which could probably be resolved by supplementary tests on the remaining SQUAW-29. The first is an analysis of the apparent 100 cycles/sec motion in the battery-room compartment which was responsible for the major strains on all three targets. The second is a determination of the true static collapse pressure of the SQUAW. We consider that all the important modes of the SQUAW can be determined by a program of tests with conventional charges in the elastic range, without doing permanent damage to the hull. After these explosion tests are completed, we suggest that the static collapse pressure can be measured on a portion of the hull in the Portsmouth pressure chamber.

We consider that this information will greatly augment the value of the Wigwam test results, at a small fraction of the initial cost. Accordingly we recommend that SQUAW-29 be made available for such a test program with adequate financial support.

APPENDIX A

EFFECT OF LEAD RESISTANCE ON CALIBRATION OF BRIDGE CIRCUIT

Assume a resistance bridge, made up of four resistors R, which is connected (1) to a power source of electromotive force E and negligible resistance and (2) to a detector of resistance R_0, by long leads whose resistances are R_1, R_2, R_3, and R_4. To determine the voltage across the detector which is caused by connecting a calibrating resistor R_C as indicated in the circuit diagram, Fig. A.1, assume mesh currents $i_1, \ldots, i_4$ as indicated. Then the equations for the currents can be written as

$$\begin{aligned}
&(2R + R_2 + R_4 + R_0)i_1 + Ri_2 - R_2i_3 - 2Ri_4 = 0\\
&Ri_1 + (2R + R_1 + R_2)i_2 - R_1i_3 - 2Ri_4 = E\\
&-R_2i_1 - R_1i_2 + (R + R_1 + R_2 + R_3)i_3 - Ri_4 = 0\\
&-2Ri_1 - 2Ri_2 - Ri_3 + Ri_4 = 0
\end{aligned} \tag{A.1}$$

and the voltage across the detector due to the calibration can be written

$$V_C = i_1R_0 = \frac{\Delta_{12}ER_0}{|R_{ij}|} = \frac{\Delta_{12}E}{R_{11}\dfrac{\Delta_{11}}{R_0} + R_{12}\dfrac{\Delta_{12}}{R_0} + R_{13}\dfrac{\Delta_{13}}{R_0} + R_{14}\dfrac{\Delta_{14}}{R_0}}$$

where R_{12} is the resistance common to meshes 1 and 2 and Δ_{12} is the cofactor of R_{12} in the determinant R_{ij}. In the limit as $R_0 \rightarrow \infty$, this becomes

$$V_C = \frac{\Delta_{12}}{\Delta_{11}} E$$

after substituting and reducing terms, and, for the special case where $R_c \gg R_1$, R_2, R_3, R_4, and R,

$$V_C = \frac{(R + 2R_1)(R + 2R_2)}{4R_C(R + R_1 + R_3)} E \tag{A.2}$$

Now $ER/(R + R_1 + R_3)$ is the supply voltage measured at the bridge, and, from the definition of gage factor F, if the bridge is measuring a strain ϵ, the voltage across the detector will be

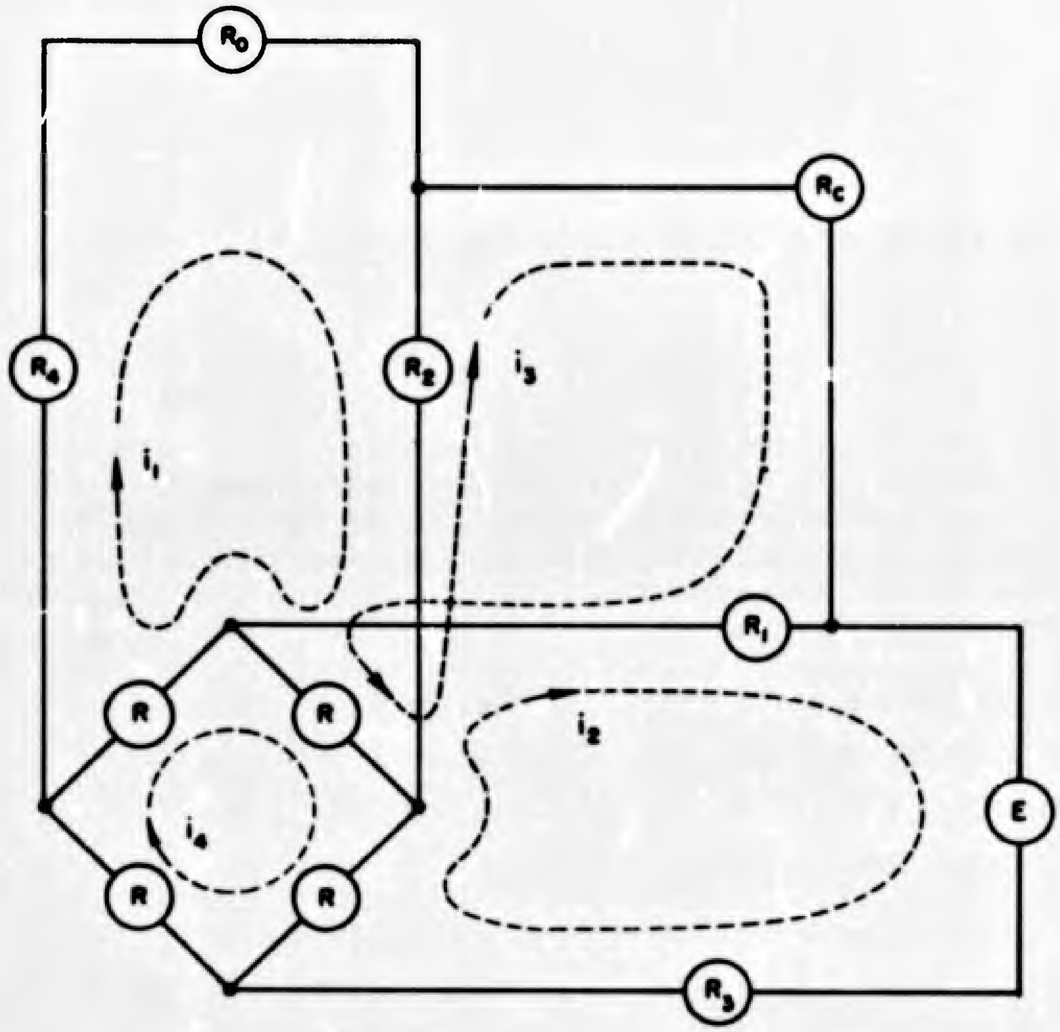

Fig. A.1—Calibration of bridge circuit with long leads.

$$V_\epsilon = F\epsilon \frac{RE}{R + R_1 + R_3} \tag{A.3}$$

Hence, comparing Eqs. A.2 and A.3, it follows that the calibration signal is equivalent to a strain

$$\epsilon_c = \frac{R}{4R_cF} \frac{R + 2R_1}{R} \frac{R + 2R_2}{R} \tag{A.4}$$

APPENDIX B

ANALYSIS OF DISPLACEMENT-GAGE CIRCUIT

The retraction wire of total resistance R_w is attached to four resistors R in a bridge circuit as shown in Fig. B.1. The bridge voltage is supplied by an electromotive force E through the mercury contact, and the unbalance voltage is measured by the detector. Then, if ρ is the resistance per unit length of the retraction wire and x is the wire length in one arm, the unbalance voltage in a detector of high impedance R_0 is

$$V = \left[\frac{R}{2R + \rho x} - \frac{R}{2R + R_w - \rho x}\right] E$$

and the rate at which this voltage changes with displacement is

$$\frac{dV}{dx} = \left[\frac{-\rho R}{(2R + \rho x)^2} - \frac{\rho R}{(2R + R_w - \rho x)^2}\right] E$$

If $R_w \ll R$, then the factor in brackets is constant and equal to the bridge factor

$$F \cong \frac{\rho}{2R}$$

Note that in this circuit it is preferable to feed the bridge voltage instead of the unbalance voltage through the mercury contact because the mercury contacts operate better at the higher current densities.

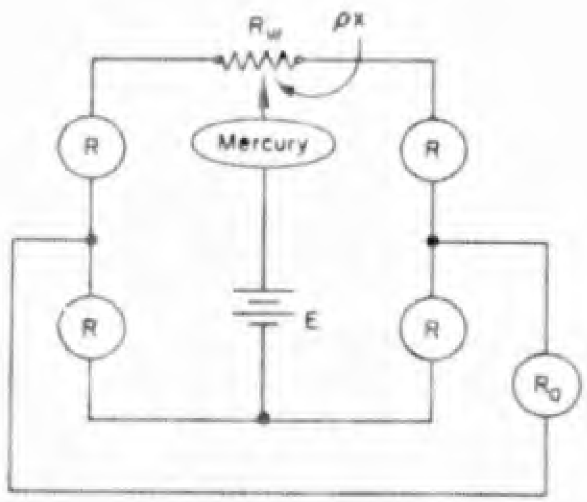

Fig. B.1—Circuit for retraction displacement gage.

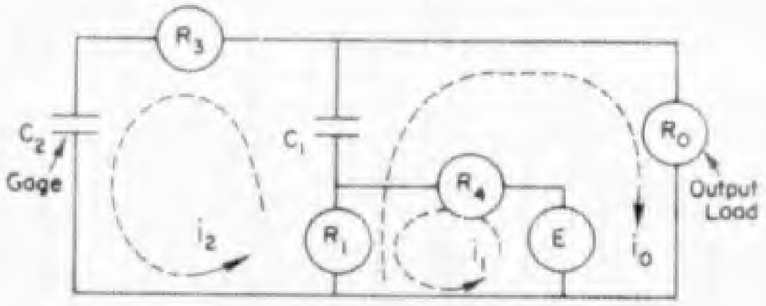

Fig. C.1—Calibration circuit for piezoelectric gages.

APPENDIX C

ANALYSIS OF PIEZOELECTRIC-GAGE CALIBRATION CIRCUIT

The termination and calibration circuit for the piezoelectric gages is shown in Fig. C.1. This is a variation of the "Q cal" circuit which has often been used in the past. However, there was originally some question as to whether the equation for the effect of a calibration signal (Eq. 4.5) might not be in error because of the possible influence of the terminating resistor R_3 and the calibration resistor R_1.

We calculate the voltage signal across the load resistance R_0 if the calibration voltage E is suddenly switched on as a step voltage. Since transient currents are involved, it is convenient to carry out the analysis in terms of Laplace transforms, which we will denote by placing a bar over the relevant variable. Thus the Laplace transform of a current i(t) is

$$\bar{I}(s) = \int_0^\infty e^{-st} i(t)\, dt$$

Assume mesh currents as indicated in the figure. The piezoelectric gage is electrically equivalent to a capacitor C_2 in series with an electromotive force KAP/C_2, where P is the instantaneous applied pressure, which is zero during calibration. Then we can write equations for the transforms of the various currents in a simple form because all the initial currents and voltages are zero.

$$\begin{aligned} &\left(R_0 + R_1 + \frac{1}{sC_1}\right)\bar{I}_0 + \left(R_1 + \frac{1}{sC_1}\right)\bar{I}_2 - R_1\bar{I}_1 = 0 \\ &\left(R_1 + \frac{1}{sC_1}\right)\bar{I}_0 + \left(R_1 + R_3 + \frac{1}{sC_1} + \frac{1}{sC_2}\right)\bar{I}_2 - R_1\bar{I}_1 = 0 \\ &-R_1\bar{I}_0 - R_1\bar{I}_2 + (R_1 + R_4)\bar{I}_1 = \frac{E}{s} \end{aligned} \tag{C.1}$$

We solve for the transform of the output voltage across R_0: $\bar{V} = \bar{I}_0 R_0$. Then, after some reduction of terms and for the special case where $R_0 \gg R_1$ and R_3, the result can be written

$$\bar{V} = \bar{I}_0 R_0 = \frac{ER_1}{R_1 + R_4}\,\frac{C_1}{C_1 + C_2}\left[\frac{1}{s + \dfrac{1}{R_0(C_1 + C_2)}} - \frac{RC_1 - R_3C_2}{(R + R_3)C}\,\frac{1}{s + \dfrac{1}{(R + R_3)C}}\right] \tag{C.2}$$

where

$$R = \frac{R_1R_4}{R_1 + R_4} \qquad C = \frac{C_1C_2}{C_1 + C_2}$$

Note that the first factor in Eq. C.2 is simply the steady-state calibrating voltage

$$E_c = \frac{ER_1}{R_1 + R_4}$$

Now we invert the transform to get the output voltage as a function of time:

$$V(t) = \frac{E_c C_1}{C_1 + C_2}\left[e^{-\{t/[R_0(C_1+C_2)]\}} - \frac{RC_1 - R_3C_2}{(R + R_3)C_1} e^{-\{t/[(R+R_3)C]\}}\right]$$

The second exponential term has a very short time constant and decays so fast that it cannot be detected on the record. The predominant first term is independent of R_1 and R_3. Hence the voltage signal due to a calibration voltage E_c is given by

$$V(t) = \frac{E_c C_1}{C_1 + C_2} e^{-\{t/[R_0(C_1+C_2)]\}} \qquad \text{(C.3)}$$

Thus the initial amplitude of the voltage signal, due to the voltage amplitude $E_c C_1/(C_1 + C_2)$, could be used as a calibration signal. However, in the actual calibration process, E (and thus E_c) is suddenly switched off, R_1 is shorted out, and the change in output voltage at this time is taken as the calibration signal. This change in voltage is taken as the signal because it is clearer, with less chatter on the record, than the initial voltage change. The change in the voltage signal is also equivalent to the voltage amplitude $E_c C_1/(C_1 + C_2)$, regardless of whether R_1 is shorted out or not. This is true because Eq. C.3 shows that V(t) is the same as though due to an electromotive force of value E_c across R_1 and is independent of the value of R_1 so long as $R_1 \ll R_0$.

THIS REPORT HAS BEEN DELIMITED
AND CLEARED FOR PUBLIC RELEASE
UNDER DOD DIRECTIVE 5200.20 AND
NO RESTRICTIONS ARE IMPOSED UPON
ITS USE AND DISCLOSURE.

DISTRIBUTION STATEMENT A

APPROVED FOR PUBLIC RELEASE;
DISTRIBUTION UNLIMITED.